AN INVESTIGATION INTO THE CAPACITY OF CELLULAR CDMA COMMUNICATION SYSTEMS WITH BEAMFORMING IN ENVIRONMENTS WITH SCATTER

by

Geoffrey W. K. Colman

A thesis submitted to the
Department of Electrical and Computer Engineering
in conformity with the requirements
for the degree of Master of Science (Engineering)

Queen's University
Kingston, Ontario, Canada
September 1998

Abstract

In recent years, humanity has looked to science for ways to increase safety and convenience in our everyday lives. This need for added security and convenience has drastically increased the demand for cellular telephony, necessitating the development of methods to increase the number of users that can be supported by a cellular system at one time. Beamforming has been proposed as a method for increasing the capacity of a cellular system. In this work, we predict the capacity of a code division multiple access (CDMA) cellular system implementing beamforming in a scattering environment.

First, we examine channel models for the auto- and cross correlation statistics of a Rayleigh fading environment with scatter. We use ARMA modelling to find a filter which matches known autocorrelation statistics. We then generalize a model for cross correlation statistics between elements of an antenna array in a scattering environment to include arbitrary distributions of angle-of-arrival statistics.

Finally, we improve a method for determining CDMA system uplink capacity given by Earnshaw and extend the analysis to determine the effect of inter-element cross correlation in an antenna array due to scatter on the overall system capacity. Capacity is determined both through analytical means and through computer simulation. The effect of high-rate data users and the problem of transmission beamforming in the downlink are also examined.

Acknowledgements

First and foremost, I would like to thank my supervisor Dr. Steven Blostein for his help, insight, patience and guidance throughout my graduate experience.

This work would not have been possible without the financial support of NSERC and CITR. I am grateful to both organizations.

I am also thankful for all of the people who gave me technical support and advice over the past two years. Special thanks go to Dr. Norman Beaulieu, Chris Tan, Dave Paranchych, Tao Luo and Cecelia Chan.

Most of all I would like to thank my parents, family, and friends for keeping me sane and putting up with me through stressful times. To Ken, Anne, Carla, Asha, Mary, Carol, Jana, 7:11, Sanjay, and Cara, I can't express my gratitute to you all.

A special word of thanks goes out to my friend and cooking instructor, Chris, from whom I have learned countless things over the past couple of years.

And, from a pact that dates back to our childhood, I thank my sister, Carol, for giving me my personality.

Contents

Abstract ii

Acknowledgements iii

List of Tables viii

List of Figures x

List of Important Symbols xiii

1 Introduction 1

1.1 Motivation 1

1.2 Literature Survey 2

1.3 Summary of Contributions 4

1.4 Thesis Outline 5

2 Autocorrelation Matching Through ARMA Modelling 7

2.1 Introduction 7

2.1.1 Chapter Outline 7

2.2 Jakes Model for Envelope Autocorrelation 8

2.2.1 Jakes Sum-of-Sinusoids Method 10

2.2.2 IDFT Method 13

2.3 ARMA Models 14

2.3.1 AR Parameter Definition 14

2.3.2 MA Parameter Definition 16

2.4 Results using ARMA methods 17
2.5 PSD Method of Matching Jakes ACF 18
2.5.1 Results 18
2.5.2 Model Order Selection 24
2.5.3 Computational Comparison with IDFT Method 24
2.6 Application to Fading Channel Gain Tracking 26
2.6.1 Analytical Performance Estimation 27
2.7 Chapter Summary 28

3 Cross Correlation **30**
3.1 Introduction 30
3.1.1 Chapter Outline 30
3.2 Scatter 31
3.3 Derivation of Cross Correlation Model 32
3.3.1 Use of a Gaussian Distribution for $P(\theta)$ 38
3.3.2 Generation of Envelopes with Proper Cross Correlation 39
3.4 Array Configurations 44
3.4.1 Linear Array 44
3.4.2 Circular Array 47
3.4.3 Confidence Intervals about Cross Correlation Values 49
3.4.4 Array Response Vectors 51
3.5 Chapter Summary 52

4 Power and Capacity Considerations **54**
4.1 Chapter Introduction 54
4.1.1 Chapter Outline 54
4.2 Power Value Calculations 55
4.2.1 Single Element Power Calculations 56
4.2.2 Multiple Antenna Element Power Calculations 57
4.2.3 Comparison with Simulated Values 61

4.3 Capacity Calculations 61
4.3.1 Single Antenna Element 61
4.3.2 Capacity Prediction with Multiple Antenna Element Arrays . 63
4.3.3 Comparison with Chip-Level Simulated Values 64
4.4 Multiple Antenna Scattering Environment 65
4.4.1 Beampattern Method 66
4.4.2 Mobile Power Prediction Using Cross-Correlation Statistics . . 67
4.4.3 Power and Capacity Prediction 77
4.4.4 Simulation Methodology 78
4.4.5 Simulation Results - Power 80
4.4.6 Simulation Results - Capacity 80
4.4.7 Capacity Prediction - Non-Uniform Placement of Mobiles . . . 82
4.5 Multi-Service/Rate Systems 91
4.6 Summary 94

5 Application to Different Beamforming Scenarios 95
5.1 Introduction 95
5.2 Methods of Beamforming 96
5.2.1 Beamforming in a Multi-Service Environment Using the Direct Matrix Inversion Algorithm 96
5.2.2 Maximum Sum of SNR Beamforming Algorithm 100
5.2.3 Beamforming in the Downlink 102
5.3 Summary 104

6 Conclusion 109
6.1 Introduction 109
6.2 Summary of Contributions 109
6.3 Future Work 111
6.4 Conclusions 111

A Application to Fading Channel Gain Tracking 113

Bibliography **120**

Vita **127**

List of Tables

2.1 Comparison of computational requirements per complex sample for the ARMA filter and IDFT method of random variate generation 26

3.1 Typical angle spreads (2Δ) in cellular applications 31

4.1 Expected values of ϕ_k 60

4.2 Predicted mean mobile and interference power values for $E_b/N_0 = 7dB$ using Eqn. (4.10) 61

4.3 Comparison of Predicted and Simulated Power Values for $N_A = 1$, and 20 mobiles 62

4.4 Comparison of Predicted and Simulated Power Values for $N_A = 3$, and 30 mobiles 62

4.5 Comparison of Predicted and Simulated Power Values for $N_A = 5$, and 30 mobiles 62

4.6 Predicted capacity values using perfect power control and correlation 1.0 between array elements. 64

4.7 Predicted and observed capacity values using perfect power control and correlation 1.0 between array elements. 65

4.8 Mobile power suppression factors $E[\mu_M]$ due to cross-correlation statistics 74

4.9 Interference suppression factors μ_{I_k} due to cross-correlation statistics and beamforming 77

4.10 Comparison of predicted capacity values (from Figure 4.5) with values observed through simulation 84

4.11 Worst-case capacity over all DOA's as a function of the outage probability and the number of antenna elements. Computed from Figs. 4.8 and 4.9 90

4.12 Worst-case capacity over all DOA's as a function of the outage probability and the number of data mobiles; computed from Fig. 4.11, it represents the case of 5 antennas and 0-4 data mobiles 91

5.1 Capacity as a function of the outage probability with 5 antenna elements, the desired voice mobile DOA at 70^o and data mobiles at DOAs of 150^o,210^o, and 290^o using the DMI algorithm to determine beamforming weights. 97

List of Figures

2.1 *The Bessel autocorrelation function presented by Jakes, $J_0(\omega_m\tau)$. Here, $\omega_m = 0.3$* 9

2.2 *Sum-of-sinusoids method for producing envelopes with the Bessel ACF* 12

2.3 *A comparison of the Jakes autocorrelation function with autocorrelation functions generated by the ARMA(7,7) filter and the AR(2) filter.* . . 19

2.4 *Power spectral density of the Jakes model.* 20

2.5 *Power spectral density of the AR(7) model.* 21

2.6 *Power spectral density of the FIR comb filter.* 22

2.7 *Combined power spectral density of the new ARMA filter.* 23

2.8 *A comparison of the Jakes autocorrelation function with autocorrelation functions generated by the new ARMA filter and the AR(2) filter.* . . 25

2.9 *An analytical estimate of the BER of DFALP with CQPSK. Compared are BER curves assuming a channel simulator with Jakes' autocorrelation statistics with those determined from the ACF of output data of ARMA and AR(2) filters.* 29

3.1 *Historical Scatter Model. The signal from user k arrives at the antenna array from a mean DOA of θ_k uniformly distributed across $[\theta_k - \Delta, \theta_k + \Delta.]$* 33

3.2 *Correlation of the real portion of the fading versus antenna spacing for $\theta = 0^o$ and angle-of-arrival uniformly distributed.* 40

3.3 *Correlation of the real portion of the fading versus antenna spacing for $\theta = 90^o$ and angle-of-arrival uniformly distributed.* 41

3.4 *Correlation of the real portion of the fading versus antenna spacing for $\theta = 0^o$ and angle-of-arrival Gaussian distributed.* 42

3.5 *Correlation of the real portion of the fading versus antenna spacing for $\theta = 90^o$ and angle-of-arrival Gaussian distributed.* 43

3.6 *Linear array geometry.* 46

3.7 *Circular array geometry.* 48

4.1 *A sample beampattern focusing on an angle-of-arrival (AOA) of 92 degrees in an array with 5 elements.* 59

4.2 *System capacity predictions for 1-5 antennas and Gaussian-distributed angle-of-arrival (AOA) statistics. The Gaussian AOA distribution has variance equal to that of a uniform distribution over 2Δ degrees.* . . . 68

4.3 *System capacity predictions for 2-5 antennas and cross-correlation statistics of a Gaussian AOA distribution with variance equal to a uniform distribution over 2Δ degrees.* 79

4.4 *Signal power to interference power ratio obtained by chip-level cell simulations with 3 and 5 antennas and Gaussian distributed angle-of-arrival statistics (stars). Compared with calculated values (lines). Gaussian AOA distribution with variance equal to a uniform distribution over 2Δ degrees.* 81

4.5 *The power-control method of capacity evaluation is used. Depicted are SNR curves for 3 antenna elements and Gaussian AOA distribution with variance equal to a uniform distribution over (-2,2) and (-90, 90) degrees.* 83

4.6 *An example probability density function for the percentage of an interferer's power passed by the spatial filter.* 85

4.7 *Interference distribution for 56-88 interferers. Power control will break down in cases where the total interference power exceeds 25.5 times the received signal power, P_R.* 87

4.8 *Outage probabilities for increasing interferers and 2,4, and 6 antenna elements. Each curve represents a different DOA in increments of* 1^o. 88
4.9 *Outage probabilities for increasing interferers and 3,5, and 7 antenna elements. Each curve represents a different DOA in increments of* 1^o. 89
4.10 *Density function for the amount of interference relative to a voice mobile that a data mobile will contribute.* 92
4.11 *Effect of number of data mobiles on system outage probability for the case of a 5 elements array.* 93

5.1 *Beampattern produced using the DMI algorithm to generate weights for a desired voice user at* 70^o *with data mobiles at* 150^o, 210^o, *and* 290^o. 98
5.2 *Outage probability for increasing interferers and 5 antenna elements for the desired mobile at* 70^o *and 3 data mobiles at* 150^o,210^o, *and* 290^o *using the DMI algorithm to determine beamforming weights.* 99
5.3 *Beampattern produced using the DMI algorithm to generate weights for a desired voice user at* 140^o *with data mobiles at* 150^o,210^o, *and* 290^o. 101
5.4 *One of the beampatterns produced using the algorithm for transmission beamforming from [28] for mobiles at* 112^o, 205^o, *and* 303^o. *Vertical spikes indicate desired directions for maximal transmission power.* . . 105
5.5 *Another beampattern produced using the algorithm for transmission beamforming from [28] for mobiles at* 161^o, 168^o, *and* 335^o. *Vertical spikes indicate desired directions for maximal transmission power.* . . 106
5.6 *Overall performance comparison of downlink performace with and without beamforming under a maximum sum of SNR criterion. Beamforming with 5,9,13,17 and 21 element circular arrays.* 107

A.1 *The DFALP algorithm for tracking phase and amplitude of frequency nonselective fading channels.* 119

List of Important Symbols

α_{ki}	relative phase of the ith entry of mobile k's array response vector
β_{ki}	signal strength due to mobile k at element i
γ_{ki}	overall phase due to mobile k at element i
2Δ	Angle spread of the arriving signal
θ_d	mean angle-of-arrival for the desired mobile
θ_k	mean angle-of-arrival for mobile k
$P(\theta)$	spatial distribution of the of the incoming signal
μ_{I_k}	net effect on interferer k's power due to cross correlation loss induced by angle-of-arrival distribution spread
μ_M	net effect on desired mobile's power due to cross correlation loss induced by angle-of-arrival distribution spread
ρ_{RiRj}	correlation coefficient between the real component of the Rayleigh fading at antenna i and the real component of the Rayleigh fading at antenna j
ρ_{RiRj}	correlation coefficient between the real component of the Rayleigh fading at antenna i and the imaginary component of the Rayleigh fading at antenna j
σ_Δ^2	variance of the spatial angle-of-arrival distribution $P(\theta)$
σ_n^2	variance of the background thermal noise
τ	correlation time lag
τ_{kd}	time delay of the kth mobile's signal relative to the dth mobile's signal
ϕ_k	fraction of interferer k's signal power passed by the spatial filter in beamforming
φ_i, φ_{pi}	realtive phase angle of the ith entry of the desired mobile's beamforming weight vector

ω_c, f_c	carrier frequency
ω_m, f_m	Doppler frequency
$\bar{a}$	array response vector
$\{a_k\}$	autoregressive filter coefficients
$\{b_k\}$	moving average filter coefficients
B	Bandwidth of the spread signal
E_b/N_0	signal to noise ratio
N_A	number of antenna array elements
N_I	number of interfering mobiles
N_M	total number of mobiles
p	order of autoregressive component of ARMA filter
P_I	total received interference power
P_R	received power due to the desired user
q	order of moving average component of ARMA filter
R	cross correlation matrix
R_B	data bit rate
R_{ki}	Rayleigh fading value at antenna i due to mobile k
$\bar{\omega}(\theta_d)$	maximum SNR beamforming weights for the desired user as a function of the angle-of-arrival θ_d

Chapter 1

Introduction

1.1 Motivation

In an age where frequency bandwidth is regarded as one of the world's natural resources, it is becoming increasingly important to optimize the bandwidth requirements of existing systems. In the midst of an already crowded system, the area of mobile communications is experiencing increasing demand without the luxury of an increased allocation of bandwidth. Because of this, there has been increased interest in multiple access techniques, which allow different users to share the same portion of the radio spectrum. TDMA (time-division multiple access) and FDMA (frequency-division multiple access) grant individual users separate time-slots or frequency bands respectively. CDMA (code-division multiple access), on the other hand, allows multiple users simultaneous use of the same frequency band, by assigning a unique individual pseudo-noise sequence to each user.

Another factor limiting the number of mobile users in a given area is defined by the signal processing limitations of the base-station. In order to maintain an acceptable quality of service, the base station must be able to maintain a signal-to-noise ratio corresponding to a desired maximum bit error rate. This is partly achieved through power control techniques, which ensure that the received power levels for all mobiles remain approximately equal. One method for increasing the number of users sustainable in a given region is through subdividing the region into

smaller and smaller cells, thereby reducing the requirements of each base station. This, however, dramatically increases the cost of the system. Recent studies have shown significant increases in the capacity of a single cell through the use of antenna array beamforming at the base station.

Beamforming takes advantage of the geometry of the antenna array by determining the phase delays of a planewave signal at the different antenna array elements. When the signals arriving from a specific direction are then co-phased, the desired signal power benefits from diversity effects, while interfering signals will tend to be randomized, decreasing their effect on the signal-to-noise ratio of the system.

The best way to determine the capacity of a CDMA system using beamforming is to implement the system and increase the number of mobile users in the system until the quality of service becomes unacceptable. Actual implementation of a CDMA system with an antenna array in the base station, however, would be both very expensive and very time-consuming. As an alternative to system creation, many effects seen in nature can be modelled accurately through statistical modelling. Through the use of both analytical arguments and computer simulation, an initial idea can be gained of the capacity of the system.

In this work, we use existing models for the autocorrelation of the Rayleigh fading envelope and cross correlation of signals received by a pair of antennas to simulate received signals in an antenna array with realistic auto- and cross correlation statistics. We then see the effect of cross correlation statistics due to a scattering environment on the capacity of a CDMA system using beamforming.

1.2 Literature Survey

One of the major contributions of this thesis is the calculation of the capacity of a CDMA system using digital beamforming. In this section, we discuss some other works that have also addressed capacity issues in a CDMA environment. Some of these papers deal strictly with the calculation of the capacity, while others analyse

the benefits of improvements to the system.

One of the first and most cited papers dealing with CDMA system capacity is [17]. Gilhousen et al. addressed the problem of calculating the capacity of a CDMA system using omnidirectional antennas with cell sectorization, taking into account path loss and shadowing, and introducing the system benefits of voice activity. In this thesis, we do not address voice activity, and so our capacity predictions are overly pessimistic. The addition of voice activity factors would be a simple extension to our work. We also modify the method of predicting downlink capacity in [17] to include transmission beamforming in the downlink.

Some other examples of capacity determination with omnidirectional antennas include [5], [8], [31] and [48]. In [5], Cameron and Woerner show a 10-30% loss in system capacity from a perfect power control scenario with the implementation of a realistic method of power control. Corazza, De Maio and Vatalaro [8] determine outage probabilities as a function of path loss, fading, shadowing and power control methods by looking at the interference contributions both from inside and outside the cell. Milstein, Rappaport and Barghouti [31] study the effects of path loss exponent, total number of users and diversity on the bit-error probability for both the uplink and downlink. In [48], the bit-error rates are also determined as a function of path-loss, fading, multiple access interference, and background noise with and without power control. The effects of selection diversity are also studied. Viterbi and Viterbi [50] determine the erlang capacity of a power controlled CDMA system by looking at the probability of system blockage from a queueing theory viewpoint.

Manji and Zhuang have extended the theory presented in [17] to include capacity calculations in multiple rate systems [29]. A further example including variable data rates is proposed by Paulrajan, Roberts and Machamer in [41]. Multiple rate system capacity is studied in Chapters 4 and 5.

Barberis [3], and Kajiwara [24] have looked at the capacity of an indoor picocellular environment.

Some methods have been proposed for improving the capacity of a cellular CDMA

system. Giannetti [15] and Giannetti et al. [16] have proposed a 50% increase in system capacity by using the 63-64 GHz band. In this band, the effects of interferers are lowered through atmospheric attenuation. Viterbi et al. [51] have proposed a soft handoff scheme that can increase coverage by more than a factor of 2. In [10], Divsalar, Simon and Raphaeli show that parallel interference cancellation dramatically improves the capacity of a CDMA system.

One of the most promising methods for increasing the capacity of a cellular CDMA system is through the use of base-station antenna arrays. In this thesis, we determine the increase in capacity due to antenna beamformimng. This work is an extension of work done by Earnshaw in [11], who studies the capacity of the uplink using beamforming for the single and multi-rate cases. Naguib and Paulraj [35] - [39], present the work most related to our own. The effects of antenna beamforming on system capacity are studied although a simplified model for interference power is used. Other works including antenna beamforming in CDMA systems as a method for increasing cell capacity include [26] and [52].

1.3 Summary of Contributions

This section presents a list of the major contributions of this thesis.

- A study of the use of Autoregressive-Moving Average (ARMA) models for matching the autocorrelation statistics of the multipath fading model presented by Jakes in [23].

- Generation of a low-order filter through the use of traditional AR modelling plus MA modelling through power spectral density analysis to match the multipath fading model presented by Jakes in [23].

- A model given by Salz and Winters in [46] for cross-correlation statistics between two antenna elements assuming uniform angle-of-arrival statistics is generalized to the case of any angle-of-arrival probability distribution $P(\theta)$.

- A method for simulating envelopes at an antenna array having the autocorrelation statistics of [23] and the cross-correlation statistics based on [46]
- Improved CDMA power and capacity predictions from Earnshaw in [11] for the multiple element antenna array case with better agreement to simulation values.
- The extension of the CDMA power and capacity predictions to the scattering environment case through analysis and simulation of the cross correlation statistics at the antenna array.
- The illustration of direction-of-arrival effects in antenna beamforming.
- The application of the methodology for power and capacity predictions to the problem of multi-service systems and transmission beamforming in the downlink.

1.4 Thesis Outline

The following chapters examine the auto- and cross-correlation statistics of an antenna array in a Rayleigh fading environment. This study is aimed at determining the capacity of a CDMA system in a scattering environment.

Chapter 2 explores the possibilities of using autoregressive-moving average (ARMA) modelling in order to match the autocorrelation statistics given in [23]. Two existing methods for matching Jakes' model are presented, followed by the proposed ARMA model. A discussion is given comparing the computational complexity of the ARMA filter with that of the FFT method proposed by Smith [47]. Finally, the developed filter is applied to the problem of channel gain tracking.

The final goal of Chapter 3 is to simulate fading envelopes with autocorrelation statistics defined in Chapter 2, with realistic cross correlation statistics. A cross-correlation model for the scattering environment derived by Salz and Winters for uniformly distributed angle-of-arrival statistics in [46] is generalized for any distribution of angle-of-arrival statistics. Using this model, the cross correlation statistics of

an antenna array can be determined. A method for generating signals with desired cross correlation statistics is then given, and the linear and circular antenna array geometries are discussed.

In Chapter 4, the power and capacity of a CDMA uplink system using beamforming are studied. The chapter commences with the improvement of system power and capacity predictions from [11] by utilising the beampattern to predict the interference power levels. Using the models developed in Chapter 3 for the inter-element cross correlation in a scattering environment, these power and capacity predictions are extended to the scattering environment case. Finally, the probability distribution of the interference power is examined in order to extend the study to a multi-service case.

Chapter 5 explores other beamforming applications using the same methodology as Chapter 4. First, the direct matrix inversion algorithm is used to null out heavy interferers in a predominantly voice mobile environment, and then an examination is made of the use of transmission beamforming in the downlink by using a downlink beamforming method developed in [28]. Finally, Chapter 6 summarizes the contributions of this thesis and presents a discussion of future research possibilities.

Chapter 2

Autocorrelation Matching Through ARMA Modelling

2.1 Introduction

The Jakes model for fading channel simulation is a commonly accepted model of the multipath fading environment [23]. In recent years the development of computationally efficient and accurate channel simulators implementing Jakes' model has been of great interest in the area of wireless communications. Methods that have been proposed include truncation to a finite impulse response filter implemented using an IDFT [47, 56]. There is also a sum-of-sinusoids method outlined by Jakes [23], as well as a recent AR(2) model described in [54]. The work in this chapter aims at reducing computational cost by employing low-order autoregressive moving-average (ARMA) processes, while maintaining high accuracy. It will then be combined with the work of Chapter 3 to generate antenna array signal envelopes with accurate auto- and inter-element cross correlation statistics for simulation purposes.

2.1.1 Chapter Outline

This chapter begins with a brief overview of the Jakes model of the fading environment. We then give an introduction to two methods for generating Rayleigh random variates with statistics defined by Jakes. The first of these methods is the

sum-of-sinusoids method given by Jakes in [23]. The second method, due to Smith [47] and improved by Young and Beaulieu in [56] utilises the IDFT.

We then present an investigation into the use of auto-regressive moving average (ARMA) modelling for fading channel simulation yielding mixed results. It will be shown that the ARMA parameter estimation methods of [25] prove unsatisfactory for our purposes, whereas a method of AR modelling from [25] combined with MA parameter determination through power spectral density analysis matches the Jakes autocorrelation function well.

In the latter part of the chapter, a comparison of the computational complexity is made between the filtering approach proposed in this chapter with the IDFT method of variate generation. Finally, the impact of the proposed filter to fading channel gain tracking on system performance is demonstrated and compared to trackers based on other channel estimation approaches.

2.2 Jakes Model for Envelope Autocorrelation

In Section 1.3.6 of [23], Jakes develops the autocorrelation function for the electric field component of the signal. This function is given in Equation (1.3-50) of [23] as

$$r(\tau) = \frac{\pi}{8} b_0 J_0^2(\omega_m \tau) \tag{2.1}$$

where J_0 is the zeroth order Bessel function of the first kind, τ is the correlation time lag, b_0 is the unmodulated signal energy and ω_m is the Doppler frequency in radians per second. In order to generate an envelope with these autocorrelation statistics, it is easiest to generate two independent sequences, corresponding to the real and imaginary, or in-phase and quadrature signals, each having an autocorrelation function approximating the Bessel function (Fig. 2.1). The Bessel squared autocorrelation is achieved by taking the square root of the sum of the squares of the two sequences.

It is desirable, then, to generate a sequence with an autocorrelation function as shown in Figure 2.1.

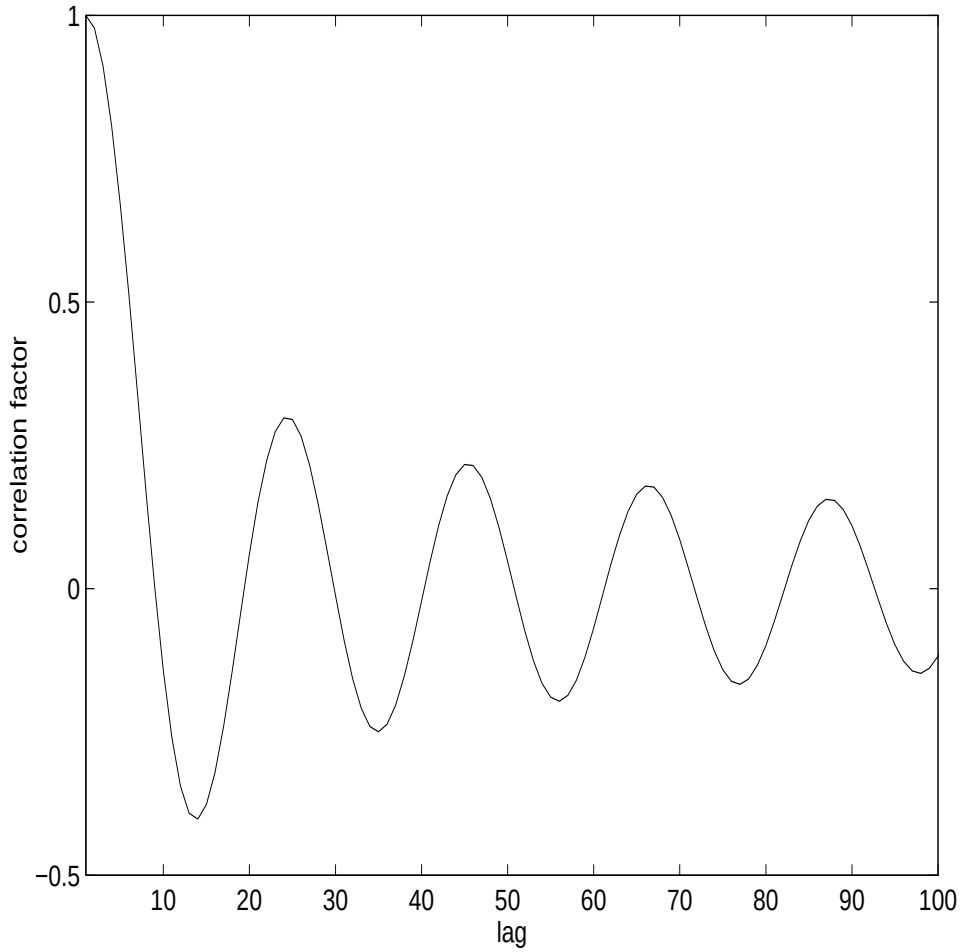

Figure 2.1: *The Bessel autocorrelation function presented by Jakes,* $J_0(\omega_m \tau)$*. Here,* $\omega_m = 0.3$

In the following sections, two different methods of generating sequences with the Bessel autocorrelation are presented. The first method, given by Jakes, is known as the sum-of-sinusoids method [23]. The second method, developed by Smith [47], uses an IFFT algorithm developed by Smith.

2.2.1 Jakes Sum-of-Sinusoids Method

In [23], the need for a method of modelling the statistical properties encountered in field testing is discussed. By modelling through computer simulation, much time and energy that would otherwise have to be spent on field measurements can be saved. In Section 1.7.1 of [23], the mathematical development of the Jakes model is given. It is reproduced in part below.

We start with an expression that represents the field as a superposition of plane waves:

$$E(t) = Re[T(t)e^{i\omega_c t}] \tag{2.2}$$

where

$$T(t) = E_0 \sum_{n=1}^{N} c_n e^{i(\omega_m t \cos\alpha_n + \phi_n)} \tag{2.3}$$

and

$$c_n^2 = p(\alpha_n)d\alpha = \frac{1}{2\pi}d\alpha \tag{2.4}$$

The arrival angles are assumed to be uniformly distributed over $[0, 2\pi]$ with $d\alpha = 2\pi/N$. This results in $c_n^2 = 1/N$, and

$$\alpha_n = \frac{2\pi n}{N}, \quad n = 1, 2, ..., N \tag{2.5}$$

By assuming N/2 is an odd integer, the series is rearranged and represented in terms of waves whose frequencies do not overlap, Jakes shows

$$T(t) = \frac{E_0}{\sqrt{N}} \left\{ \sqrt{2} \sum_{n=1}^{N_0} [e^{i(\omega_m t \cos\alpha_n + \phi_n)} + e^{-i(\omega_m t \cos\alpha_n + \phi_{-n})}] \right. \tag{2.6}$$

$$\left. + \quad e^{i(\omega_m t + \phi_N)} + e^{-i(\omega_m t + \phi_{-N})} \right\}, \qquad N_0 = \frac{1}{2}\left(\frac{N}{2} - 1\right) \tag{2.7}$$

The autocorrelation function of $T(t)$ is then shown to be

$$R_T(\tau) = \frac{b_0}{N} \cos(\omega_c \tau) \left[4 \sum_{n=1}^{N_0} \cos\left(\omega_m \tau \cos\frac{2\pi n}{N}\right) + 2\cos(\omega_m \tau) \right]. \tag{2.8}$$

It is recognized that (2.8) is of the form of a carrier multiplied by a low frequency factor. As $J_0(x)$ is defined as

$$J_0(x) = \frac{2}{\pi} \int_0^{\pi/2} \cos(x \cos\alpha) d\alpha, \tag{2.9}$$

from [23]

$$2 \sum_{n=1}^{N_0} \cos\left(\omega_m \tau \cos\frac{2\pi n}{N}\right) + \cos(\omega_m \tau) \approx \frac{N}{2} J_0(\omega_m \tau). \tag{2.10}$$

Using this analysis, a method for simulation is clear and is depicted in Figure 2.2. In this figure,

$$\omega_n = \omega_m \cos(2\pi n/N) \tag{2.11}$$

$$N_0 = \frac{1}{2}\left(\frac{N}{2} - 1\right) \tag{2.12}$$

$$\alpha = \frac{\pi}{4} \tag{2.13}$$

$$\beta_n = \frac{\pi n}{N_0}. \tag{2.14}$$

It should be noted that the output sequence is deterministic for a set of offset oscillator phases. For further discussion of the realisation of this method, see section (1.7.2) of [23].

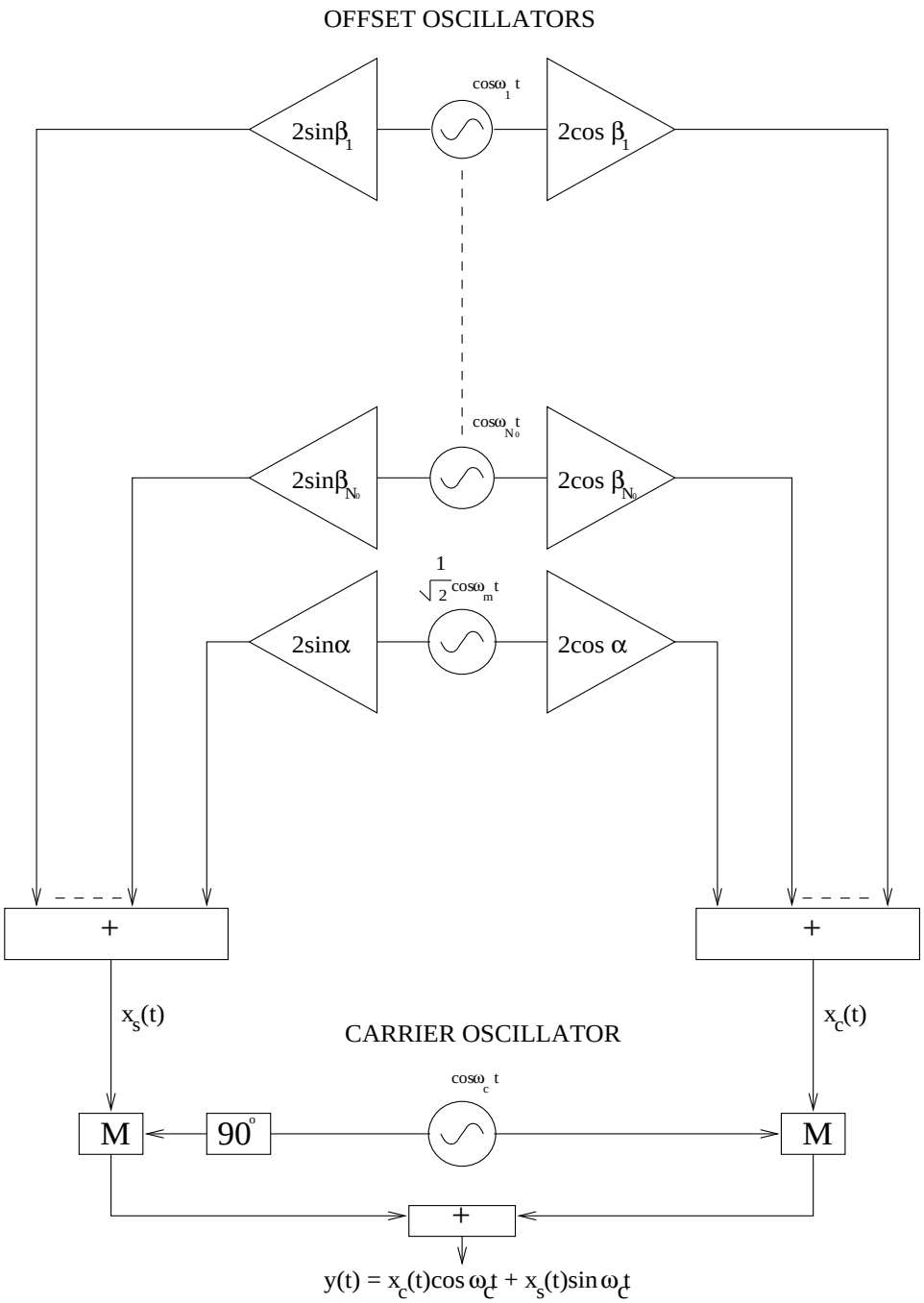

Figure 2.2: *Sum-of-sinusoids method for producing envelopes with the Bessel ACF*

2.2.2 IDFT Method

A second method for generating sequences with autocorrelation functions that match the model given in [23] uses the inverse discrete Fourier transform (IDFT) and was developed by Smith [47], and modified by Young and Beaulieu [56]. In the first step of this method, in generating a sequence with N samples, a complex sequence $\{X[k]\}$, $k = 0, 1, ..., N-1$ is formed.

$$X[k] = F[k]A[k] - jF[k]B[k] \tag{2.15}$$

where $\{A[k]\}$ and $\{B[k]\}$ are i.i.d. Gaussian variates, and $\{F[k]\}$ are filter coefficients defined to match the Jakes spectrum $S_J(f)$.

$$S_J(f) = \frac{1.5}{\pi f_m \sqrt{1 - \left(\frac{f}{f_m}\right)^2}}, \quad |f| \leq f_m \tag{2.16}$$

The filter coefficients are defined in [56] as

$$F[k] = \begin{cases} 0 & k = 0 \\ \frac{1}{\sqrt{2}} F_S[k] & k = 1, 2, ..., \frac{N}{2} - 1 \\ F_S[k] & k = \frac{N}{2} \\ \frac{1}{\sqrt{2}} F_S[N-k] & k = \frac{N}{2} + 1, ..., N-1 \end{cases} \tag{2.17}$$

and

$$F_S[k] = \begin{cases} 0 & k = 0 \\ \sqrt{\frac{1}{\sqrt{1 - \left(\frac{k}{N f_m / f_s}\right)}}} & k = 1, 2, ..., k_m - 1 \\ \sqrt{\frac{\pi}{2} - \arctan\left(\frac{k_m - 1}{\sqrt{2k_m - 1}}\right)^2} & k = k_m \\ 0 & elsewhere \end{cases} \tag{2.18}$$

where f_m is the Doppler frequency, f_s is the sample rate, $f_p = f_s/N$. and $k_m = \lfloor f_m / f_p \rfloor$.

An IDFT is then taken of the $X[k]$ sequence from Equation (2.15) to attain the desired sequence $x[n]$ which has real and imaginary components, each of which is Gaussian distributed with an autocorrelation function approximating the Bessel function. This method is block-based and requires a large memory allocation when generating long sequences.

2.3 ARMA Models

Autoregressive and Moving-Average models are commonly used to approximate many discrete-time random processes [25]. They are often chosen due to their relationship to linear filters with rational transfer functions, and their ability, through a random input sequence, to simulate noiselike behaviour accurately. Autoregressive (AR) models are used most commonly, due to the ease in calculating parameters by solving a set of equations. AR models are most effectively used in systems with power spectral densities (PSDs) with sharp peaks. Moving-Average models are useful in characterising systems whose PSDs have sharp nulls and wide peaks. ARMA models are most useful in cases where the PSD can not be modelled accurately by either a pure AR or MA model. Unfortunately, there is no simple way of determining an optimal ARMA estimator, although there are several standard methods for determining the AR and MA parameters to be used in the ARMA model.

The following sections give a brief outline of the least squares modified Yule Walker equation (LSMYWE) method of AR estimation [25], chosen because it makes use of many lags of the nonrational Jakes autocorrelation function in determining AR parameters, as well as the Durbin method for MA parameter definition.

2.3.1 AR Parameter Definition

In the following equations p denotes the order of the AR term, while q denotes the order of the MA term. The basic relationship between the autocorrelation function (ACF) $\{r_{xx}(m)\}$ and the ARMA(p,q) parameters is given by [44]:

$$r_{xx}(m) = \begin{cases} -\sum_{k=1}^{p} a_k r_{xx}(m-k) & m > q \\ -\sum_{k=1}^{p} a_k r_{xx}(m-k) + \sigma_w^2 \sum_{k=0}^{q-m} h(k) b_{k+m} & 0 \leq m \leq q \\ r_{xx}^*(-m) & m < 0 \end{cases} \tag{2.19}$$

where σ_w^2 is the variance of a white noise input sequence to the desired filter having an impulse response of $h(k)$. In a purely AR process, this simplifies to

$$r_{xx}(m) = \begin{cases} -\sum_{k=1}^{p} a_k r_{xx}(m-k) & m > 0 \\ -\sum_{k=1}^{p} a_k r_{xx}(m-k) + \sigma_w^2 & m = 0 \\ r_{xx}^*(-m) & m < 0 \end{cases} . \tag{2.20}$$

This gives rise to the Yule-Walker equations which when solved yield the autoregressive filter coefficients $\{a_k\}$.

$$\begin{bmatrix} r_{xx}(0) & r_{xx}(-1) & \cdots & r_{xx}(-p+1) \\ r_{xx}(1) & r_{xx}(0) & \ddots & r_{xx}(-p+2) \\ \vdots & \ddots & \ddots & \vdots \\ r_{xx}(p-1) & r_{xx}(p-2) & \cdots & r_{xx}(0) \end{bmatrix} \begin{bmatrix} a_1 \\ a_2 \\ \vdots \\ a_p \end{bmatrix} = - \begin{bmatrix} r_{xx}(1) \\ r_{xx}(2) \\ \vdots \\ r_{xx}(p) \end{bmatrix} \tag{2.21}$$

This system of equations can be solved easily and efficiently using the Levinson algorithm.

It was found that AR modelling was unsatisfactory in approximating the Jakes autocorrelation sequence. Higher-order models ($p > 8$) yielded filters with poles outside the unit circle, and lower-order models resulted in very low accuracy. This stability problem motivated the use of the LSMYWE method to find the AR parameters, though at the cost of destroying the correlation-matching property of AR modelling [25].

With LSMYWE, the information contained in the higher order samples of the ACF is used. The equations are of the following form [25]; where the number of lags used in the calculation $M > p$

$$\begin{bmatrix} r_{xx}(q+1) \\ r_{xx}(q+2) \\ \vdots \\ r_{xx}(M) \end{bmatrix} = - \begin{bmatrix} r_{xx}(q) & r_{xx}(q-1) & r_{xx}(q-2) & \cdots & r_{xx}(q-p+1) \\ r_{xx}(q+1) & r_{xx}(q) & r_{xx}(q-1) & \ddots & r_{xx}(q-p+2) \\ \vdots & \ddots & \ddots & \ddots & \vdots \\ r_{xx}(M-1) & r_{xx}(M-2) & \cdots & \cdots & r_{xx}(M-p) \end{bmatrix} \begin{bmatrix} a_1 \\ a_2 \\ \vdots \\ a_p \end{bmatrix} \tag{2.22}$$

which can be represented in matrix-vector form as

$$\mathbf{r_{xx}} = -\mathbf{R_{xx}a} \tag{2.23}$$

It follows from this that a least-squares estimate of $\mathbf{a}$ can be found by

$$\hat{\mathbf{a}} = -(\mathbf{R_{xx}^H R_{xx}})^{-1}\mathbf{R_{xx}^H r_{xx}} \tag{2.24}$$

where $\mathbf{R_{xx}^H}$ denotes the Hermitian transpose of $\mathbf{R_{xx}}$.

An important advantage of this method is that a large number of ACF samples are used in the computation of the filter coefficients. The optimal number of equations to be used in this method, however, is not known a priori. For the Jakes ACF, satisfactory results were obtained using $M - q = 23$ equations in computing a $p = 7$ order AR process.

2.3.2 MA Parameter Definition

The parameters of the MA model are related to the ACF using (2.19) where $a_k = 0$, and $h(k) = b_k$ for $1 \leq k \leq q$. In this case, Equation (2.19) simplifies to:

$$r_{xx}(m) = \begin{cases} 0 & m > q \\ \sigma_w^2 \sum_{k=0}^{q-m} b_k b_{k+m} & 0 \leq m \leq q \\ r_{xx}^*(-m) & m < 0 \end{cases} . \tag{2.25}$$

One method for calculating the $\{b_k\}$ parameters is based on a high-order AR approximation to the MA process, and is attributed to Durbin [25, 44]. In this method, the $MA(q)$ process is modelled by an $AR(p')$ process where $p' \gg q$. (In our design, the AR process was of order 300 to determine the MA(7) parameters.)

In matching the MA process to the AR process, we have the z-transform relationship $B(z) = 1/A(z)$ or $B(z)A(z) = 1$. This can be represented by a convolutional sum

$$\hat{a}_n + \sum_{k=1}^{q} b_k \hat{a}_{n-k} = \begin{cases} 1 & n = 0 \\ 0 & n \neq 0 \end{cases} \tag{2.26}$$

A better fit for the $\{b_k\}$ parameters is found by using a least-squares error criterion. The squared error $\mathcal{E}$ is formed

$$\mathcal{E} = \sum_{n=0}^{p'} [\hat{a}_n + \sum_{k=1}^{q} b_k \hat{a}_{n-k}]^2 - 1 \tag{2.27}$$

where $\hat{a}_0 = 1$, $\hat{a}_k = 0$ for $k < 0$ and $\hat{a}_k = a_k$ for $1 \leq k \leq p'$ given by the high-order AR solution to (2.21).

The result of this minimization is

$$\hat{b} = -\mathbf{R_{aa}^{-1}} \mathbf{r_{aa}} \tag{2.28}$$

where the $|i-j|$-th element of matrix R_{aa} is given by

$$R_{aa}(|i-j|) = \sum_{n=0}^{p'-|i-j|} \hat{a}_n \hat{a}_{n+|i-j|} \quad i,j = 1,2,\cdots,q \tag{2.29}$$

and the ith component of vector r_{aa} is

$$r_{aa}(i) = \sum_{n=0}^{p'-i} \hat{a}_n \hat{a}_{n+i} \quad i = 1,2,\cdots,q \tag{2.30}$$

2.4 Results using ARMA methods

Using the method outlined above, and a normalized Doppler frequency of $2\pi f_m = 0.3$, an ARMA(7,7) filter was obtained with the following transfer function:

$$H(z) = \frac{1 + 0.0338z^{-1} + 0.0569z^{-2} + 0.00357z^{-3} + 0.00337z^{-4} + 0.00468z^{-5} + 0.00563z^{-6} + 0.0323z^{-7}}{1 - 3.5282z^{-1} + 4.1031z^{-2} - 0.8564z^{-3} - 1.4288z^{-4} + 0.4452z^{-5} + 0.4939z^{-6} + 0.2275z^{-7}} \tag{2.31}$$

When zero-mean white Gaussian noise with variance 1 was passed through this filter and after 5000 samples were discarded for start-up transients to become negligible, an output waveform with the autocorrelation function shown in Figure 2.3

was produced. Also shown in this figure is the AR(2) model of [54]. As can be seen from this plot, the autocorrelation function of the output sequence does not match the bessel autocorrelation closely. A modification to the algorithm to ensure a good fit to the autocorrelation function is proposed in the following sections.

2.5 PSD Method of Matching Jakes ACF

As the results of existing methods for determining the coefficients for the filter taps seemed inaccurate, information contained in the Jakes' power spectral density (PSD) was used match the system more closely to theory.

The PSD of of the Jakes model is depicted in Figure (2.4).

The power spectral density of the Autoregressive portion of the ARMA model developed earlier in this chapter shows a similarity to the theoretical PSD (Fig 2.5).

In order for the PSD to match the Jakes PSD more closely, the MA component must contribute to the system.

It was found that if a comb filter [44] is used in the numerator of the filter, nulls can be placed in desired locations in order to make the roll-off of the filter steeper. Using the AR(7) model found earlier and a 15th order comb filter, improved results were obtained. The following diagrams show an example of a system with a Doppler frequency $\omega_m = 0.3$. Figure 2.5 shows the PSD of the AR(7) process, Figure 2.6 shows the PSD of the comb filter, and finally Figure 2.7 shows the PSD of the complete system. As can be seen in this graph, the total power spectral density of the system resembles the Jakes PSD quite closely; it has a much steeper rolloff at the doppler frequency than the AR(7) PSD.

2.5.1 Results

Using the method outlined in the previous sections for determining the filter taps, a digital filter was implemented in order to test this fading generator.

When zero-mean white Gaussian noise with unit variance was passed through

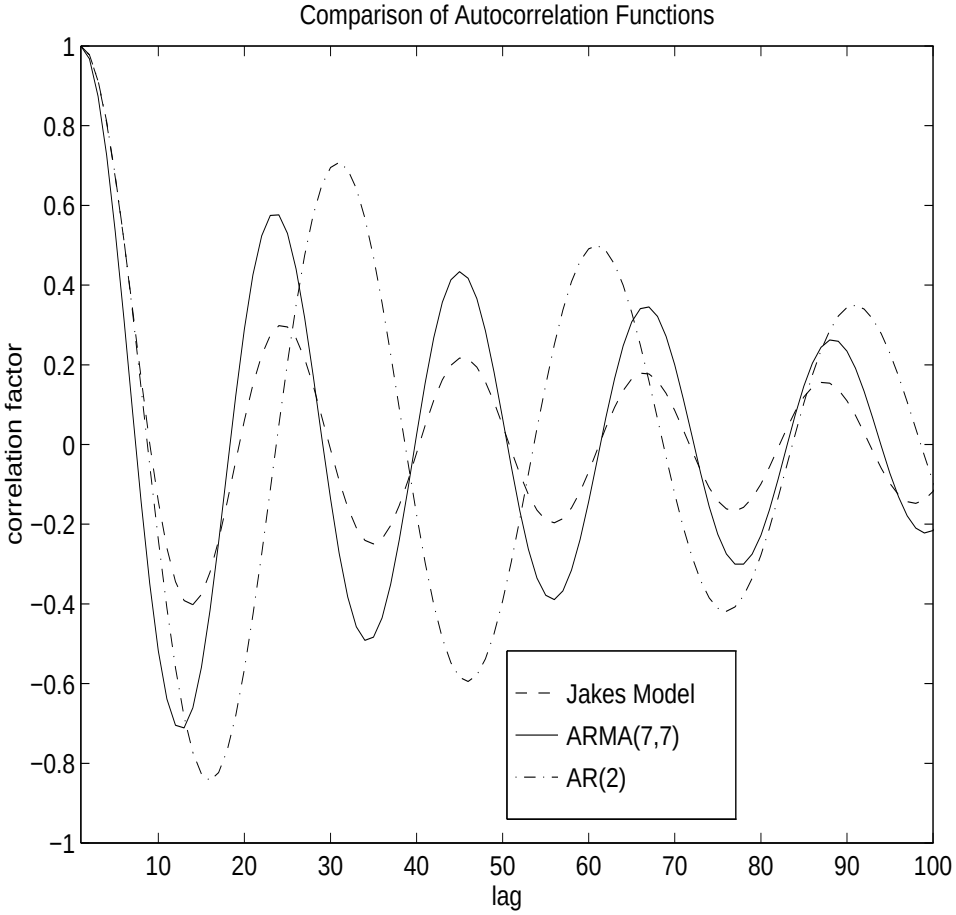

Figure 2.3: *A comparison of the Jakes autocorrelation function with autocorrelation functions generated by the ARMA(7,7) filter and the AR(2) filter.*

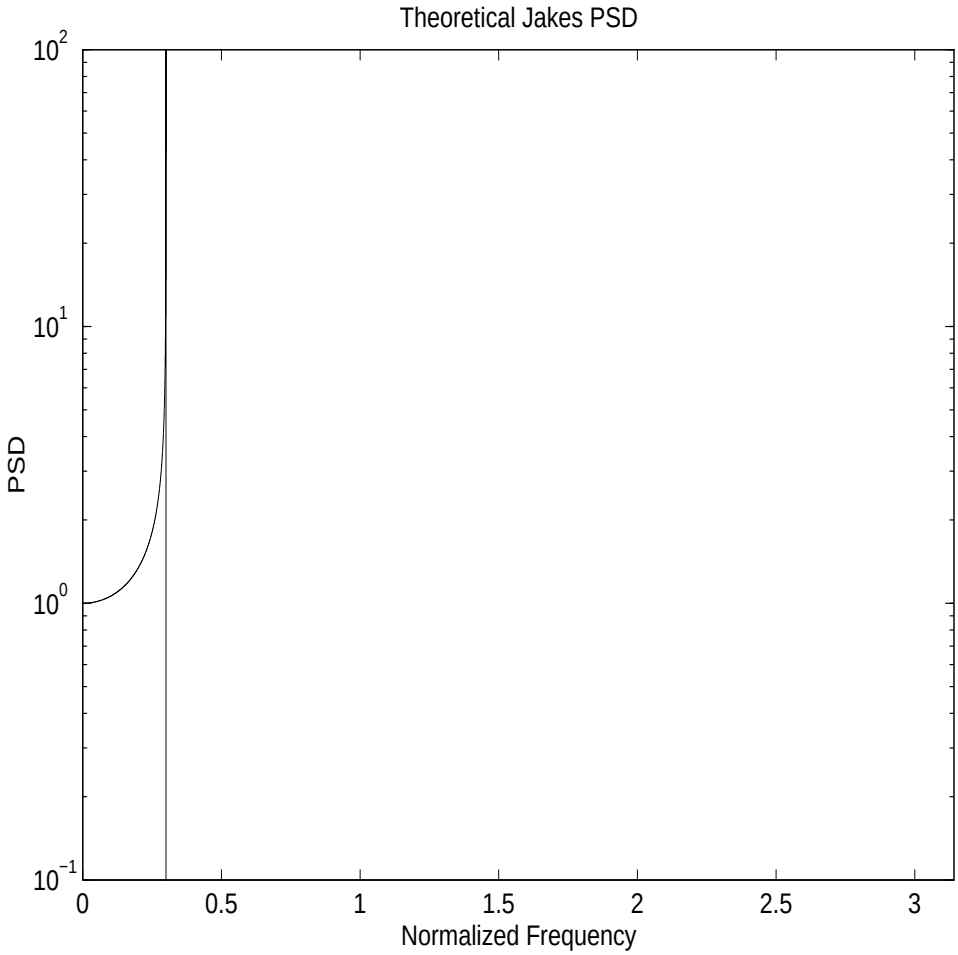

Figure 2.4: *Power spectral density of the Jakes model.*

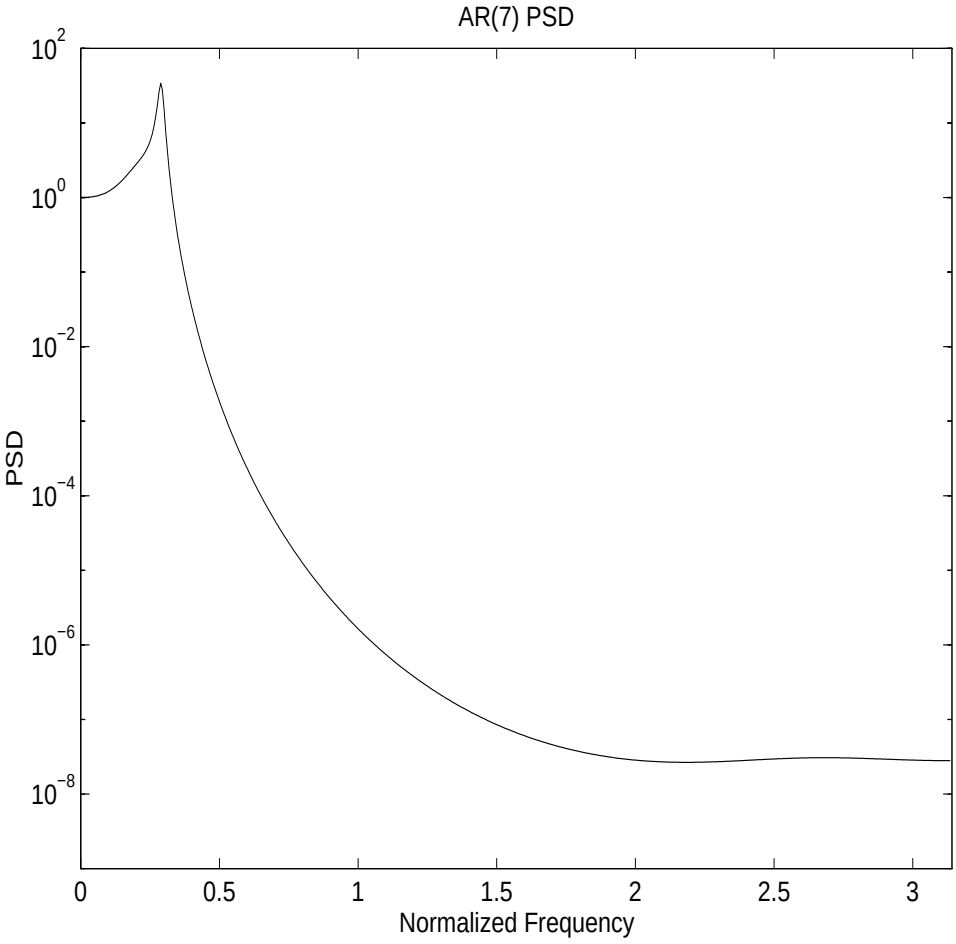

Figure 2.5: *Power spectral density of the AR(7) model.*

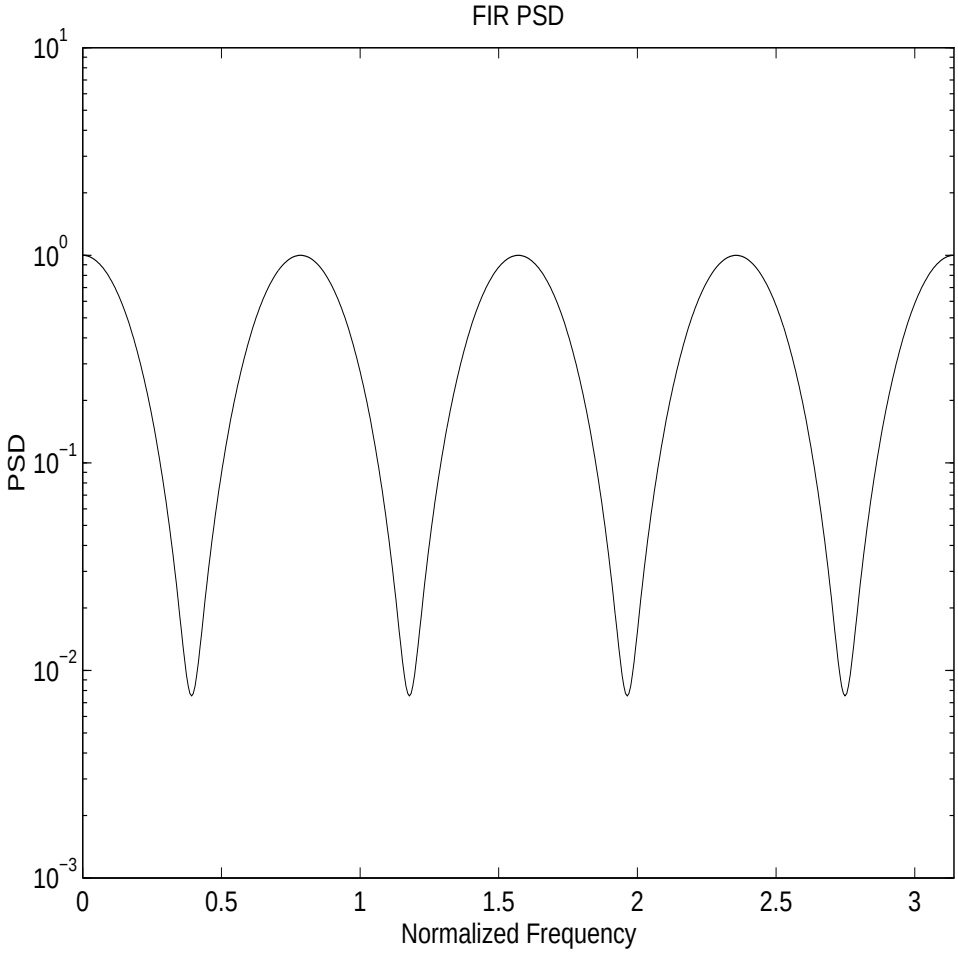

Figure 2.6: *Power spectral density of the FIR comb filter.*

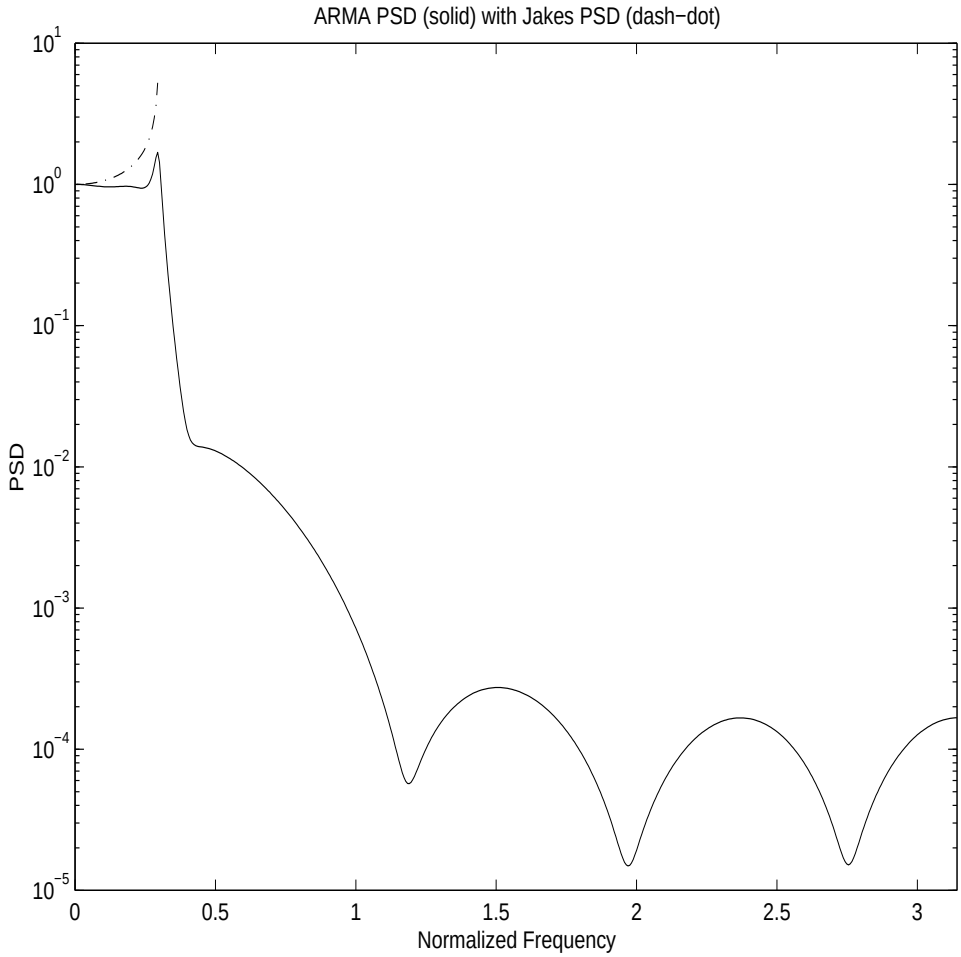

Figure 2.7: *Combined power spectral density of the new ARMA filter.*

this filter and discarding 5000 samples for transient effects to become negligible, an output waveform with the autocorrelation function shown in Figure 2.8 was produced. As can be seen from this plot, the autocorrelation function of the output sequence matches the bessel ACF much more closely than the filter produced by the ARMA methods of [25].

2.5.2 Model Order Selection

The model order of an ARMA process has been studied by Merhav in [30] and Hannan and Rissanen in [19]. Both of these methods assume a data sequence y_k is being modelled. Unfortunately, the nature of our problem is different, as we are trying to model a known ACF with a true model order that is infinite.

2.5.3 Computational Comparison with IDFT Method

One of the main goals of the development of an ARMA filter to generate correlated Rayleigh random variates was to minimize the computation time. In [56], the complexity of the IDFT method of generation compared favorably to the sum-of-sinusoids method described earlier in the chapter. In this section we compare the computational complexity of the IIR filter with the IDFT method for random variate generation.

If a filter has M non-zero entries in the numerator and N non-zero entries in the denominator of the transfer function, it will require $M + N$ real additions and $M+N+1$ real multiplications per output sample [44]. The filter derived in this chapter therefore requires 9 additions and 10 multiplications per sample or 18 additions and 20 multiplications per complex sample.

This compares favourably with the IDFT method [56] which requires $3\log_2 N$ real adds per complex sample and $2\log_2 N$ real multiplications per complex sample. Table 2.1 compares the computations required per complex sample to generate a complex sequence of length 2^N. Table 2.1 illustrates the computational benefit of the ARMA filter especially if the data set to be generated is long.

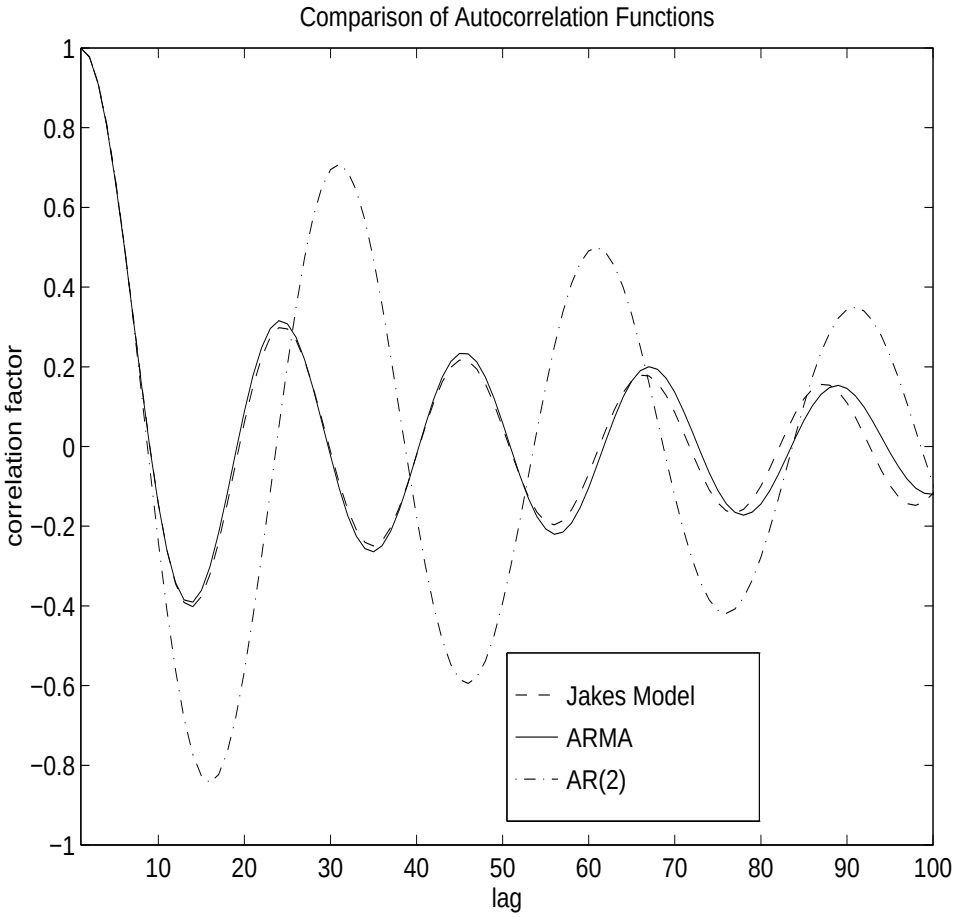

Figure 2.8: *A comparison of the Jakes autocorrelation function with autocorrelation functions generated by the new ARMA filter and the AR(2) filter.*

Sequence Length	ARMA filter	IDFT Method
$2^{12} = 4096$	18 adds, 20 mults	36 adds, 24 mults
$2^{14} = 16384$	18 adds, 20 mults	42 adds, 28 mults
$2^{16} = 65536$	18 adds, 20 mults	48 adds, 32 mults
$2^{18} = 262144$	18 adds, 20 mults	54 adds, 36 mults
$2^{20} = 1048576$	18 adds, 20 mults	60 adds, 40 mults

Table 2.1: Comparison of computational requirements per complex sample for the ARMA filter and IDFT method of random variate generation

Some other advantages of the ARMA filter method over the IDFT method include memory efficiency and a recursive rather than block calculation. These computational benefits are multiplied when being used to simulate antenna array situations.

2.6 Application to Fading Channel Gain Tracking

To detect an information sequence transmitted coherently and reliably over a fading channel, it is necessary to estimate the channel phase and amplitude. This is motivated by the fact that coherent detection of signals over fading channels is superior to non-coherent detection if accurate channel state information is available [43]. Prediction of fading dynamics can be applied to channel estimation in systems employing coherent modulation. In [27], Liu and Blostein propose a decision feedback and adaptive linear prediction (DFALP) algorithm which is reproduced for reference in Appendix A. [27] assumes the Rayleigh fading channel given in [23], and produces bit-error-rate (BER) curves of system performance based on that assumption. In the following section, we illustrate the importance of model accuracy on simulation validity.

2.6.1 Analytical Performance Estimation

According to [27], the bit error rate (BER) of symbol-by-symbol CPSK signal detection for an SNR per symbol γ_s is

$$P_e = \frac{1}{2}\left(1 - \frac{1}{\sqrt{1 + \frac{\sigma_{\hat{c}}^2 \log_2 q + \gamma_s^{-1}}{1-\sigma_{\hat{c}}^2}}}\right) \tag{2.32}$$

where $\sigma_{\hat{c}}^2$ is the mean-square-error of the unbiased minimum mean square error (MMSE) estimator $\hat{c}_k$ of c_k and $q = 2$ for BPSK and $q = 4$ for QPSK. It is seen that the BER performance is dependent only on the MSE of the channel gain estimator $\hat{c}_k$.

An estimated MSE of the channel gain estimator $\hat{c}_k$ for DFALP is derived in [27] as

$$\sigma_{\hat{c}}^2 \approx r_0 - \vec{r}^T (R_c + \frac{1}{\gamma_s} I_{N\times N})^{-1} \vec{r} \tag{2.33}$$

where R_c is the covariance matrix of the channel gain $\vec{c}(k) = (c_{k-1}, ..., c_{k-N})^T$, $\vec{r}$ is the covariance between c_k and $\vec{c}(k)$, $I_{N\times N}$ is the identity matrix. The approximation in (2.33) is due to the fact that errorless decision feedback is assumed in step 1.4 of the algorithm (Appendix A). For the Jakes fading model, the autocorrelation sequence, r_k, is given by

$$r_k = r_0 J_0(2\pi f_m T k) \tag{2.34}$$

where r_0 is the variance of the input sequence (assumed to be unity). Also,

$$f_m T = \frac{v}{\lambda} T = \frac{v f}{v_l f_s} \tag{2.35}$$

is the normalized fading bandwidth with v the vehicle speed, f the wave frequency, f_s the symbol rate and v_l the speed of light. Eqs.(2.32) and (2.33) can be used to estimate the BER performance of the DFALP algorithm when the channel matches Jakes' model perfectly.

In simulation of the DFALP algorithm, a channel simulator must be used in order to generate channel gain values. The choice of the channel simulator is an important

one as its accuracy will determine the system performance. Figure 2.9 plots the analytical estimate of the BER performance of the DFALP algorithm using CQPSK, comparing the the BER performance of the system if driven by ARMA filter developed in this chapter with an AR(2) filter used by Wu and Duel-Hallen in [54]. The performance curve obtained by truncating Jakes' autocorrelation function to 200 samples is also plotted for reference. It can be seen from this plot that the performance of the system using the ARMA filter comes much closer to matching the curve produced using the theoretical autocorrelation function than that of the AR(2) filter. However, at higher SNR, the ARMA filter may not provide autocorrelation statistics accurate enough for all simulation purposes.

2.7 Chapter Summary

In this chapter, we have investigated the use of autoregressive moving-average (ARMA) modelling to design a digital filter which matches the Jakes autocorrelation function of the multipath fading environment. ARMA modellingas in [25] proved ineffective in matching the Bessel autocorrelation output. However, the use of the Jakes PSD in order to improve the response of the overall filter proved an effective way to achieve satisfactory results while maintaining the benefit of a low-order filter in order to decrease simulation run-time.

The ARMA filter was then applied to the problem of fading channel gain tracking. This illustrated the importance of model accuracy in simulation.

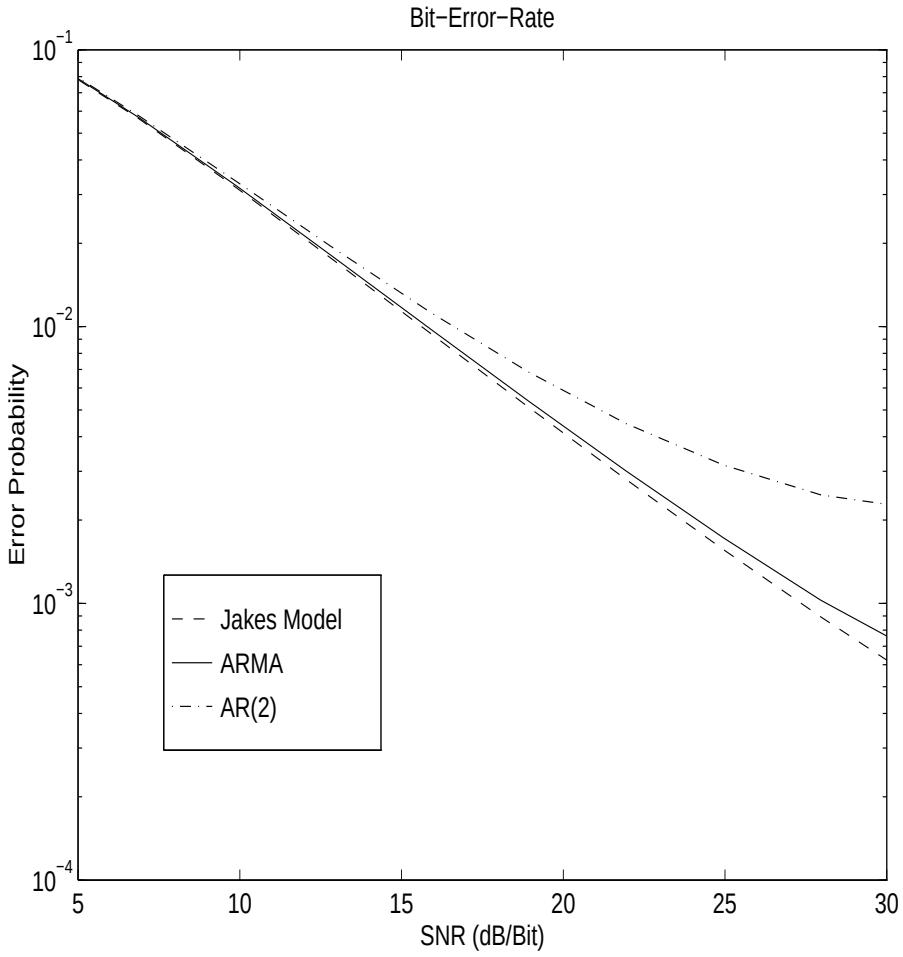

Figure 2.9: *An analytical estimate of the BER of DFALP with CQPSK. Compared are BER curves assuming a channel simulator with Jakes' autocorrelation statistics with those determined from the ACF of output data of ARMA and AR(2) filters.*

Chapter 3

Cross Correlation

3.1 Introduction

In the past, much of the research and simulation work involving antenna arrays assumed either that the envelopes of the signals received at each of the antenna elements in the array were uncorrelated (in the case of diversity research) or perfectly correlated (in the case of research in beamforming). In this chapter we examine the cross-correlation statistics between antennas within an antenna array. The goal of this is to model the effects of cross-correlation statistics more accurately both in analysis and simulation.

3.1.1 Chapter Outline

The beginning of this chapter deals with a model for the cross-correlation statistics between signals received from the same source at a pair of antennas. This model has derivations in [4], [46], and [35]. The derivation by Bramley [4] is followed closely in this chapter. The final model presented in [46] and [35] is then generalized to an arbitrary angle-of-arrival distribution.

The second part of the chapter deals with linear and circular antenna arrays. First, a method for generating signals with desired cross-correlation statistics is presented followed by a discussion of linear and circular array structures. This method is then

Environment	Angle Spread (2Δ)
Flat Rural (Macro)	1 degree
Urban (Macro)	20 degrees
Hilly (Macro)	30 degrees
Microcell (Mall)	120 degrees
Picocell (Indoors)	360 degrees

Table 3.1: Typical angle spreads (2Δ) in cellular applications

verified using some sample data. Finally, the array response vectors for linear and circular arrays are presented.

3.2 Scatter

In the analysis and simulation of a wireless multipath system, it is important to take the effects of scatter into account. Scatter occurs when signals from a single source arrive at a base station from several directions within an angular region after being reflected by objects in the surrounding vicinity. This effect is depicted in Figure 3.1 where the signal is shown to arrive within $[\theta_k - \Delta, \theta_k + \Delta]$. Typical angle spreads for different environments are given in [42] and are shown for reference in Table 3.1.

In [13], Ertel et al. discuss a number of spatial channel models including the Gaussian Wide Sense Stationary Uncorrelated Scattering (GWSSUS), Gaussian Angle of Arrival (GAA), Typical Urban (TU), and Bad Urban (BU) models. Much of the work in this chapter deals with the cross-correlation statistics between elements of an antenna array in a scattering environment. Throughout the remainder of this thesis, the distribution of the arriving signal power, $P(\theta)$, plays a significant role. In this chapter, a model for determining cross correlation statistics given by Salz and

Winters in [46], which assumes a uniform distribution of arrival statistics, is generalized for any distribution of arrival statistics. In [2], a discussion is raised of the appropriateness of a Gaussian distributed angle-of-arrival (AOA) model versus a uniformly distributed AOA model. It has been suggested in [2] that the Gaussian AOA model more accurately represents the environment in rural and suburban environments, whereas environments with much higher angle spread may be more accurately modelled by a uniform AOA model. The model that is then chosen for analysis and simulation throughout this work is the GAA model by applying a Gaussian distribution of arrival statistics. It should be noted that the same methodology can be applied to distributions corresponding to other environments as well.

3.3 Derivation of Cross Correlation Model

This section presents the derivation for the cross-correlation statistics of the multipath fading channel. It is based on and similar to a derivation given in [4], and yields similar results to derivations found in [46] and [35]. In the latter derivations, the assumption is made that the information arriving at the receiver is contained within a beamwidth of 2Δ, and that it is uniformly distributed therein. This derivation takes the model one step further by assuming no specific distribution so that any distribution can be used with the result of the derivation.

Assume that two identical antennas i and j, spaced at a distance d are receiving signals from the same source. Let the direction of the rth wave make an angle θ_{k_r} with the line ij, and let the rth wave produce voltages

$$v_{ir} = a_r \cos\left(\omega t + \psi_r + \frac{\pi d}{\lambda}\cos(\theta_{k_r})\right) \tag{3.1}$$

and

$$v_{jr} = a_r \cos\left(\omega t + \psi_r - \frac{\pi d}{\lambda}\cos(\theta_{k_r})\right) \tag{3.2}$$

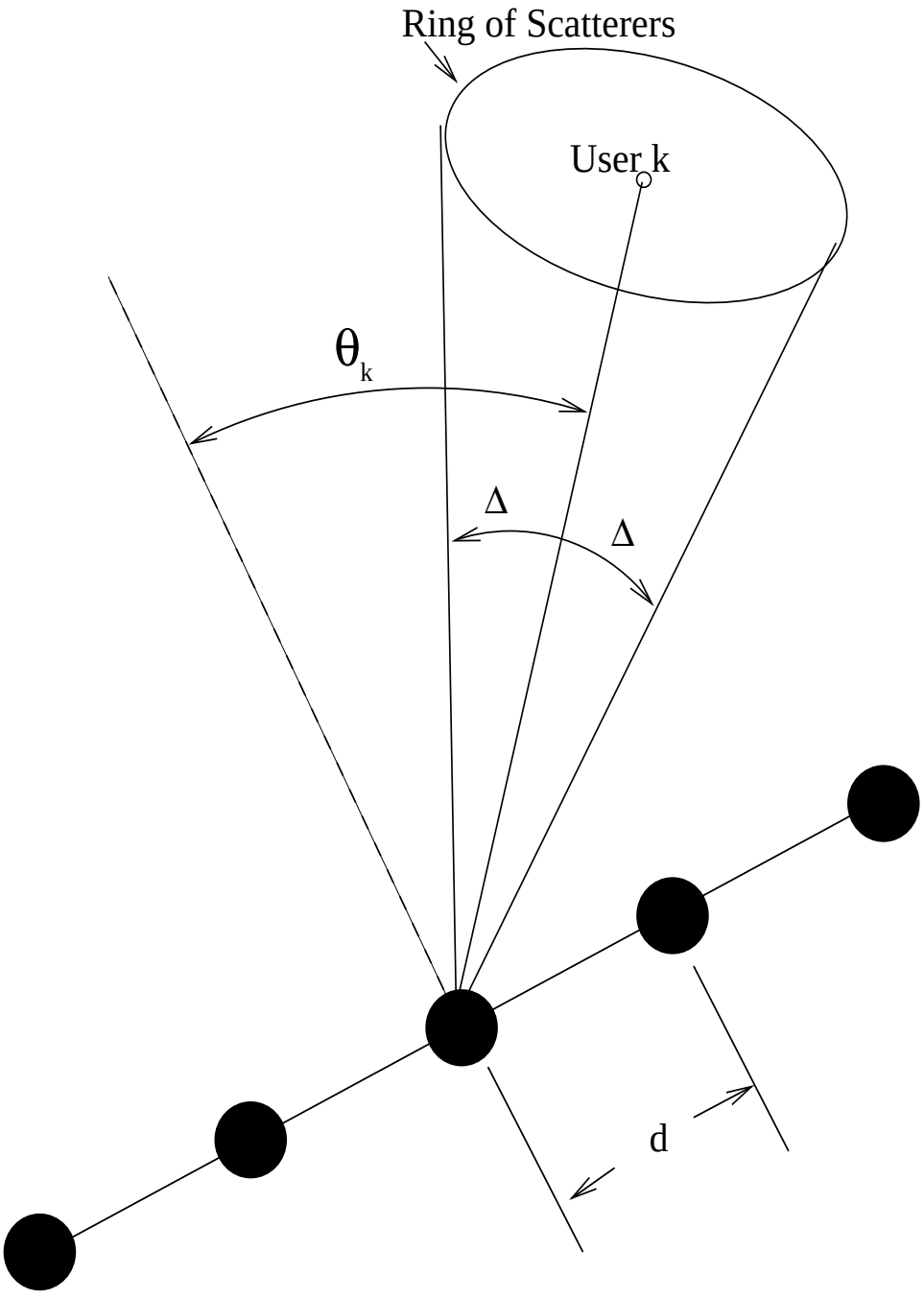

Figure 3.1: *Historical Scatter Model. The signal from user k arrives at the antenna array from a mean DOA of* θ_k *uniformly distributed across* $[\theta_k - \Delta, \theta_k + \Delta.]$

in i and j for a coplanar ray of frequency $f = \omega/2\pi$ with wavelength λ. The quantity ψ_r represents the phase delay of ray r, and a_r represents the amplitude of ray r.

Then the total voltages produced by all the waves at i and j are then:

$$v_i = \sum_{r=1}^{n} a_r \cos\left(\omega t + \psi_r + \frac{\pi d}{\lambda}\cos(\theta_{k_r})\right) \tag{3.3}$$

and

$$v_j = \sum_{r=1}^{n} a_r \cos\left(\omega t + \psi_r - \frac{\pi d}{\lambda}\cos(\theta_{k_r})\right) \tag{3.4}$$

If Eqs. (3.3) and (3.4) are written in the following form

$$v_i = A_1 \cos(\omega t + \Psi_1) \tag{3.5}$$

and

$$v_j = A_2 \cos(\omega t + \Psi_2) \tag{3.6}$$

then the amplitudes and the phases at the two antennas will, in general, be different. It can readily be shown from Eq.(3.3) and Eq.(3.4) that the mean signal voltage at i or j is:

$$\bar{v}_1 = \bar{v}_2 = 0 \tag{3.7}$$

The mean square signal voltage at i or j is

$$\bar{v}_1^2 = \bar{v}_2^2 = \frac{1}{2}\sum_{r=1}^{n} a_r^2 \tag{3.8}$$

The mean square signal amplitude at i or j is

$$\bar{A}_1^2 = \bar{A}_2^2 = \sum_{r=1}^{n} a_r^2 \tag{3.9}$$

The mean product of v_1 and v_2 is

$$\overline{v_1 v_2} = \frac{1}{2} \sum_{r=1}^{n} a_r^2 \cos\left(\frac{2\pi d}{\lambda} \cos(\theta_{k_r})\right) \tag{3.10}$$

When the individual rays above are now dealt with as distributions of rays, the summations in Eqs. (3.8), (3.9), and (3.10) are replaced by integrals over the distribution of received waves.

The total power received from the whole distribution of waves is

$$P_0 = \int_0^{2\pi} P(\theta) d\theta \tag{3.11}$$

Equations (3.8), (3.9), and (3.10) now become

$$\bar{v}_1^2 = \bar{v}_2^2 = P_0 = \int_0^{2\pi} P(\theta) d\theta \tag{3.12}$$

$$\bar{A}_1^2 = \bar{A}_2^2 = 2P_0 = 2\int_0^{2\pi} P(\theta) d\theta \tag{3.13}$$

$$\overline{v_1 v_2} = \int_0^{2\pi} P(\theta) \cos\left(\frac{2\pi d}{\lambda} \cos(\theta)\right) d\theta \tag{3.14}$$

From Eqs. (3.7), (3.12), and (3.14) the correlation coefficient between the instantaneous signals at the two antennas is given by:

$$\rho_v = \frac{\overline{v_1 v_2}}{\bar{v}_1^2} = \frac{\int_0^{2\pi} P(\theta) \cos\left(\frac{2\pi d}{\lambda} \cos(\theta)\right) d\theta}{\int_0^{2\pi} P(\theta) d\theta} \tag{3.15}$$

In practice, it is the signal amplitude that is observed, and we need to find the correlation coefficient between A_1 and A_2.

Eqs. (3.5) and (3.6) may be written

$$v_1 = B_{1c}\cos(\omega t) + B_{1s}\sin(\omega t) \tag{3.16}$$

and

$$v_2 = B_{2c}\cos(\omega t) + B_{2s}\sin(\omega t) \tag{3.17}$$

where

$$B_{1c} = A_1\cos(\Psi_1) = \sum_{r=1}^{m} a_r\cos(\psi_r + \chi_r) \tag{3.18}$$

$$B_{2c} = A_2\cos(\Psi_2) = \sum_{r=1}^{m} a_r\cos(\psi_r - \chi_r) \tag{3.19}$$

$$B_{1s} = A_1\sin(\Psi_1) = \sum_{r=1}^{m} a_r\sin(\psi_r + \chi_r) \tag{3.20}$$

$$B_{2s} = A_2\sin(\Psi_2) = \sum_{r=1}^{m} a_r\sin(\psi_r - \chi_r) \tag{3.21}$$

and

$$\chi_r = \frac{\pi d}{\lambda}\cos(\theta_{k_r}) \tag{3.22}$$

Since the phase angles, ψ, are assumed to be random, and m is assumed to be large, B_{1c}, B_{2c}, B_{1s}, and B_{2s}, are each distributed normally with mean zero.

The joint probability distribution of A_1 and A_2 is determined by the second moments: $\bar{B}_{1c}^2$, $\bar{B}_{2c}^2$, $\bar{B}_{1s}^2$, $\bar{B}_{2s}^2$, $\overline{B_{1c}B_{2c}}$, $\overline{B_{1s}B_{2s}}$, $\overline{B_{1c}B_{1s}}$, $\overline{B_{2c}B_{2s}}$, $\overline{B_{1c}B_{2s}}$, and $\overline{B_{2c}B_{1s}}$.

$$\bar{B}_{1c}^2 = \bar{B}_{2c}^2 = \bar{B}_{1s}^2 = \bar{B}_{2s}^2 = \frac{1}{2}\sum_{r=1}^{m} a_r^2 = P_0 = \int_0^{2\pi} P(\theta)d\theta \tag{3.23}$$

$$\overline{B_{1c}B_{2c}} = \overline{B_{1s}B_{2s}} = \frac{1}{2}\sum_{r=1}^{m} a_r^2 \cos\left(\frac{2\pi d}{\lambda}\cos(\theta_{k_r})\right) \tag{3.24}$$

$$= \int_0^{2\pi} P(\theta)\cos\left(\frac{2\pi d}{\lambda}\cos(\theta)\right)d\theta = \rho_{RiRj} \tag{3.25}$$

$$\overline{B_{1c}B_{1s}} = \overline{B_{2c}B_{2s}} = 0 \tag{3.26}$$

$$\overline{B_{1c}B_{2s}} = -\overline{B_{2c}B_{1s}} = -\frac{1}{2}\sum_{r=1}^{m} a_r^2 \sin\left(\frac{2\pi d}{\lambda}\cos(\theta_{k_r})\right) \tag{3.27}$$

$$= -\int_0^{2\pi} P(\theta)\sin\left(\frac{2\pi d}{\lambda}\cos(\theta)\right)d\theta = \rho_{RiIj} \tag{3.28}$$

Where the notation ρ_{RiRj} denotes the cross-correlation factor of the real component of the Rayleigh fading value at antenna element i with the real component of the Rayleigh fading value at element j. In the same way, ρ_{RiIj} denotes the cross-correlation factor of the real component of the Rayleigh fading value at antenna element i with the imaginary component of the Rayleigh fading value at element j.

Equations (3.25) and (3.28) agree with Equations (6) and (7) given by Salz and Winters in [45] and are the end result of the derivation by Bramley in [4]. At this point in the derivation, both [45] and [35] assume that $P(\theta)$ is uniform on the beamwidth $[\theta_k - \Delta, \theta_k + \Delta]$. If that is followed through, Eqn. (3.25) becomes:

$$\begin{aligned}\rho_{RiRj} &= \frac{1}{2\Delta}\int_{\theta_k-\Delta}^{\theta_k+\Delta}\cos\left(\frac{2\pi d}{\lambda}\cos(\theta)\right)d\theta \\ &= \frac{1}{2\Delta}\int_{\theta_k-\Delta}^{\theta_k+\Delta}[J_0(\frac{2\pi d}{\lambda}) + 2\sum_{m=1}^{\infty} J_{2m}(\frac{2\pi d}{\lambda})\cos 2m\theta]d\theta \\ &= J_0(\frac{2\pi d}{\lambda}) + 2\sum_{m=1}^{\infty} J_{2m}(\frac{2\pi d}{\lambda})\cos 2m\theta_k \frac{\sin(2m\Delta)}{2m\Delta}\end{aligned} \tag{3.29}$$

and Eqn. (3.28) becomes:

$$\rho_{RiIj} = 2\sum_{m=1}^{\infty} J_{2m+1}(\frac{2\pi d}{\lambda})\sin((2m+1)\theta_k)\frac{\sin((2m+1)\Delta)}{(2m+1)\Delta} \tag{3.30}$$

which is the final result of the derivation in both [45] and [35]. Instead, we make no assumption for the distribution of $P(\theta)$. Eqn. (3.25) becomes:

$$\begin{aligned}
\rho_{RiRj} &= \int_0^{2\pi} P(\theta)\cos\left(\frac{2\pi d}{\lambda}\cos(\theta)\right)d\theta \\
&= \int_0^{2\pi} P(\theta)[J_0(\frac{2\pi d}{\lambda}) + 2\sum_{m=1}^{\infty} J_{2m}(\frac{2\pi d}{\lambda})\cos 2m\theta]d\theta \\
&= J_0(\frac{2\pi d}{\lambda}) + 2\sum_{m=1}^{\infty} J_{2m}(\frac{2\pi d}{\lambda})\int_0^{2\pi} P(\theta)\cos(2m\theta)d\theta \qquad (3.31)
\end{aligned}$$

and Eqn. (3.28) becomes:

$$\begin{aligned}
\rho_{RiIj} &= -\int_0^{2\pi} P(\theta)\sin\left(\frac{2\pi d}{\lambda}\cos(\theta_r)\right)d\theta \\
&= -\int_0^{2\pi} P(\theta)2\sum_{m=1}^{\infty} J_{2m+1}(\frac{2\pi d}{\lambda})\sin((2m+1)\theta)d\theta \\
&= -2\sum_{m=1}^{\infty} J_{2m+1}(\frac{2\pi d}{\lambda})\int_0^{2\pi} P(\theta)\sin((2m+1)\theta)d\theta \qquad (3.32)
\end{aligned}$$

Equations (3.31) and (3.32), each contain an integral consisting of the probability distribution function of the angle-of-arrival statistics multiplied by a sinusoid. These integrals are very closely related with the definition for the real and imaginary components of the Fourier transform of $P(\theta)$. This result enables a closed-form expression for the cross correlation statistics to be found for any angle-of-arrival distribution $P(\theta)$ for which the Fourier transform of $P(\theta)$ has a closed-form expression.

In this work we propose the use of a Gaussian distribution for $P(\theta)$. The next section outlines the theory and results of this model.

3.3.1 Use of a Gaussian Distribution for $P(\theta)$

If a Gaussian distribution is used for $P(\theta)$ with mean AOA θ_k and variance σ_Δ^2

$$P(\theta) = \frac{1}{\sqrt{2\pi\sigma_\Delta^2}} e^{\frac{-(\theta-\theta_k)^2}{2\sigma_\Delta^2}} \qquad (3.33)$$

Eqs. (3.31) and (3.32) become:

$$\rho_{RiRj} = J_0(\frac{2\pi d}{\lambda}) + 2\sum_{m=1}^{\infty} J_{2m}(\frac{2\pi d}{\lambda})\cos(2m\theta_k)e^{-2m^2\sigma_\Delta^2} \tag{3.34}$$

and

$$\rho_{RiIj} = 2\sum_{m=0}^{\infty} J_{2m+1}(\frac{2\pi d}{\lambda})\sin((2m+1)\theta_k)e^{\frac{-(2m+1)^2\sigma_\Delta^2}{2}} \tag{3.35}$$

In determining (3.34) and (3.35), integrals are taken over $[0, 2\pi)$. It should be noted that for these integrals, the Gaussian AOA distibution is being truncated. As σ_Δ^2 increases, (3.34) and (3.35) become more approximate.

The following graphs show the relationship between the cross correlation of the antennas and the antenna spacing for arrival angles of 0^o and 90^o. The graphs show the relationships for the cross correlation factors between the real components of the Rayleigh fading between two antennas as a function of antenna spacing. Figures (3.2) and (3.3) show results assuming a uniform distribution within the beamwidth. Figures (3.4) and (3.5) assume a Gaussian angle of arrival distribution as in Eqn. (3.34). As a means of comparison, these graphs are plotted for a Gaussian distribution with the same variance as the corresponding uniform distributions. Similar plots can also be made of the correlation factor between the real component of the Rayleigh Fading value at one antenna and the imaginary component of the Rayleigh fading value at another antenna using Eqn. (3.35).

3.3.2 Generation of Envelopes with Proper Cross Correlation

From the previous chapter, we saw that it was possible to create sequences of data that had desirable autocorrelation sequences. A major goal of this work is to have signals arriving at an antenna array with proper auto- as well as cross correlation statistics. In order for this to be possible we filter uncorrelated data, denoted by

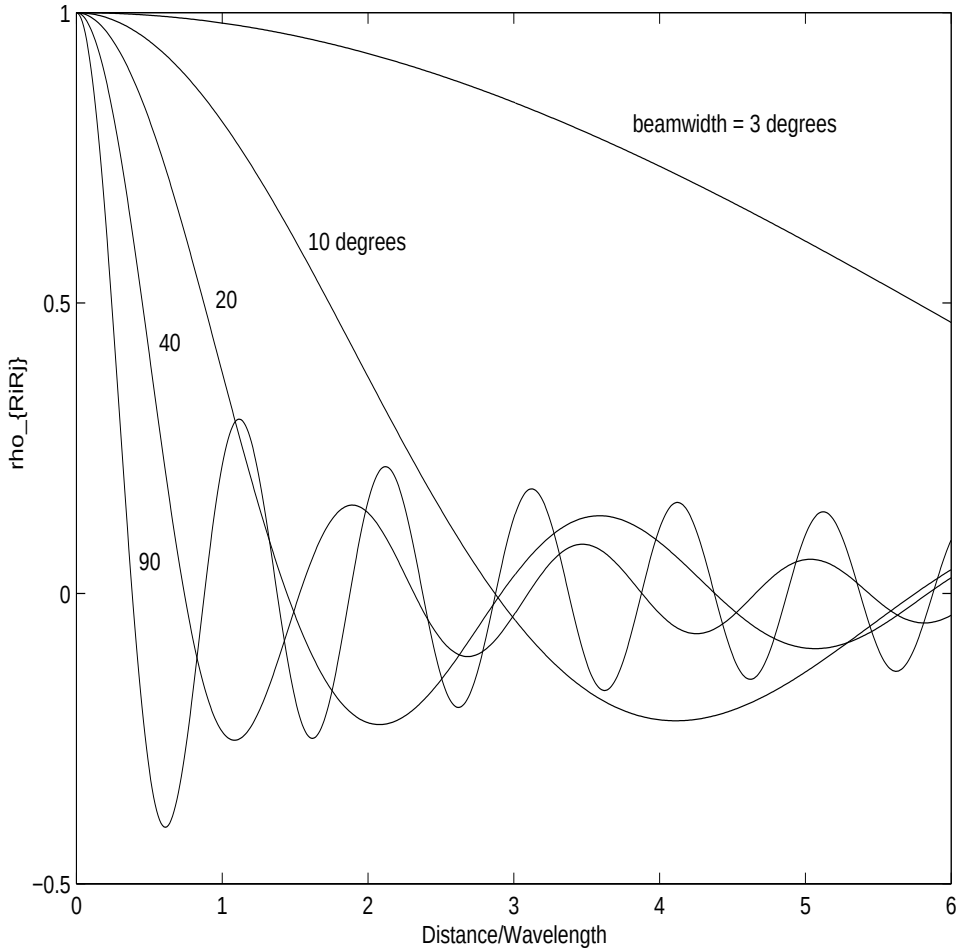

Figure 3.2: *Correlation of the real portion of the fading versus antenna spacing for* $\theta = 0^o$ *and angle-of-arrival uniformly distributed.*

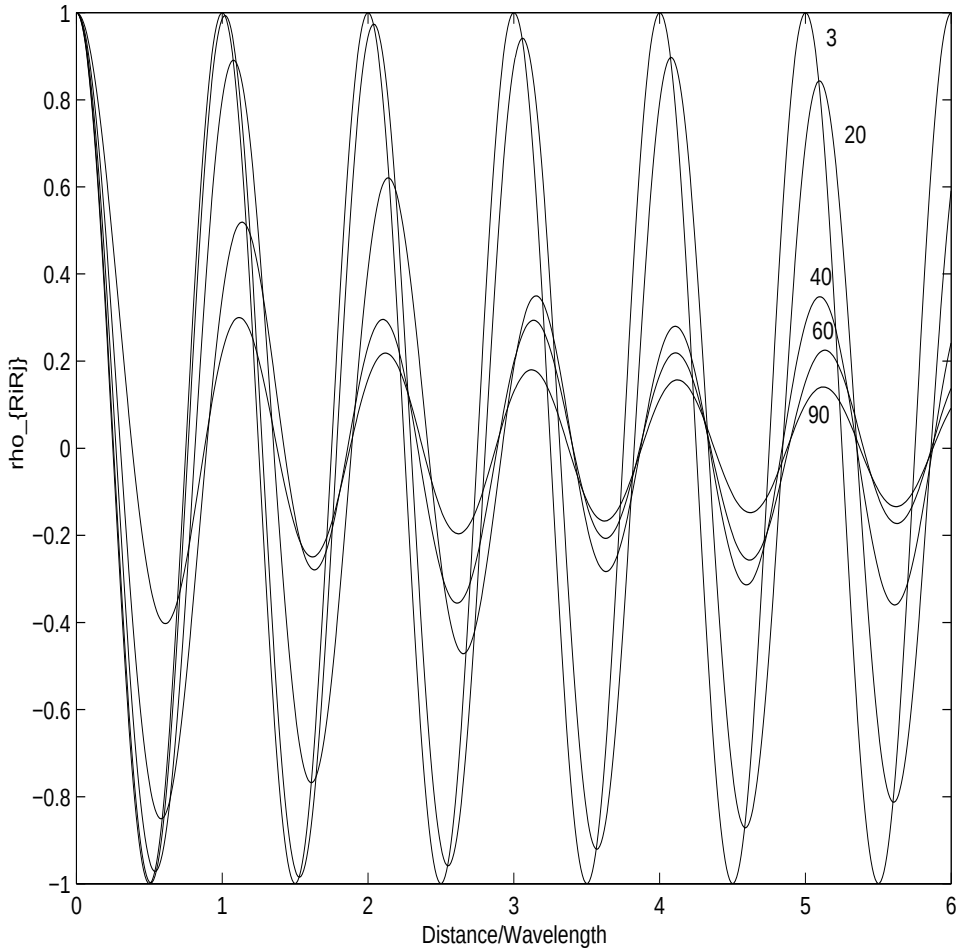

Figure 3.3: *Correlation of the real portion of the fading versus antenna spacing for* $\theta = 90^o$ *and angle-of-arrival uniformly distributed.*

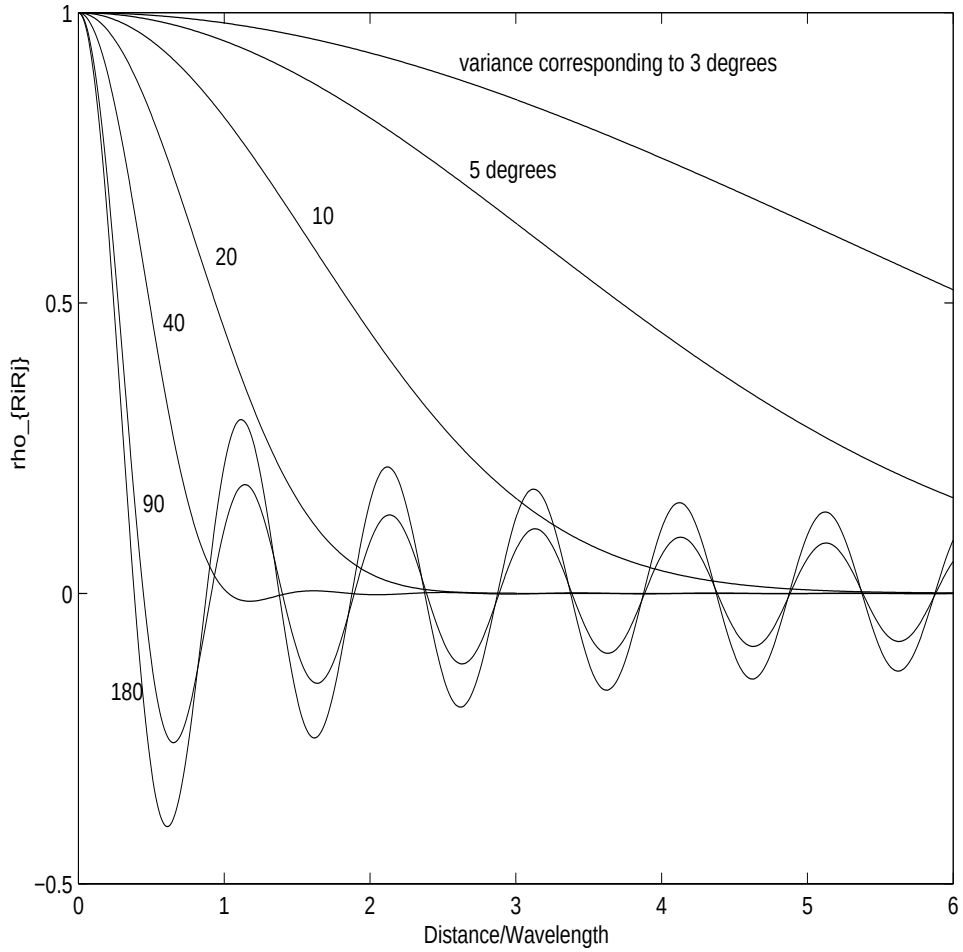

Figure 3.4: *Correlation of the real portion of the fading versus antenna spacing for* $\theta = 0^o$ *and angle-of-arrival Gaussian distributed.*

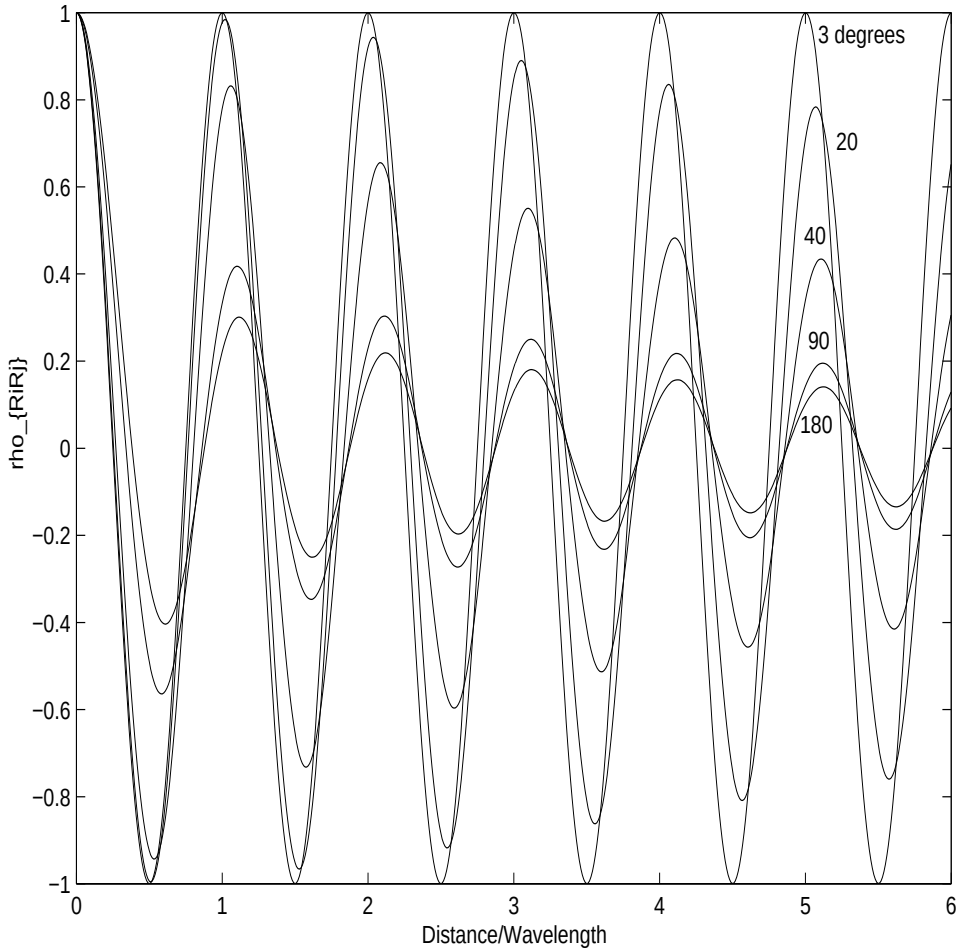

Figure 3.5: *Correlation of the real portion of the fading versus antenna spacing for* $\theta = 90^o$ *and angle-of-arrival Gaussian distributed.*

the multi-channel vector $\bar{y}$, to produce correlated data, denoted by the multi-channel vector $\bar{x}$:

$$\bar{x} = A\bar{y} \tag{3.36}$$

where A is a matrix containing the filter coefficients to be determined.

First, note that

$$\bar{x}\bar{x}^T = A\bar{y}\bar{y}^T A^T \tag{3.37}$$

Taking the expected value of both sides of this equation yields:

$$R = E\{\bar{x}\bar{x}^T\} = E\{A\bar{y}\bar{y}^T A^T\} \tag{3.38}$$

Where R is the desired cross correlation matrix. This simplifies to:

$$\begin{aligned} R = E\{\bar{x}\bar{x}^T\} &= AE\{\bar{y}\bar{y}^T\}A^T \\ &= AIA^T \\ &= AA^T \end{aligned} \tag{3.39}$$

Therefore, in order to generate data with the proper auto and cross correlation statistics denoted by the matrix R, it is only necessary to generate uncorrelated data and multiply it by matrix A.

3.4 Array Configurations

3.4.1 Linear Array

If the antennas are arranged in a linear array of N_A elements, as shown in Figure 3.6, calculations to determine the desired cross correlation matrix are simplified considerably. The spacing between neighbouring antennas is simply $\lambda/2$, making the

possible separation of pairs of antennas multiples of $\lambda/2$. The angle of arrival, unlike that of a circular antenna array, is the same for each pair of antennas, as the assumed distance to the mobile is much larger than the length of the antenna array.

Defining the 2 x 2 matrix:

$$\begin{aligned} D_{|i-j|} &= \begin{bmatrix} \rho_{RiRj} & \rho_{RiIj} \\ \rho_{IiRj} & \rho_{IiIj} \end{bmatrix} \\ &= \begin{bmatrix} \rho_{RiRj} & \rho_{RiIj} \\ -\rho_{RiIj} & \rho_{IiIj} \end{bmatrix} \end{aligned} \tag{3.40}$$

where $i, j = 1, ...N_A$, the cross correlation matrix R can be defined as:

$$R \equiv \begin{bmatrix} I_{2\times2} & D_1 & D_2 & \cdots & D_{N_A} \\ D_1^T & I_{2\times2} & D_1 & \ddots & D_{N_A-1} \\ D_2^T & D_1^T & I_{2\times2} & \ddots & D_{N_A-1} \\ \vdots & \ddots & \ddots & \ddots & \vdots \\ D_{N_A}^T & D_{N_A-1}^T & D_{N_A-2}^T & \cdots & I_{2\times2} \end{bmatrix} \tag{3.41}$$

An example of such a cross correlation matrix for an antenna array with 5 antenna elements with the signals coming from $\theta = 5^o$ with a beamwidth $\Delta = 5^o$ yields a cross correlation matrix as follows:

$$R = \begin{bmatrix} 1.00 & 0.00 & 0.95 & 0.26 & 0.81 & 0.49 & 0.61 & 0.65 & 0.38 & 0.73 \\ 0.00 & 1.00 & -0.26 & 0.95 & -0.49 & 0.81 & -0.65 & 0.61 & -0.73 & 0.38 \\ 0.95 & -0.26 & 1.00 & 0.00 & 0.95 & 0.26 & 0.81 & 0.49 & 0.61 & 0.65 \\ 0.26 & 0.95 & 0.00 & 1.00 & -0.26 & 0.95 & -0.49 & 0.81 & -0.65 & 0.61 \\ 0.81 & -0.49 & 0.95 & -0.26 & 1.00 & 0.00 & 0.95 & 0.26 & 0.81 & 0.49 \\ 0.49 & 0.81 & 0.26 & 0.95 & 0.00 & 1.00 & -0.26 & 0.95 & -0.49 & 0.81 \\ 0.61 & -0.65 & 0.81 & -0.49 & 0.95 & -0.26 & 1.00 & 0.00 & 0.95 & 0.26 \\ 0.65 & 0.61 & 0.49 & 0.81 & 0.26 & 0.95 & 0.00 & 1.00 & -0.26 & 0.95 \\ 0.38 & -0.73 & 0.61 & -0.65 & 0.81 & -0.49 & 0.95 & -0.26 & 1.00 & 0.00 \\ 0.73 & 0.38 & 0.65 & 0.61 & 0.49 & 0.81 & 0.26 & 0.95 & 0.00 & 1.00 \end{bmatrix} \tag{3.42}$$

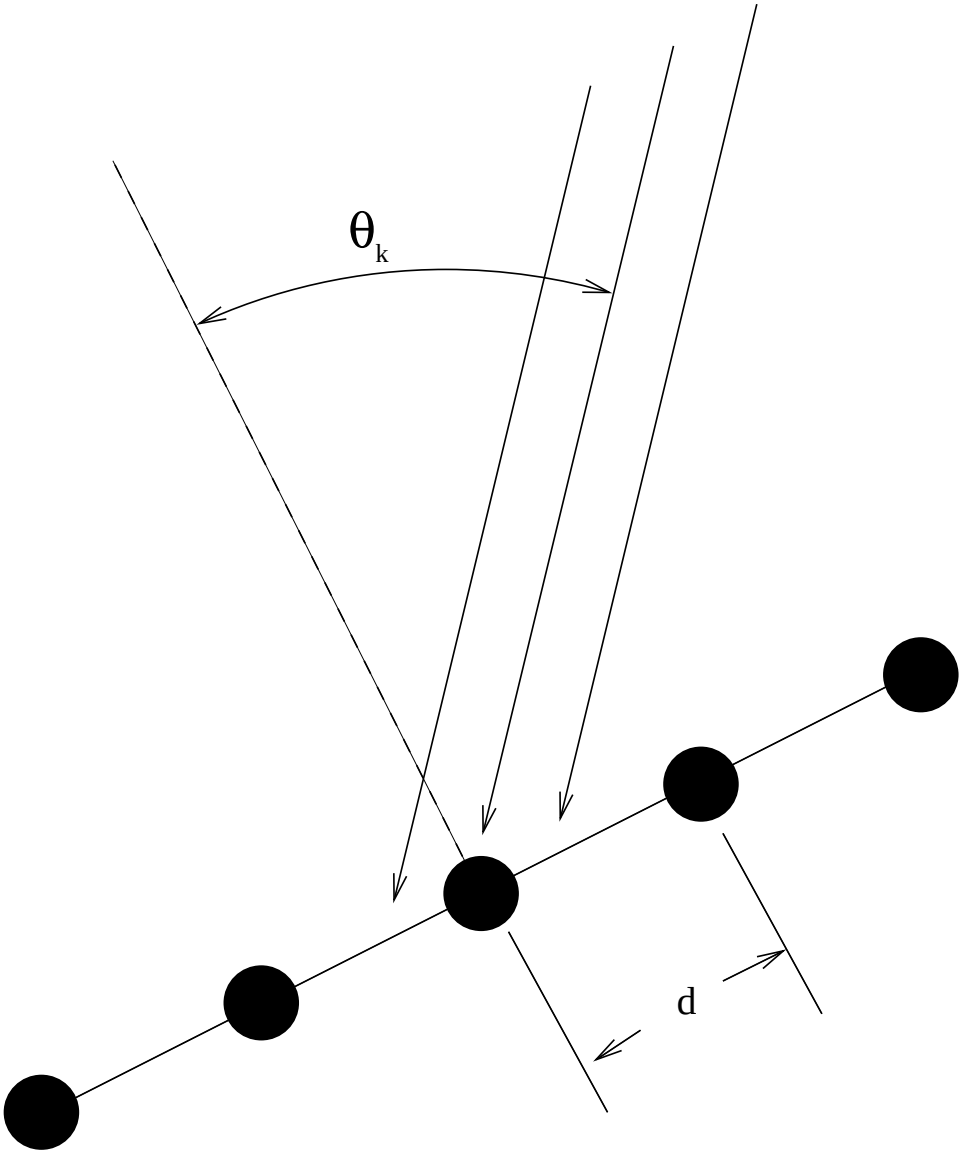

Figure 3.6: *Linear array geometry.*

3.4.2 Circular Array

If the antennas are arranged in a circular array, as shown in Figure 3.7, the calculations to determine the cross correlation matrix are more mathematically involved. The cross correlation coefficients between any two antennas are calculated simply by determining the distance between the pair of antennas and the angle of arrival in relation to the geometry of the two antennas. The distance between neighbouring antennas in the array is assumed to be $\lambda/2$. Using this information and the number of antennas in the array, the distance between any pair of antenna elements can be calculated. The distances between pairs of antenna elements can be calulated using the cosine law and the geometry of the circular array. For example, the distance between antennas 1 and 3, d_{13} is given by

$$d_{13}^2 = 2\left(\frac{\lambda}{2}\right)^2\left(1-\cos\left(\frac{\pi(N_A-2)}{N_A}\right)\right) \tag{3.43}$$

Once the entire geometry of the circular array is defined, a cross correlation matrix can be calculated.

An example of such a cross correlation matrix for an antenna array with 5 antenna elements with the signals coming from $\theta = 5^o$ with a beamwidth $\Delta = 5^o$ yeilds a cross correlation matrix as follows:

$$R = \begin{bmatrix} 1.00 & 0.00 & 0.95 & 0.26 & 0.23 & 0.97 & -0.84 & 0.49 & -0.47 & 0.88 \\ 0.00 & 1.00 & -0.26 & 0.95 & -0.97 & 0.23 & -0.49 & 0.84 & -0.88 & -0.47 \\ 0.95 & -0.26 & 1.00 & 0.00 & -0.04 & 0.99 & -0.96 & -0.18 & -0.04 & -0.99 \\ 0.26 & 0.95 & 0.00 & 1.00 & -0.99 & -0.04 & 0.18 & -0.96 & 0.99 & -0.04 \\ 0.23 & -0.97 & -0.04 & -0.99 & 1.00 & 0.00 & -0.97 & -0.25 & 0.87 & -0.41 \\ 0.97 & 0.23 & 0.99 & -0.04 & 0.00 & 1.00 & 0.25 & -0.97 & 0.41 & 0.87 \\ -0.84 & -0.49 & -0.96 & 0.18 & -0.97 & 0.25 & 1.00 & 0.00 & -0.99 & -0.08 \\ 0.49 & -0.84 & -0.18 & -0.96 & -0.25 & -0.97 & 0.00 & 1.00 & 0.08 & -0.99 \\ -0.47 & -0.88 & -0.04 & -0.99 & 0.87 & 0.41 & -0.99 & 0.08 & 1.00 & 0.00 \\ 0.88 & -0.47 & 0.99 & -0.04 & -0.41 & 0.87 & -0.08 & -0.99 & 0.00 & 1.00 \end{bmatrix} \tag{3.44}$$

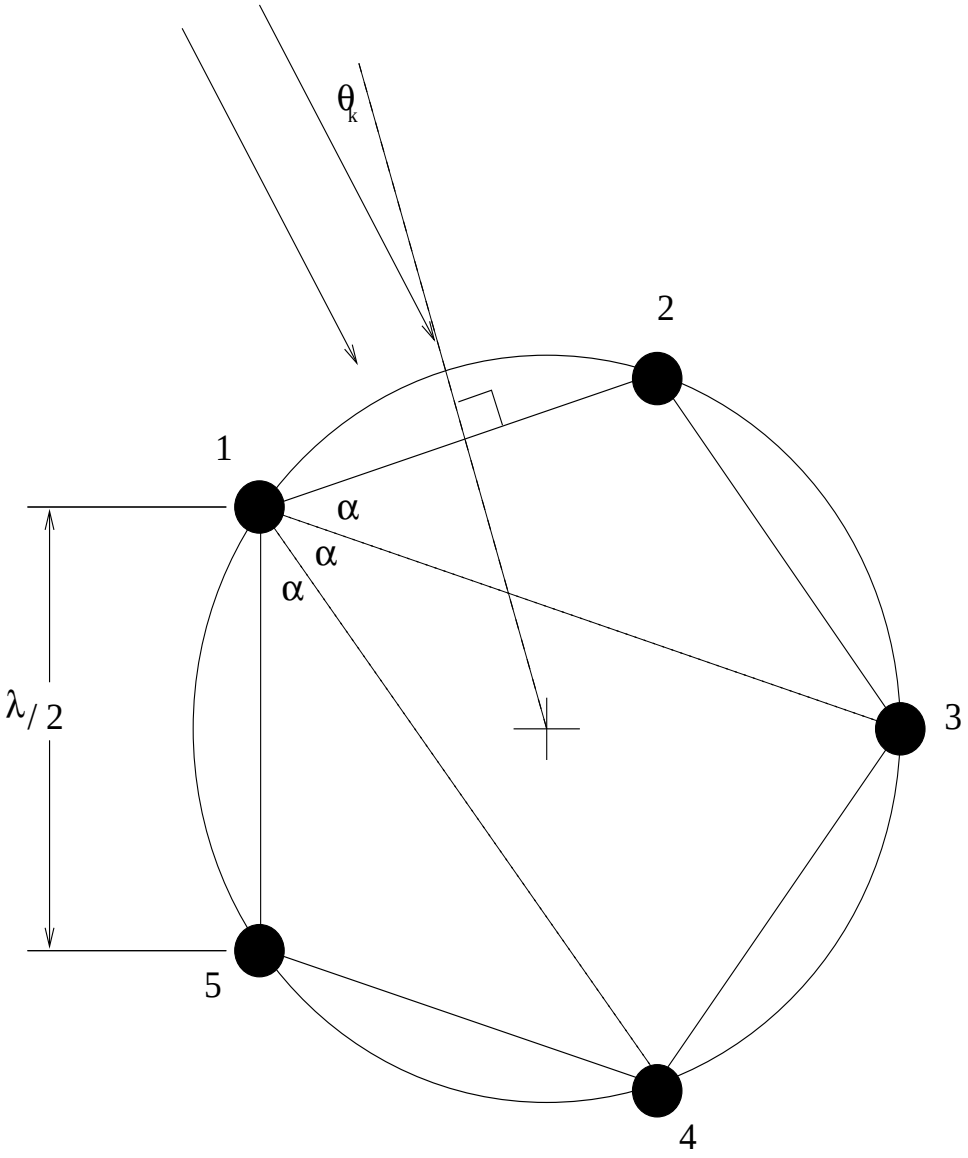

Figure 3.7: *Circular array geometry.*

3.4.3 Confidence Intervals about Cross Correlation Values

In order to ensure the accuracy of simulated results, it is important to determine an acceptable range into which simulation results should fall. In determining whether the cross correlation statistics come within an acceptable range of values about the desired value, a confidence interval can be set for each value in the cross correlation matrix.

A method for determining this confidence interval is given by Myers and Well in [34]. If the cross correlation coefficient of the data is given by r, and the Fisher Z-Transform of r is given by

$$Z_r = \frac{1}{2} \ln \left[\frac{1+r}{1-r} \right] \tag{3.45}$$

Then the 95% confidence interval for Z_r is given by

$$Z = Z_r \pm \frac{1.96}{\sqrt{N-3}} \tag{3.46}$$

where N is the number of samples in each of the Gaussian sequences.

The inverse Fisher Z-Transform of the confidence interval for Z_r then yields the confidence interval around r.

$$\rho_{max,min} = \frac{e^{2Z}-1}{e^{2Z}+1} \tag{3.47}$$

As an example of this, and as an illustration of the effectiveness of the strategy for generating envelopes with correct cross-correlation statistics, a sample cross correlation matrix of the Gaussian components of the Rayleigh fading using a 3 element circular array is given by R:

$$R = \begin{bmatrix} 1.0000 & 0.0000 & -0.8156 & -0.3412 & 0.4311 & -0.2367 \\ 0.0000 & 1.0000 & 0.3412 & -0.8156 & 0.2367 & 0.4311 \\ -0.8156 & 0.3411 & 1.0000 & 0.0000 & -0.5254 & 0.5400 \\ -0.3411 & -0.8156 & 0.0000 & 1.0000 & -0.5400 & -0.5254 \\ 0.4312 & 0.2367 & -0.5254 & -0.5400 & 1.0000 & 0.0000 \\ -0.2367 & 0.4311 & 0.5400 & -0.5254 & 0.0000 & 1.0000 \end{bmatrix} \tag{3.48}$$

The cross correlation matrix of the six 10000 sample sequences is denoted by ϱ

$$\varrho = \begin{bmatrix} 1.0000 & 0.0040 & -0.8144 & -0.3409 & 0.4271 & -0.2467 \\ 0.0040 & 1.0000 & 0.3371 & -0.8191 & 0.2439 & 0.4195 \\ -0.8144 & 0.3371 & 1.0000 & -0.0001 & -0.5232 & 0.5447 \\ -0.3409 & -0.8191 & -0.0001 & 1.0000 & -0.5378 & -0.5124 \\ 0.4271 & 0.2439 & -0.5232 & -0.5378 & 1.0000 & -0.0090 \\ -0.2467 & 0.4195 & 0.5447 & -0.5124 & -0.0090 & 1.0000 \end{bmatrix} \tag{3.49}$$

Now using the method outlined ablove, the 95% confidence interval is determined for the individual elements of the matrix ϱ. From ϱ, the individual cross correlation values, ρ, are upper bounded by:

$$\varrho_{max} = \begin{bmatrix} 1.0000 & 0.0236 & -0.8077 & -0.3235 & 0.4430 & -0.2282 \\ 0.0236 & 1.0000 & 0.3543 & -0.8126 & 0.2623 & 0.4355 \\ -0.8077 & 0.3543 & 1.0000 & 0.0195 & -0.5088 & 0.5584 \\ -0.3235 & -0.8126 & 0.0195 & 1.0000 & -0.5238 & -0.4978 \\ 0.4430 & 0.2623 & -0.5088 & -0.5238 & 1.0000 & 0.0106 \\ -0.2282 & 0.4355 & 0.5584 & -0.4978 & 0.0106 & 1.0000 \end{bmatrix} \tag{3.50}$$

and lower bounded by:

$$\varrho_{min} = \begin{bmatrix} 1.0000 & -0.0156 & -0.8209 & -0.3581 & 0.4109 & -0.2650 \\ -0.0156 & 1.0000 & 0.3196 & -0.8255 & 0.2254 & 0.4032 \\ -0.8209 & 0.3196 & 1.0000 & -0.0197 & -0.5373 & 0.5308 \\ -0.3581 & -0.8255 & -0.0197 & 1.0000 & -0.5516 & -0.5267 \\ 0.4109 & 0.2254 & -0.5373 & -0.5516 & 1.0000 & -0.0286 \\ -0.2650 & 0.4032 & 0.5308 & -0.5267 & -0.0286 & 1.0000 \end{bmatrix} \tag{3.51}$$

As can be seen by these matrices, every value contained in R fits in the 95% confidence interval established by matrix ϱ. This shows that this method for generating sequences with specific cross-correlation statistics is satisfactory in the above statistical sense.

3.4.4 Array Response Vectors

When multi-element antenna arrays are used to receive signals, it is necessary to determine the array response vector $\bar{a}$ for a signal arriving from direction θ_k. This vector comprises the relative phases of the received signal at each of the antenna elements, and is important in beamforming as a means to co-phase the signals arriving from a specified direction. The process of co-phasing the signal for a given direction will tend to randomize the phases of signals arriving from other directions. The net effect of this is the amplification of desired signals and the suppression of undesired signals, known as a type of spatial filtering called beamforming. In this section we present the array response vectors for both linear and circular arrays.

3.4.4.1 Array Response Vector for a Linear Array

The relative phase of a signal at θ_k being received at the ith element of a linear array of N_A elements is given by Van Veen and Buckley in [49].

$$\bar{a} = \begin{bmatrix} 1 \\ e^{j\pi\cos(\theta_k)} \\ e^{j2\pi\cos(\theta_k)} \\ \vdots \\ e^{j(N_A-1)\pi\cos(\theta_k)} \end{bmatrix} \tag{3.52}$$

3.4.4.2 Array Response Vector for a Circular Array

The array response vector of a circular array is considerably more complicated to derive than that of the linear array. It has been derived by Earnshaw in [11]. The relative phase of a signal at θ_k being received at the ith element of a circular array is given by

$$\bar{a} = \begin{bmatrix} 1 \\ e^{-j\alpha_1} \\ e^{-j\alpha_2} \\ \vdots \\ e^{-j\alpha_{N_A-1}} \end{bmatrix} \tag{3.53}$$

where the phase delays at each antenna α_i are:

$$\alpha_i(\theta_k) = \frac{\pi\cos(\theta_k - i\frac{2\pi}{N_A})}{2\sin(\frac{\pi}{N_A})} \tag{3.54}$$

3.5 Chapter Summary

In this chapter, we presented a model given in [4], [46], and [35] for the cross-correlation factor for the envelope of a quadrature signal arriving at a pair of antennas. We then generalized the model to include any angle of arrival distribution. For illustration purposes, a comparison was made between the cross correlation statistics of a system assuming a uniform AOA distribution with a system assuming a Gaussian AOA distribution.

A method was then shown to generate signals with specific cross-correlation statistics from uncorrelated signals. This was then verified using confidence intervals from some sample data. Finally, the array response vectors for both linear and circular arrays were presented.

Chapter 4

Power and Capacity Considerations

4.1 Chapter Introduction

Beamforming is a widely studied technique for improving the signal-to-noise ratio of a received signal. Through the use of an antenna array, signals arriving from a desired direction can be isolated by multiplying the total signal received at the different antenna elements by a series of beamforming weights. These weights are chosen to co-phase the desired signal, while randomizing the signals arriving from other directions. In this chapter, new techniques for power levels and system capacity evaluation of a CDMA system using beamforming are determined both through analytical means and through computer simulation. This chapter will deal with four main topics: power prediction, uplink capacity prediction, the extension to scattering environments, and finally, the extension to other beamforming applications such as a multi-service environment.

4.1.1 Chapter Outline

The first main topic of this chapter deals with power value prediction. Analysis starts with the simple case of a single antenna element in a CDMA system. This is then extended to include the case of multiple antenna element arrays by utilising the beampattern in order to determine power levels that are influenced by interfering

mobiles. A comparison of predicted values with simulation results given in [11] is then presented.

The second topic, the capacity of the CDMA system uplink, is investigated by using the previously derived power value expressions in order to determine the threshold for the number of mobiles that the system can handle before power control starts to fail. These values are also compared with simulation results from [11].

In the third section, this analysis is extended to the case of a scattering environment. A basic calculation is made through information contained within the beampattern only, which yields an overly pessimistic view on the power levels and capacity of the system. The second method converts the effects of increased scatter into decreased cross-correlation statistics as derived in Chapter 3. These results are also compared with chip-level and power-control-level simulation results.

The final part of the chapter further presents extensions of this work. Firstly, the capacity of the system is studied in a more in-depth manner by determining the probability distribution of the interference. This analysis enables an introductory look at the multi-service case.

4.2 Power Value Calculations

The analysis in this chapter is closely related to that presented by Earnshaw in [11]. Some of the differences between [11] and our work are outlined below.

In Eqs. (3.3) and (3.4) in [11], the received power values for the in-phase and quadrature components of the k^{th} mobile when beamforming coefficients for the d^{th} mobile are used are shown for an N_A element array to be, respectively:

$$P_{I_{dk}} = \frac{1}{4}\beta_k^2 \left\{ \left[\sum_{i=1}^{N_A} \cos(\varphi_{di} - \alpha_{ki} - 2\pi f_c \tau_{kd}) \right]^2 + \left[\sum_{i=1}^{N_A} \sin(\varphi_{di} - \alpha_{ki} - 2\pi f_c \tau_{kd}) \right]^2 \right\} \quad (4.1)$$

$$P_{Q_{dk}} = \frac{1}{4}\beta_k^2 \left\{ \left[\sum_{i=1}^{N_A} \sin(\varphi_{di} - \alpha_{ki} - 2\pi f_c \tau_{kd}) \right]^2 + \left[\sum_{i=1}^{N_A} \cos(\varphi_{di} - \alpha_{ki} - 2\pi f_c \tau_{kd}) \right]^2 \right\} \quad (4.2)$$

where β_k is the received signal strength, α_{ki} is the relative phase of the i^{th} entry of mobile k's array response vector, and φ_{di} is the relative phase angle of the i^{th} entry of mobile d's beamforming weight vector. It should be noted that these quantities are equal.

In Chapter 6 of his thesis, Earnshaw simplifies (4.1) and (4.2) by defining $\Phi_{dki} \equiv \varphi_{di} - \alpha_{ki} - 2\pi f_c \tau_{kd}$. He then assumes that the Φ_{dki} values are independent random variables, and in power calculations assumes that $(\sum_{i=1}^{N_A} \sin(\Phi_{dki}))^2$ is independent of $(\sum_{i=1}^{N_A} \cos(\Phi_{dki}))^2$. These approximations are made in order to derive closed-form expressions, but adversely affect the accuracy of the analysis. In this work, we do not make these assumptions. Rather, we derive insight from the information contained within the beampattern which enables a more accurate, yet simpler, view of the problem.

4.2.1 Single Element Power Calculations

In a system where perfect power control [11] is employed and only a single antenna element is used, each mobile k in the system will contribute an amount of interference power, P_{I_k}, equivalent to the signal power P_R.

For a voice activity factor of unity, this means

$$P_I = N_I P_R \quad (4.3)$$

where $N_I = N_M - 1$ is the number of interferers.

Substituting Eqn. (4.3) into the definition for the signal-to-noise ratio (Equation (6.23) from [11]):

$$\frac{E_b}{N_0} = \frac{P_R/R_B}{P_I/B + \sigma_n^2} \tag{4.4}$$

with R_B representing the single data bit rate for all users, B the bandwidth of the spread signal and σ_n^2 the variance of the background thermal noise. Solving Eqn. (4.4)for P_R yields:

$$P_R = \left(\frac{E_b}{N_0}\right) \sigma_n^2 \left\{ \frac{1}{R_B} - \frac{N_I}{B} \left(\frac{E_b}{N_0}\right) \right\}^{-1} \tag{4.5}$$

From Eqn. (4.5), the signal power and the interference power can be predicted for one antenna element and a given target signal-to-noise ratio.

4.2.2 Multiple Antenna Element Power Calculations

Calculations for predicted power values in the multiple-antenna-element case are essentially the same as in the single-element case, except that, due to beamforming, signals coming from certain directions will be suppressed more than others. This can be illustrated by a sample beampattern. In Figure 4.1, the desired signal is arriving from the direction where the beampattern is at its peak, and signals arriving from other mobiles that are evenly positioned around the cell will be suppressed as illustrated by the beampattern.

In the multiple antenna element case, the SNR equation from (4.4) becomes:

$$\frac{E_b}{N_0} = \frac{P_R/R_B}{P_I/B + N_A\sigma_n^2} \tag{4.6}$$

where N_A is the number of antenna elements in the array, and P_R is the total received signal power at the antenna array. Note that the factor of N_A in (4.6) is due to independent noise at each array element. The interference contributed by a given mobile k is given by:

$$P_{I_k} = \phi_k P_R \tag{4.7}$$

where

$$\sum_{k=1}^{N_I} P_{I_k} = P_I \tag{4.8}$$

where ϕ_k is the fraction of interferer k's signal power passed by the beamforming weights.

The expected interference power is then given by:

$$E[P_I] = E[\phi_k] N_I P_R \tag{4.9}$$

In the same way as the single element case, this value can be substituted into Eq(4.6) in order to solve for the predicted power level. In this case the received power is:

$$E[P_R] = \left(\frac{E_b}{N_0}\right) N_A \sigma_n^2 \left\{ \frac{1}{R_B} - \frac{E[\phi_k] N_I}{B} \left(\frac{E_b}{N_0}\right) \right\}^{-1} \tag{4.10}$$

4.2.2.1 Calculation of $E[\phi_k]$

For illustration purposes, the maximum SNR beamforming weights for a desired user d at an angle of θ_d in a circular array are calculated in the following way:

$$\vec{w}(\theta_d) = \begin{bmatrix} e^{j\alpha_0} \\ e^{j\alpha_1} \\ \vdots \\ e^{j\alpha_{N_A-1}} \end{bmatrix} \tag{4.11}$$

where the phase delays at each antenna α_i were defined by Eq. (3.54) as:

$$\alpha_i(\theta_d) = \frac{\pi \cos(\theta_d - i\frac{2\pi}{N_A})}{2\sin(\frac{\pi}{N_A})} \tag{4.12}$$

This method may be extended to other array geometries as well.

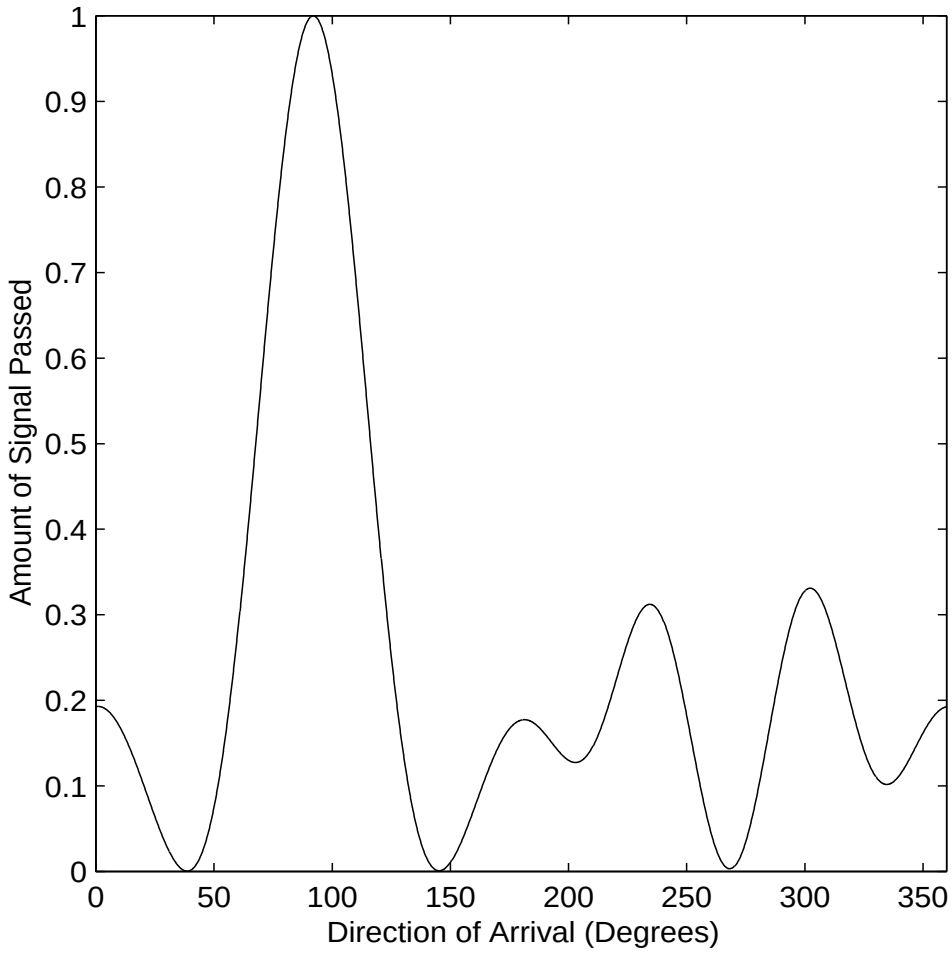

Figure 4.1: *A sample beampattern focusing on an angle-of-arrival (AOA) of 92 degrees in an array with 5 elements.*

Number of Antennas (N_A)	$E[\phi_k]$
1	1.0000
2	0.5463
3	0.3950
4	0.3241
5	0.2460
6	0.2058
7	0.1956
8	0.1682

Table 4.1: Expected values of ϕ_k

The amount of interference power seen from an interferer k at direction-of-arrival of θ_k is then:

$$\phi_k(\theta_d, \theta_k) = |\vec{w}^{\mathbf{H}}(\theta_d)\vec{a}(\theta_k)|^2 \tag{4.13}$$

where $\vec{w}^{\mathbf{H}}(\theta_d)$ denotes the complex conjugate transpose of $\vec{w}(\theta_d)$.

Assuming that both θ_d and θ_k are random variables uniformly distributed on $(0, 2\pi]$, the expected value of ϕ_k can be calculated by substituting (4.11) into (4.13) and calculating the expected value of the result. For the case of a circular array,

$$E[\phi_k(\theta_d, \theta_k)] = \frac{1}{4\pi^2 N_A} \int_0^{2\pi} \int_0^{2\pi} \left| \sum_{q=1}^{N_A} e^{j\left(\frac{\pi \cos(\theta_d - q\frac{2\pi}{N_A})}{2\sin(\frac{\pi}{N_A})} - \frac{\pi \cos(\theta_k - q\frac{2\pi}{N_A})}{2\sin(\frac{\pi}{N_A})} \right)} \right|^2 d\theta_d d\theta_k \tag{4.14}$$

Table 4.1 shows the calculated expected values for ϕ_k as a function of the number of antennas; these values were obtained by numerically integrating (4.14).

Now using the results from Table 4.1 and Eqs. (4.9) and (4.10), the mean mobile power and mean interference power can be predicted for different values of N_A. The results of these calculations are presented in Table 4.2.

# of Ants (N_A)	# of Mobs (N_M)	Mean Mobile Power	Mean Interference Power
1	20	3.8052×10^{-16}	7.2299×10^{-15}
2	30	5.1324×10^{-16}	8.1311×10^{-15}
3	30	5.3002×10^{-16}	6.0714×10^{-15}
4	30	6.1667×10^{-16}	5.7960×10^{-15}
5	30	6.7598×10^{-16}	4.8225×10^{-15}
6	30	7.6286×10^{-16}	4.5529×10^{-15}
7	30	8.7675×10^{-16}	4.9733×10^{-15}
8	30	9.6347×10^{-16}	4.6996×10^{-15}

Table 4.2: Predicted mean mobile and interference power values for $E_b/N_0 = 7dB$ using Eqn. (4.10)

4.2.3 Comparison with Simulated Values

PN-chip level simulation of the CDMA environment has been performed by Earnshaw in [11]. A comparison of simulation results with predicted values from Table 4.2 are given in Tables 4.3, 4.4, and 4.5. As can be seen from these tables, the results from simulation come much closer to matching the predictions from Eq. (4.10) than from [11]. This is likely due to the assumptions Earnshaw makes in his power calculations for the multiple element antenna array case as discussed in Section 4.2.

4.3 Capacity Calculations

4.3.1 Single Antenna Element

In calculating the maximum number of mobiles that the system can handle, we look at the expression for calculating mean mobile power Eq.(4.5).

Quantity	Observed Value via Simulation	Predicted Value Eq. (4.5)	Predicted Value in [11]
Mean mobile power	3.8041×10^{-16}	3.8052×10^{-16}	3.8052×10^{-16}
Mean interference power	7.2275×10^{-15}	7.2299×10^{-15}	7.2299×10^{-15}

Table 4.3: Comparison of Predicted and Simulated Power Values for $N_A = 1$, and 20 mobiles

Quantity	Observed Value via Simulation	Predicted Value Eq. (4.10)	Predicted Value in [11]
Mean mobile power	5.4193×10^{-16}	5.3002×10^{-16}	4.7656×10^{-16}
Mean interference power	6.3758×10^{-15}	6.0714×10^{-15}	4.6068×10^{-15}

Table 4.4: Comparison of Predicted and Simulated Power Values for $N_A = 3$, and 30 mobiles

Quantity	Observed Value via Simulation	Predicted Value Eq. (4.10)	Predicted Value in [11]
Mean mobile power	6.7858×10^{-16}	6.7598×10^{-16}	6.3219×10^{-16}
Mean interference power	4.8870×10^{-15}	4.8225×10^{-15}	3.6667×10^{-15}

Table 4.5: Comparison of Predicted and Simulated Power Values for $N_A = 5$, and 30 mobiles

$$P = \left(\frac{E_b}{N_0}\right)\sigma_n^2\left\{\frac{1}{R_B} - \frac{N_I}{B}\left(\frac{E_b}{N_0}\right)\right\}^{-1} \tag{4.15}$$

It is easy to see from this equation that as the number of users in the system increases, the power level will decrease and eventually become negative. Solving this equation for the maximum number of mobiles still yielding a positive result yields:

$$N_M = \left\lfloor \frac{B}{R_B(E_b/N_0)} \right\rfloor + 1 \tag{4.16}$$

where $\lfloor . \rfloor$ is the floor function. This expression for capacity is derived based on a single desired user with interferers and is optimistic. Information on power control and a multi-user based criterion for capacity determination is found in [11].

4.3.2 Capacity Prediction with Multiple Antenna Element Arrays

In the same way as the single element case, an estimate for the capacity of the system is found by finding the minimum number of mobiles needed to make Eq. (4.10) become negative. In the multiple antenna element case, the expression for the predicted capacity of the single cell is:

$$N_M = \left\lfloor \frac{1}{E[\phi_k]}\left(\frac{B}{R_B(E_b/N_0)}\right) \right\rfloor + 1 \tag{4.17}$$

Predicted capacities for the single and multiple element cases for the capacity of a single cell are given in Table 4.6. As can be seen from this table, as the number of antenna elements in the array increases, the number of mobiles that can be supported increases as well. These values show some discrepancy from the values predicted in [11], especially for low numbers of antenna elements, where Earnshaw's Gaussian approximations would be especially poor.

(N_A)	Capacity Eq. (4.17)	Capacity From [11]
1	26	26
2	47	37
3	65	59
4	79	82
5	104	104
6	125	128

Table 4.6: Predicted capacity values using perfect power control and correlation 1.0 between array elements.

4.3.3 Comparison with Chip-Level Simulated Values

Through PN-chip-level simulation, the capacity of the system can also be estimated by increasing the number of mobile users in the system until the BER of the received signals exceeds 10^{-3}. This method of simulation is computationally expensive, especially as the number of mobile users and the number of elements in the antenna array increase. It is for this reason that Earnshaw performed chip-level simulations for cases only up to 3 antenna elements. Table 4.7 compares the analytical prediction of capacity with the chip-level simulation results from [11]. As can be seen from this table, the agreement for the single element case is closer than that for the multiple elements case. This is due to the averaging effect of the interference power over the beampattern. For some mobile arrangements in the multiple antenna case, a greater amount of interference will be seen (due to several mobiles being clustered around the maximum of the beampattern). This will tend to degrade the capacity in the multiple antenna case as is evident from table 4.7. This effect is studied in more detail in sections 4.4.6 and 4.4.7.

(N_A)	Capacity Eq. (4.17)	Simulation Capacity From [11]
1	26	26
2	47	41
3	65	60
4	79	-
5	104	-
6	125	-

Table 4.7: Predicted and observed capacity values using perfect power control and correlation 1.0 between array elements.

4.4 Multiple Antenna Scattering Environment

In Section 3.2, an introduction was given to scatter. Typical values for angle spread, and different methods for modelling angle-of-arrival (AOA) statistics were discussed. In the remainder of this chapter, the model that is implemented for the AOA statistics is the Gaussian Angle of Arrival model, as discussed in [13]. This model assumes that the scattered signal arrives at the antenna array Gaussian distributed around a mean angle of θ_k with a variance of σ_Δ^2, where σ_Δ^2 denotes a variance equivalent to a uniform distribution over $[\theta_k - \Delta, \theta_k + \Delta]$. The AOA distribution is denoted by $P(\theta)$.

In this section, we extend the work of this chapter to the case of scattering environments. This is done in using two separate methods. The first uses the beampattern. The second method deals with increasing scatter through decreasing the envelope correlation within the antenna array. In both cases, the effects of phase delay are ignored.

4.4.1 Beampattern Method

This simple method to give an indication of possible system behaviour in the scattering environment uses the beampattern to determine the amount that the desired signal will be suppressed due to scattering. Power predictions, in the scattering case with an AOA distribution of $P(\theta)$, can be calculated much in the same way as those without scattering, except that the signal is assumed to be made up of a large number of individual paths that will all behave in the way that the signal behaved with no scatter.

So in this case the interference contributed by a mobile k is given by:

$$P_{I_k} = \phi_k P_R \tag{4.18}$$

where ϕ_k is the relative percentage of the signal power of an interferer passed by the beamforming weights. The expected interference power in this case is the same as in the previous case as each individual path will still be suppressed by its location in the beam pattern.

$$E[P_I] = E[\phi_k] N_I P \tag{4.19}$$

Again, this value can be substituted into Eqn. (4.6) in order to solve for the predicted power level. In this case, however, some of the desired signal itself will be suppressed due to the fact that not all of the signal is located at the maximum of the spatial filter corresponding to the maximum SNR beamformer. The percentage of the desired signal passed by the beam pattern for a mean angle-of-arrival θ_d is given by:

$$\phi_d = \int_0^{2\pi} P(\theta) \left| \sum_{q=1}^{N_A} e^{j\left(\frac{\pi \cos(\theta_d - q\frac{2\pi}{N_A})}{2\sin(\frac{\pi}{N_A})} - \frac{\pi \cos(\theta - q\frac{2\pi}{N_A})}{2\sin(\frac{\pi}{N_A})} \right)} \right|^2 d\theta \tag{4.20}$$

If $P(\theta)$ is assumed to be Gaussian with mean θ_d and variance equivalent to that of a uniform distribution over $[\theta_d - \Delta, \theta_d + \Delta]$ as illustrated in Figure 3.1, (4.20) becomes:

$$\phi_d = \sqrt{\frac{3}{2\pi\Delta^2}} \int_0^{2\pi} e^{-3(\theta-\theta_d)^2/\Delta^2} \left| \sum_{q=1}^{N_A} e^{j\left(\frac{\pi\cos(\theta_d - q\frac{2\pi}{N_A})}{2\sin(\frac{\pi}{N_A})} - \frac{\pi\cos(\theta - q\frac{2\pi}{N_A})}{2\sin(\frac{\pi}{N_A})} \right)} \right|^2 d\theta \quad (4.21)$$

The expected value of (4.21) can be calculated as

$$E[\phi_d] = \frac{1}{2\pi}\sqrt{\frac{3}{2\pi\Delta^2}} \int_0^{2\pi}\int_0^{2\pi} e^{-3(\theta-\theta_d)^2/\Delta^2} \left| \sum_{q=1}^{N_A} e^{j\left(\frac{\pi\cos(\theta_d - q\frac{2\pi}{N_A})}{2\sin(\frac{\pi}{N_A})} - \frac{\pi\cos(\theta - q\frac{2\pi}{N_A})}{2\sin(\frac{\pi}{N_A})} \right)} \right|^2 d\theta d\theta_d \quad (4.22)$$

Again, similar calculations as in the preceding sections can be performed numerically yielding analytically predicted values for mobile and interference powers and from the, analytical evaluations of system capacity. The equation for system capacity in this case is given by:

$$N_M = \left\lfloor \frac{1}{E[\phi_k]} \left(\frac{E[\phi_d]B}{R(E_b/N_0)} \right) \right\rfloor + 1 \quad (4.23)$$

Assuming the angle-of-arrival statistics are Gaussian-distributed about some nominal angle, θ_d, the predicted system capacities are calculated and shown shown in Figure 4.2.

4.4.2 Mobile Power Prediction Using Cross-Correlation Statistics

In Eqs.(3.3) and (3.4) in [11], the received power values for the in-phase and quadrature components of the k^{th} mobile when beamforming coefficients for the d^{th}

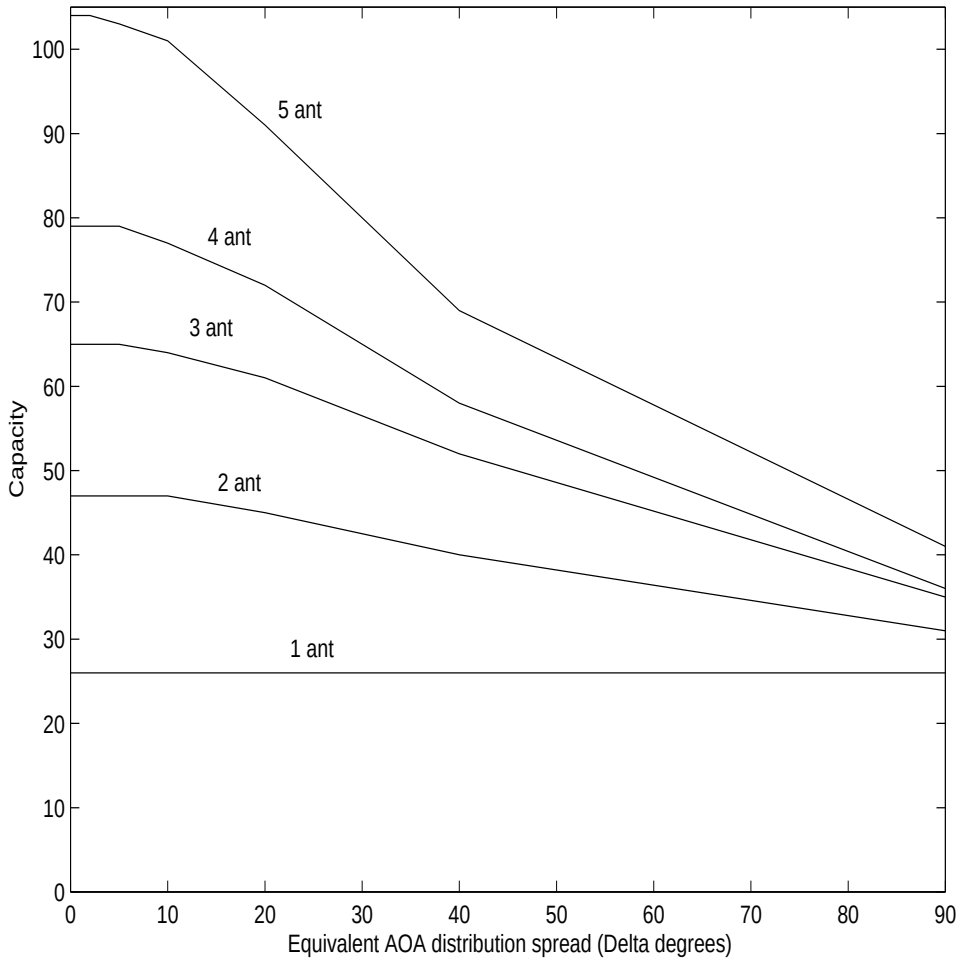

Figure 4.2: *System capacity predictions for 1-5 antennas and Gaussian-distributed angle-of-arrival (AOA) statistics. The Gaussian AOA distribution has variance equal to that of a uniform distribution over 2Δ degrees.*

mobile are used are given, respectively, by:

$$P_{I_{dk}} = \frac{1}{4}\beta_k^2 \left\{ \left[\sum_{i=1}^{N_A} \cos(\varphi_{di} - \alpha_{ki} - 2\pi f_c \tau_{kd}) \right]^2 + \left[\sum_{i=1}^{N_A} \sin(\varphi_{di} - \alpha_{ki} - 2\pi f_c \tau_{kd}) \right]^2 \right\} \quad (4.24)$$

$$P_{Q_{dk}} = \frac{1}{4}\beta_k^2 \left\{ \left[\sum_{i=1}^{N_A} \sin(\varphi_{di} - \alpha_{ki} - 2\pi f_c \tau_{kd}) \right]^2 + \left[\sum_{i=1}^{N_A} \cos(\varphi_{di} - \alpha_{ki} - 2\pi f_c \tau_{kd}) \right]^2 \right\} \quad (4.25)$$

where β_k is the received signal strength, α_{ki} is the relative phase of the i^{th} entry of mobile k's array response vector, and φ_{di} is the relative phase angle of the i^{th} entry of mobile d's beamforming weight vector. In [11], it was assumed that the signal strength of the received signal at the different antenna elements was the same. In the following, this artificial assumption is not made. Letting β_{ki} denote the signal strength due to mobile k at element i, the received power values for the in-phase and quadrature components of the k^{th} mobile when beamforming coefficients for the d^{th} mobile are used are generalized from Eqs. (4.24) and (4.25) to:

$$P_{I_{dk}} = \frac{1}{4} \left\{ \left[\sum_{i=1}^{N_A} \beta_{ki} \cos(\varphi_{di} - \alpha_{ki} - 2\pi f_c \tau_{kd}) \right]^2 + \left[\sum_{i=1}^{N_A} \beta_{ki} \sin(\varphi_{di} - \alpha_{ki} - 2\pi f_c \tau_{kd}) \right]^2 \right\} \quad (4.26)$$

$$P_{Q_{dk}} = \frac{1}{4} \left\{ \left[\sum_{i=1}^{N_A} \beta_{ki} \sin(\varphi_{di} - \alpha_{ki} - 2\pi f_c \tau_{kd}) \right]^2 + \left[\sum_{i=1}^{N_A} \beta_{ki} \cos(\varphi_{di} - \alpha_{ki} - 2\pi f_c \tau_{kd}) \right]^2 \right\} \quad (4.27)$$

For notational simplicity, the following term may be defined:

$$\gamma_{idk} \equiv \varphi_{di} - \alpha_{ki} - 2\pi f_c \tau_{kd} \quad (4.28)$$

Then the total received power by substituting (4.28) into (4.26) and (4.27) is:

$$\begin{aligned} P_{dk} &= P_{I_{dk}} + P_{Q_{dk}} \\ &= \frac{1}{2}\left\{\left[\sum_{i=1}^{N_A}\beta_{ki}\cos(\gamma_{idk})\right]^2 + \left[\sum_{i=1}^{N_A}\beta_{ki}\sin(\gamma_{idk})\right]^2\right\} \end{aligned} \tag{4.29}$$

Without loss of generality, we simplify the notation and define the reference mobile corresponding to $d = 1$. In the following, if $k = 1$, reference is made to the desired signal, otherwise it refers to the interferer k, where $k \neq 1$. This notation modifies (4.28) to

$$\gamma_{ik} = \varphi_i - \alpha_{ki} - 2\pi f_c \tau_k \tag{4.30}$$

By expanding (4.29), the interference power due to mobile k, P_k, becomes:

$$\begin{aligned} P_k &= \frac{1}{2}\{[\beta_{k1}\beta_{k1}\cos^2(\gamma_{1k}) + \beta_{k1}\beta_{k2}\cos(\gamma_{1k})\cos(\gamma_{2k}) \\ &+ \beta_{k1}\beta_{k3}\cos(\gamma_{1k})\cos(\gamma_{3k}) + ... + \beta_{kN_A}\beta_{kN_A}\cos^2(\gamma_{N_Ak})] \\ &+ [\beta_{k1}\beta_{k1}\sin^2(\gamma_{1k}) + \beta_{k1}\beta_{k2}\sin(\gamma_{1k})\sin(\gamma_{2k}) \\ &+ \beta_{k1}\beta_{k3}\sin(\gamma_{1k})\sin(\gamma_{3k}) + ... + \beta_{kN_A}\beta_{kN_A}\sin^2(\gamma_{N_Ak})]\} \end{aligned} \tag{4.31}$$

Using the identity $\cos(A)\cos(B) + \sin(A)\sin(B) = \cos(A - B)$, (4.31) simplifies to

$$P_k = \frac{1}{2}\sum_{i=1}^{N_A}\sum_{j=1}^{N_A}\beta_{ki}\beta_{kj}\cos(\gamma_{ik} - \gamma_{jk}) \tag{4.32}$$

Note that in this equation $\cos(\gamma_{ik} - \gamma_{jk}) = 1$ for $i = j$ regardless of whether k is the reference mobile.

Equation (4.32) can now be used to aid in the calculation of both the mobile and interference power. In calculating reference mobile power, ($k = 1$), we substitute (4.30) into (4.32)

$$P_k = \frac{1}{2}\sum_{i=1}^{N_A}\sum_{j=1}^{N_A}\beta_{ki}\beta_{kj}\cos((\varphi_i - \alpha_{ki} - 2\pi f_c\tau_k) - (\varphi_j - \alpha_{kj} - 2\pi f_c\tau_k)) \quad (4.33)$$

$$= \frac{1}{2}\sum_{i=1}^{N_A}\sum_{j=1}^{N_A}\beta_{ki}\beta_{kj}\cos((\varphi_i - \alpha_{ki}) - (\varphi_j - \alpha_{kj})) \quad (4.34)$$

Using maximum SNR beamforming [49] for the reference mobile ($k = 1$), the relative phase of the i^{th} element of the array response vector, α_{1i}, will equal the relative phase of the i^{th} beamforming weight, φ_i. Therefore, $\cos((\varphi_i - \alpha_{1i}) - (\varphi_j - \alpha_{1j})) = \cos(0) = 1$, and (4.34) becomes

$$P_1 = \frac{1}{2}\sum_{i=1}^{N_A}\sum_{j=1}^{N_A}\beta_{1i}\beta_{1j} \quad (4.35)$$

The mean power is then

$$E[P_1] = \frac{1}{2}\sum_{i=1}^{N_A}\sum_{j=1}^{N_A}E[\beta_{1i}\beta_{1j}] \quad (4.36)$$

where β_{1i} is the signal strength received at element i, which is proportional to the Rayleigh fading random variables for mobile 1 at element i, R_{1i} . We write $\beta_{1i} = \eta_1 R_{1i}$, where η_1 models other effects such as path loss and shadowing, which are assumed to be independent of the Rayleigh fading and equal across the antenna array. Eqn. (4.37) becomes

$$E[P_1] = \frac{1}{2}\sum_{i=1}^{N_A}\sum_{j=1}^{N_A}E[\eta_1 R_{1i}\eta_1 R_{1j}]$$

$$= \frac{1}{2}E[\eta_1^2]\sum_{i=1}^{N_A}\sum_{j=1}^{N_A}E[R_{1i}R_{1j}] \quad (4.37)$$

where R_{1i} and R_{1j} are both Rayleigh-distributed random variables that are each a function of two Gaussian distributed random variables. The second-order statistics among these four Gaussian distributed random variables are given by the cross-correlation matrix between antenna elements i and j, $\mathcal{R}_{ij}$

$$\mathcal{R}_{ij} = \begin{bmatrix} \rho_{RiRi} & \rho_{RiIi} & \rho_{RiRj} & \rho_{RiIj} \\ \rho_{IiRi} & \rho_{IiIi} & \rho_{IiRj} & \rho_{IiIj} \\ \rho_{RjRi} & \rho_{RjIi} & \rho_{RjRj} & \rho_{RjIj} \\ \rho_{IjRi} & \rho_{IjIi} & \rho_{IjRj} & \rho_{IjIj} \end{bmatrix} \tag{4.38}$$

This can be simplified to

$$\mathcal{R}_{ij} = \begin{bmatrix} 1 & 0 & \rho_{RiRj} & \rho_{RiIj} \\ 0 & 1 & -\rho_{RiIj} & \rho_{RiRj} \\ \rho_{RiRj} & -\rho_{RiIj} & 1 & 0 \\ \rho_{RiIj} & \rho_{RiRj} & 0 & 1 \end{bmatrix} \tag{4.39}$$

where ρ_{RiRj} is defined as the cross-correlation factor between the real component of the Rayleigh fading value at antenna i with the real component of the Rayleigh value at antenna j, and ρ_{RiIj} is defined as the cross-correlation factor between the real component of the Rayleigh fading at antenna i with the imaginary component of the Rayleigh fading at antenna j. The quantities ρ_{RiRj} and ρ_{RiIj} are calculated based on the cross-correlation model derived in Section 3.3. In this case, $E[R_{ki}R_{kj}]$, the cross-correlation between the Rayleigh distributed random variables at antennas i and j due to mobile k, is given in terms of the confluent hypergeometric function ${}_2F_1(-\frac{1}{2}, -\frac{1}{2}; 1; .)$ as shown by Davenport and Root in [9]

$$E[R_{ki}R_{kj}] = \frac{\pi}{2}({}_2F_1(-\frac{1}{2}, -\frac{1}{2}; 1; \zeta_{ji}^2)) \tag{4.40}$$

with $\zeta_{ji}^2 = \rho_{RiRj}^2 + \rho_{RiIj}^2$. In the case of maximum correlation between antenna elements, $E[R_{ki}R_{kj}] = 2$. As the inter-element correlation decreases, $E[R_{ki}R_{kj}]$ will also decrease to a minimum of $\frac{\pi}{2}$. In the channel model for the case of no scattering, if the angle-of-arrival distribution has zero variance, then all of the Rayleigh cross-correlation values will equal 2. On the other hand, for the case of scattering, the AOA statistics are more spread out, and values in the cross-correlation matrix off the main diagonal will decrease as the AOA distribution variance, σ_Δ^2 increases. σ_Δ^2 is equal to the variance of a uniformly distributed random variable over $\pm\Delta^o$.

4.4.2.1 Mobile Power Effect due to Cross-Correlation

We denote the quantity μ_M to represent the net effect of correlation loss induced by angle-of-arrival distribution spread. This value can be used as a factor in determining the mean mobile power. In the SNR equation (4.6), P_R can be replaced by $\mu_M P_R$. Without loss of generality, we consider mobile 1. We define μ_M as

$$\mu_M \equiv \frac{E[P_1|\text{AOA dist variance} = \sigma_\Delta^2]}{E[P_1|\text{AOA dist variance} = 0]} \tag{4.41}$$

From (4.37), (4.41) can be written as

$$\mu_M = \frac{\frac{1}{2}\eta_1^2 \sum_{i=1}^{N_A} \sum_{j=1}^{N_A} E[R_{1i}R_{1j}|\text{AOA dist variance} = \sigma_\Delta^2]}{\frac{1}{2}\eta_1^2 \sum_{i=1}^{N_A} \sum_{j=1}^{N_A} E[R_{1i}R_{1j}|\text{AOA dist variance} = 0]} \tag{4.42}$$

Evaluating the confluent hypergeometric function as discussed in the previous section, (4.42) can be simplified to:

$$\mu_M = \frac{\sum_{i=1}^{N_A} \sum_{j=1}^{N_A} E[R_{ki}R_{kj}|\text{AOA dist variance} = \sigma_\Delta^2]}{2N_A^2} \tag{4.43}$$

Values of μ_M can be calculated using the hypergeometric function and $E[\mu_M]$ calculated by averaging μ_M over all directions-of-arrival, and are presented in Table 4.8. In this table, AOA distribution Δ indicates a Gaussian angle-of-arrival distribution with variance equivalent to a uniform distribution of $\pm\Delta$ degrees. As expected, the cross-correlation effects are more pronounced as the AOA distribution variance increases, and as the number of antenna elements increases (increasing the percentage of elements in the cross-correlation matrix affected by cross-correlation, and increasing the diameter of the circular array).

4.4.2.2 Interference Power Effect Due to Cross-Correlation

Calculations for the effect on an interferer's power due to the amplitude cross-correlation effects are similar to the calculations of the cross-correlation effect on the

AOA Distribution Δ	$N_A = 2$	$N_A = 3$	$N_A = 4$	$N_A = 5$
0	1.0000	1.0000	1.0000	1.0000
2	0.9998	0.9997	0.9995	0.9993
5	0.9985	0.9980	0.9970	0.9956
10	0.9942	0.9922	0.9886	0.9840
20	0.9799	0.9733	0.9628	0.9510
40	0.9475	0.9300	0.9119	0.8965
90	0.9108	0.8811	0.8650	0.8525
180	0.9024	0.8699	0.8545	0.8385

Table 4.8: Mobile power suppression factors $E[\mu_M]$ due to cross-correlation statistics

mobile power. Define μ_{I_k} to be the effect on an interferer's power due to beamforming as well as cross-correlation effects. By determining μ_{I_k}, interference power P_I in the SNR equation (4.6) can be replaced by $\mu_{I_k} P_R N_I$ in order to solve for the mobile and interference power. μ_{I_k} is defined as

$$\mu_{I_k} \equiv \frac{E[P_{I_k} | \text{AOA dist variance} = \sigma_\Delta^2]}{E[P_1 | \text{AOA dist variance} = 0]} \tag{4.44}$$

Using equations (4.32) and (4.37), (4.44) can be rewritten as:

$$\mu_{I_k} = \frac{\frac{1}{2}E[\eta_k^2] \sum_{i=1}^{N_A} \sum_{j=1}^{N_A} E[R_{ki} R_{kj} \cos(\gamma_{ik} - \gamma_{jk}) | \text{AOA dist variance} = \sigma_\Delta^2]}{\frac{1}{2}E[\eta_1^2] \sum_{i=1}^{N_A} \sum_{j=1}^{N_A} E[R_{1i} R_{1j} | \text{AOA dist variance} = 0]} \tag{4.45}$$

But $E[R_{1i} R_{1j}] = 2$ for all i, j in the case of AOA distribution variance = 0. Also, it is assumed that due to perfect power control, $\mathrm{E}[\eta_1^2] = E[\eta_k^2]$, and (4.45) simplifies to

$$\mu_{I_k} = \frac{\sum_{i=1}^{N_A} \sum_{j=1}^{N_A} E[R_{ki} R_{kj} \cos(\gamma_{ik} - \gamma_{jk}) | \text{AOA dist variance} = \sigma_\Delta^2]}{2N_A^2} \tag{4.46}$$

It is assumed that the fading information (R_{ki},R_{kj}) is independent of the angles γ_{ik} and γ_{jk}. With this assumption, (4.46) factors to

$$\mu_{I_k} = \frac{\sum_{i=1}^{N_A}\sum_{j=1}^{N_A} E[R_{ki}R_{kj}|\text{AOA dist variance} = \sigma_\Delta^2]\cos(\gamma_{ik}-\gamma_{jk})}{2N_A^2} \tag{4.47}$$

In Section 4.2.2.1 a similar expression was calculated for beamforming by ignoring the cross-correlation effects and analysing the beampattern. The amount that an interferer k was suppressed was defined as ϕ_k, and this corresponded the amount of signal passed by the spatial filter. The analysis in Section 4.2.2.1 is equivalent to the case of perfect correlation at the antenna elements (AOA distribution variance = 0). For perfect correlation, $E[R_{ki}R_{kj}] = 2$ regardless of the antenna pair i and j, and

$$\mu_{I_k} = \phi_k = \frac{1}{2N_A^2}\sum_{i=1}^{N_A}\sum_{j=1}^{N_A} 2\cos(\gamma_{ik}-\gamma_{jk}) \tag{4.48}$$

or

$$\sum_{i=1}^{N_A}\sum_{j=1}^{N_A}\cos(\gamma_{ik}-\gamma_{jk}) = \phi_k N_A^2 \tag{4.49}$$

By removing all values in the summation for which $i = j$ and hence $\cos(\gamma_{ik}-\gamma_{jk}) = 1$, (4.49) becomes:

$$\sum_{i=1}^{N_A}\sum_{j=1,j\neq i}^{N_A}\cos(\gamma_{ik}-\gamma_{jk}) = \phi_k N_A^2 - N_A \tag{4.50}$$

This result will now be used to analyse cross-correlation degradation. By removing the terms in (4.47) for which $i = j$ and hence $\cos(\gamma_{ik}-\gamma_{jk}) = 1$, (4.47) becomes

$$\mu_{I_k} = \frac{1}{2N_A^2}\left(2N_A + \sum_{i=1}^{N_A}\sum_{j=1,j\neq i}^{N_A} E[R_{ki}R_{kj}|\text{AOA dist variance} = \sigma_\Delta^2]\cos(\gamma_{ik}-\gamma_{jk})\right) \tag{4.51}$$

The $E[R_{ki}R_{kj}]$ terms for which $i \neq j$ can be calculated using the confluent hypergeometric function for a given direction-of-arrival and AOA distribution variance σ_Δ^2. From the properties of the hypergeometric function, $\frac{\pi}{2} \leq E[R_{ki}R_{kj}] \leq 2$. Letting ϵ_k represent the average off-diagonal cross-correlation value, (4.51) can be approximated by:

$$\mu_{I_k} \approx \frac{1}{2N_A^2}\left(2N_A + \sum_{i=1}^{N_A}\sum_{j=1,j\neq i}^{N_A} \epsilon_k \cos(\gamma_{ik} - \gamma_{jk})\right) \tag{4.52}$$

$$= \frac{1}{2N_A^2}\left(2N_A + \epsilon_k \sum_{i=1}^{N_A}\sum_{j=1,j\neq i}^{N_A} \cos(\gamma_{ik} - \gamma_{jk})\right) \tag{4.53}$$

Substituting the result from (4.50), this becomes

$$\mu_{I_k} \approx \frac{1}{2N_A^2}\left(2N_A + \epsilon_k(\phi_k N_A^2 - N_A)\right) \tag{4.54}$$

Averaging this result over all directions-of-arrival

$$E[\mu_{I_k}] \approx \frac{1}{2N_A^2}\left(2N_A + E[\epsilon_k](E[\phi_k]N_A^2 - N_A)\right) \tag{4.55}$$

$$= \frac{1}{N_A} + \frac{E[\epsilon_k]E[\phi_k]}{2} - \frac{E[\epsilon_k]}{2N_A} \tag{4.56}$$

The interference suppression factors due to cross-correlation statistics and beamforming effects are calculated numerically, and are given in Table 4.9. As in the table of μ_M values, the values decrease as the number of antennas increases, and as the AOA distribution variance increases.

The two methods outlined in this section for determining the amount of suppression due to scatter yielded drastically different results. The first method, using information from the beampattern exclusively, showed a drastic decrease in the signal power as the angle spread increased. A more in-depth method, using the cross correlation information caused by the scatter seems to indicate that the effects on power due to scatter, may, in fact, be quite small, suggesting that beamforming will still provide significant capacity benefits, even in high scatter environments.

AOA Distribution Δ	$N_A = 2$	$N_A = 3$	$N_A = 4$	$N_A = 5$
0	0.5463	0.3950	0.3241	0.2460
2	0.5463	0.3950	0.3241	0.2460
5	0.5462	0.3948	0.3238	0.2457
10	0.5458	0.3943	0.3230	0.2451
20	0.5444	0.3925	0.3204	0.2432
40	0.5414	0.3885	0.3154	0.2400
90	0.5380	0.3840	0.3108	0.2375
180	0.5373	0.3830	0.3097	0.2367

Table 4.9: Interference suppression factors μ_{I_k} due to cross-correlation statistics and beamforming

4.4.3 Power and Capacity Prediction

Once again, the same calculations as in the preceding sections can be performed numerically yielding predicted values for mobile and interference power as well as predictions for system capacity. Repeating the multiple antenna expression for SNR (4.6) here:

$$\frac{E_b}{N_0} = \frac{P_R/R_B}{P_I/B + N_A\sigma_n^2} \tag{4.57}$$

As mentioned in the previous sections, if P_R is replaced by $E[\mu_M]P_R$, and P_I replaced by $E[\mu_{I_k}]P_R N_I$, (4.57) becomes:

$$\frac{E_b}{N_0} = \frac{E[\mu_M]P_R/R_B}{E[\mu_{I_k}]P_1 N_I/B + N_A\sigma_n^2} \tag{4.58}$$

Solving this for P_R yields:

$$P_R = \left(\frac{E_b}{N_0}\right) N_A \sigma_n^2 \left\{ \frac{E[\mu_M]}{R_B} - \frac{E[\mu_I] N_I}{B} \left(\frac{E_b}{N_0}\right) \right\}^{-1} \tag{4.59}$$

The equation for system capacity, i.e. the maximum value of $N_M = N_I + 1$ that will still yield a positive result in (4.59), is given by:

$$N_M = \left\lfloor \left(\frac{E[\mu_M] B}{E[\mu_I] R_B (E_b/N_0)}\right) \right\rfloor + 1 \tag{4.60}$$

Assuming the angle-of-arrival statistics are Gaussian-distributed about some nominal angle, θ_k, the system capacities can be predicted and are shown in Figure 4.3.

The previous sections have all assumed mobiles that are distributed uniformly in a cell. In the following sections we extend this to include the possibility of nonuniformly distributed mobiles in the cell. This will also enable the analysis of a multi-service system.

4.4.4 Simulation Methodology

For additional verification, a detailed system simulation has been performed taking into account inter-element cross-correlation statistics. A version of the simulator developed by Earnshaw in [11] was obtained and modified to allow inclusion of inter-element cross-correlation statistics within the antenna array. Salz and Winters have considered inter-element statistical correlation for the case of uniformly distributed scatterers [45]. A modified relationship for a Gaussian scatter distribution was derived in Chapter 3, and is given by

$$\rho_{RiRj} = J_0\left(\frac{2\pi d}{\lambda}\right) + 2 \sum_{m=1}^{\infty} J_{2m}\left(\frac{2\pi d}{\lambda}\right) \cos 2m\theta_k e^{-2m^2\sigma_\Delta^2} \tag{4.61}$$

and

$$\rho_{RiIj} = 2 \sum_{m=0}^{\infty} J_{2m+1}\left(\frac{2\pi d}{\lambda}\right) \sin((2m+1)\theta_k) e^{\frac{-(2m+1)^2\sigma_\Delta^2}{2}} \tag{4.62}$$

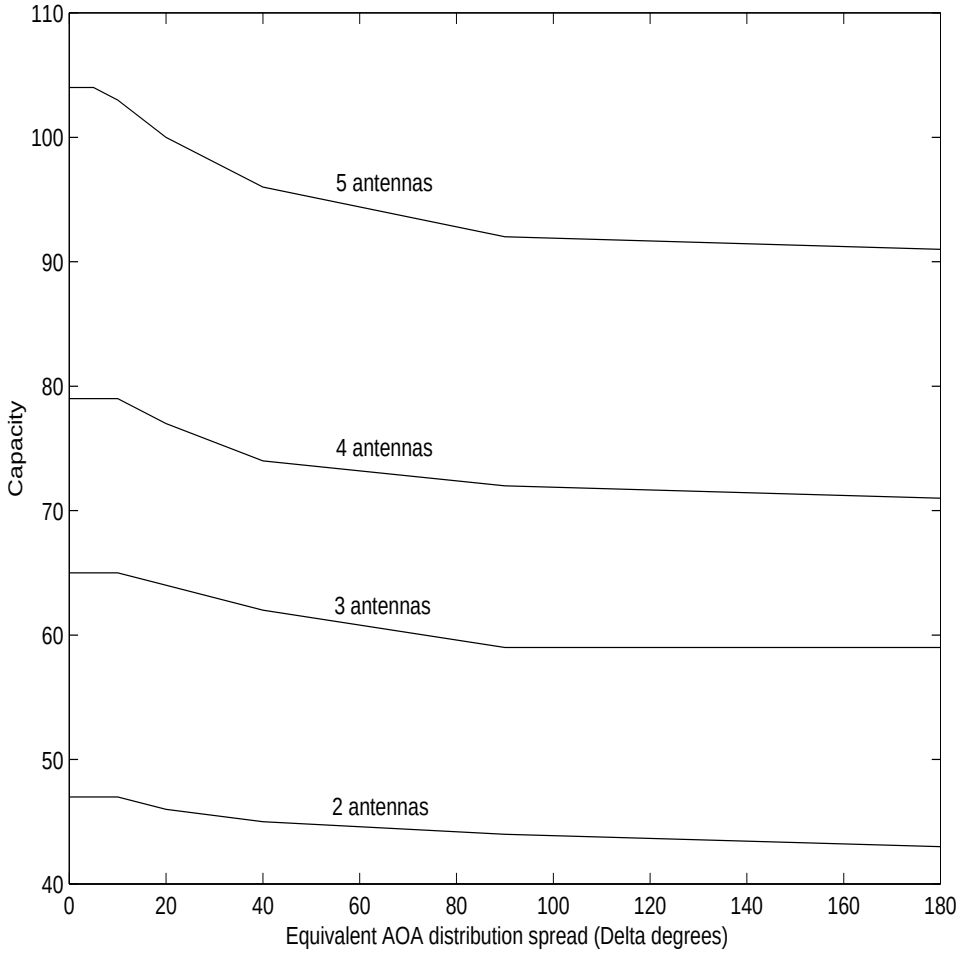

Figure 4.3: *System capacity predictions for 2-5 antennas and cross-correlation statistics of a Gaussian AOA distribution with variance equal to a uniform distribution over* 2Δ *degrees.*

where θ is the mean angle-of-arrival, σ_Δ^2 is the variance of the Gaussian angle-of-arrival distribution, and ρ_{RiRj} refers to the correlation coefficient between the real component of the Rayleigh fading at antenna i and the real component of the Rayleigh fading at antenna j.

4.4.5 Simulation Results - Power

An important aspect of confirming analytical calculations for system power and capacity is the confirmation of the results through computer simulation. Using perfect power control, chip-level simulations were run to examine the effect of inter-element statistical correlation on mean mobile power and interference power. The results for 3 and 5 element antenna arrays are shown in Figure 4.4.

From Figure 4.4, a general trend of degradation of signal to interference (SIR) power ration is observed as the variance, σ_Δ^2, of the angle-of-arrival distribution is increased. However, this decrease in SIR is negligible for low σ_Δ^2 and is quite small even for high σ_Δ^2. This suggests that even though there is lowered inter-element correlation the, users' array responses remain fairly distinct.

4.4.6 Simulation Results - Capacity

There are several ways of testing the capacity of the system through simulation. A direct approach is to perform a PN-chip-level simulation, and continue to add mobiles until the BER of the system drops below some accepable level such as 10^{-3}. This method is computationally very expensive, especially for large numbers of mobiles and large antenna elements. In order to make these simulations more computationally efficient, capacity was determined through power-control-level simulation instead [11]. In this approach, power levels are periodically determined such that the signal-to-noise ratio for each mobile is kept fixed at 7dB. As the number of mobiles increases, however, there comes a point where the solution to the power control problem starts to break down. The point where valid solutions to the power control system of equations cannot be found is taken to be the capacity of the system. Examples of the

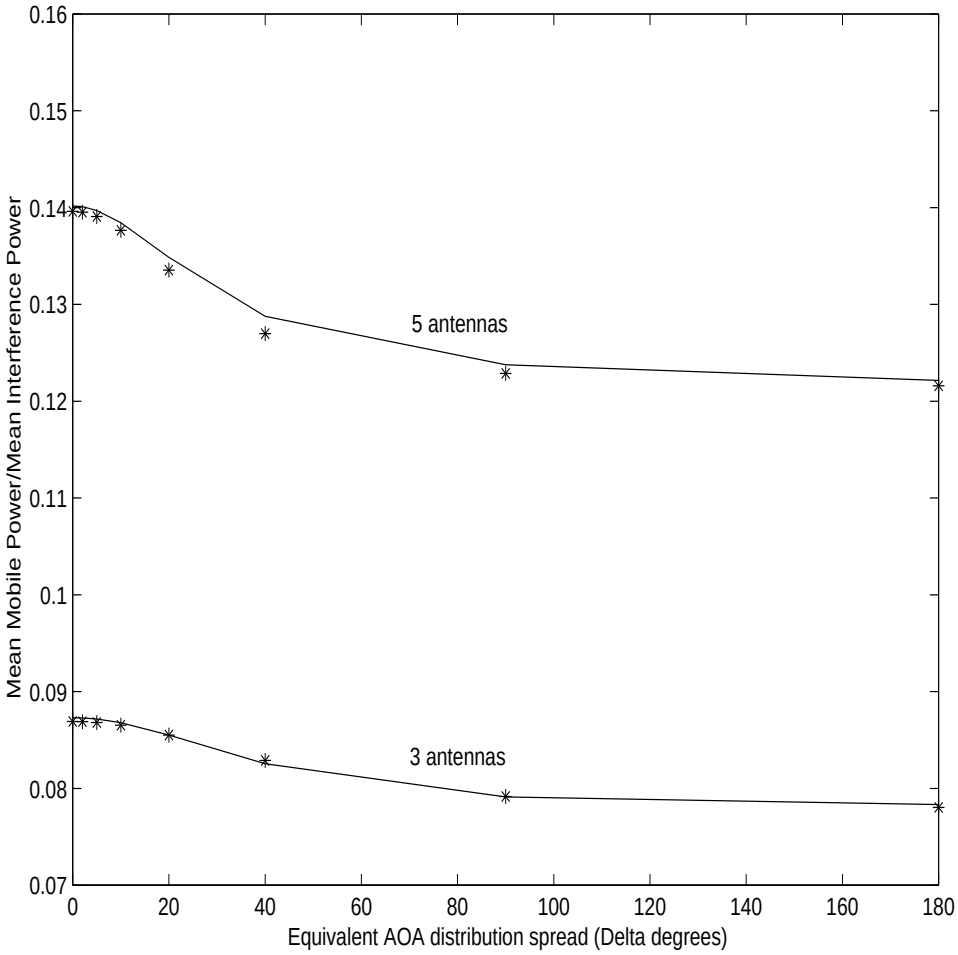

Figure 4.4: *Signal power to interference power ratio obtained by chip-level cell simulations with 3 and 5 antennas and Gaussian distributed angle-of-arrival statistics (stars). Compared with calculated values (lines). Gaussian AOA distribution with variance equal to a uniform distribution over 2Δ degrees.*

SNR curves for 3 antenna elements and angle-of-arrival distribution with equivalent variance to uniform distributions over $\pm 2^o$ and over $\pm 90^0$ are plotted in Figure 4.5. Due to computer processing resource limitations, it was only feasible to run these simulations for 3 antenna elements, and even then not for enough trials to produce smooth SNR curves.

These curves were generated using the power control method of simulation. Similar curves were also obtained for AOA distributions with variance equivalents to $\pm\Delta$ where $\Delta = 0, 2, 5, 10, 20, 40, 90$, and 180 degrees. It is difficult to obtain a specific capacity value for the point when power control starts to break down. If the maximum point on the SNR curve is taken as the breakdown point, then the capacity of the system is given in Table 4.10. As can be seen in this table, the performace degrades as the AOA distribution variance increases, but no significant degredation is seen with small AOA distribution variance. It is also noted that the predicted capacity value from Eq. (4.60) is consistently higher than the values obtained through simulation. This is caused by a built-in assumption in the predicted value that the mobiles are uniformly distributed about the cell. In the simulation, the location of each mobile is generated randomly, allowing cases where mobiles are clustered. These cases account for a decrease in the overall capacity. The effects on non-uniform placement of mobiles is studied in the next section.

4.4.7 Capacity Prediction - Non-Uniform Placement of Mobiles

In this section the interference power distribution is calculated and used to determine the proportion of interference power that will be seen by a mobile. In the previous sections, it was assumed that the mobiles were uniformly distributed about the cell, thus ignoring situations where large numbers of mobiles may be clustered in one area increasing their mutual interference.

Recall in Fig. 4.1 that a sample beampattern was shown for a 5-antenna-element circular array. As can be seen from this example, there is a small probability that a

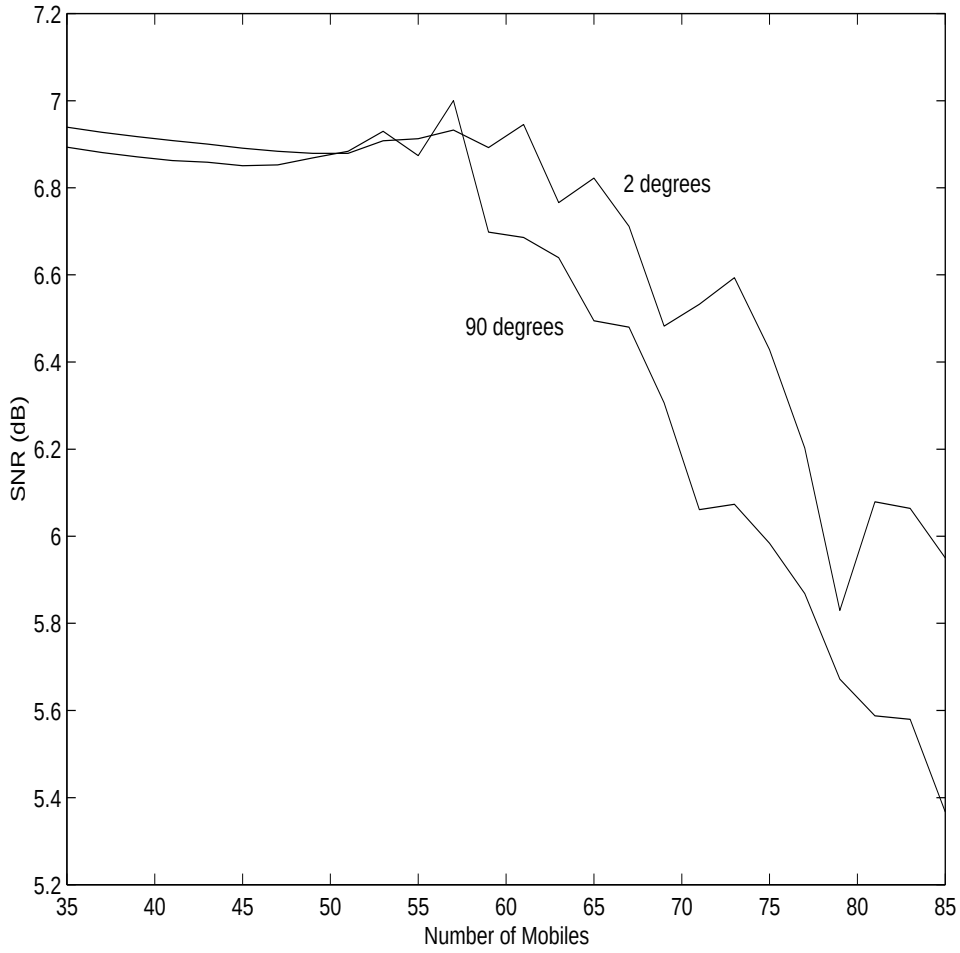

Figure 4.5: *The power-control method of capacity evaluation is used. Depicted are SNR curves for 3 antenna elements and Gaussian AOA distribution with variance equal to a uniform distribution over (-2,2) and (-90, 90) degrees.*

Δ	Predicted Value Eq. (4.60)	Simulation
0	65	61
2	65	61
5	65	61
10	65	61
20	64	61
40	62	59
90	59	57
180	59	53

Table 4.10: Comparison of predicted capacity values (from Figure 4.5) with values observed through simulation

randomly placed interferer will have 90-100% of its power passed by the spatial filter (i.e. the direction of arrival is approximately 92^o), a moderately small probability that 35-90% of the interferer's power is passed by the spatial filter, and a relatively high probability that 0-35% of the interferer's power is passed. In other words, the information contained within the beampattern can therefore be used to determine a probability density function for the percentage of an interferer's power that will be passed by the spatial filter defined by the beamforming weights. The probability density function corresponding to the beampattern given in Fig. 4.1 is shown in Fig. 4.6

As more mobiles are added to the system, the overall interference affecting each user will increase. Using the probability density function (Fig. 4.6) for a single interferer, the density function of the total interference can be determined numerically through repeated convolution. Fig. 4.7 shows the overall probability distribution of the total interference with a 5-element antenna array and 56,64,72,80, and 88

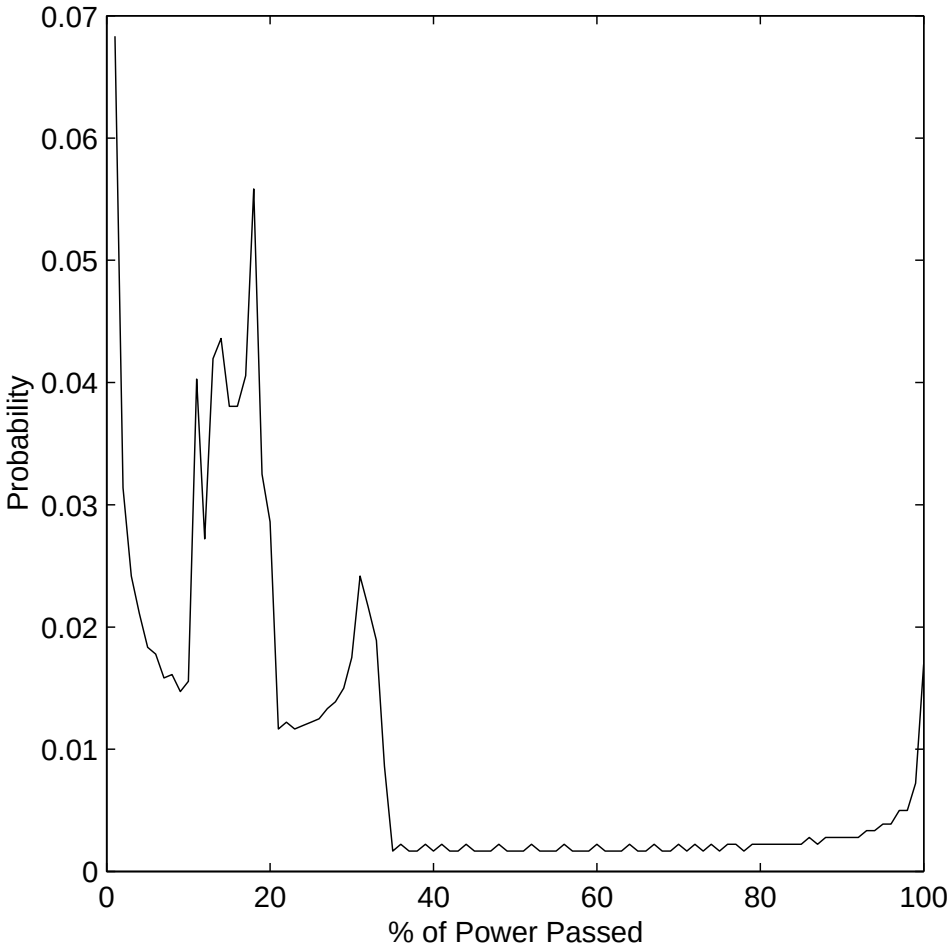

Figure 4.6: *An example probability density function for the percentage of an interferer's power passed by the spatial filter.*

interferers.

4.4.7.1 Capacity Revisited

Reexamining the expression for the Signal to Noise Ratio (SNR) in the multiple antenna case (Eq. (4.6))

$$\frac{E_b}{N_0} = \frac{P_R/R_B}{P_I/B + N_A\sigma_n^2} \tag{4.63}$$

with a large number of interferers, under the condition that the interference is much greater than the effects due to thermal noise, and from Eq. (4.63) we obtain

$$\frac{P_R/R_B}{P_I/B} \approx \frac{E_b}{N_0} \tag{4.64}$$

For an SNR of 7.0 dB, $R_B = 9600Hz$, and $B = 128 \times 9600Hz$, for each user, we require the total interference power P_I over the total received signal power P_R to be

$$\frac{P_I}{P_R} \leq 25.5 \tag{4.65}$$

As can be seen in Fig. 4.7, for 5 antennas and a direction-of-arrival of 92 degrees, this expression holds for almost all cases for 56-72 mobiles, but starts to break down in some cases with 80-88 mobiles.

4.4.7.2 Capacity Sensitivity to DOA

The probability density function in Fig. (4.6) corresponds to a single beampattern, which in turn correspnds to a single direction-of-arrival for a given number of antennas. As the direction-of-arrival changes, so does the probability density function for the interference. This variation due to direction-of-arrival will decrease as the number of antennas tends to infinity removing the directionality of the circular array.

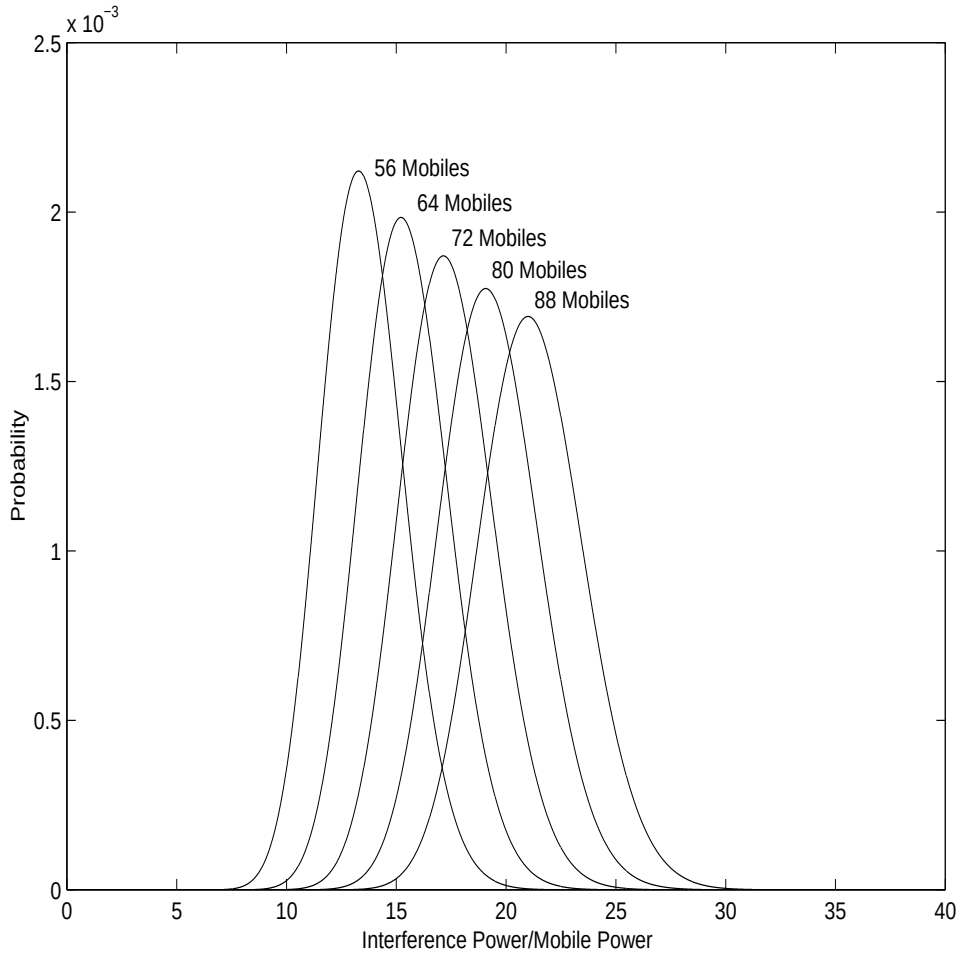

Figure 4.7: *Interference distribution for 56-88 interferers. Power control will break down in cases where the total interference power exceeds 25.5 times the received signal power,* P_R.

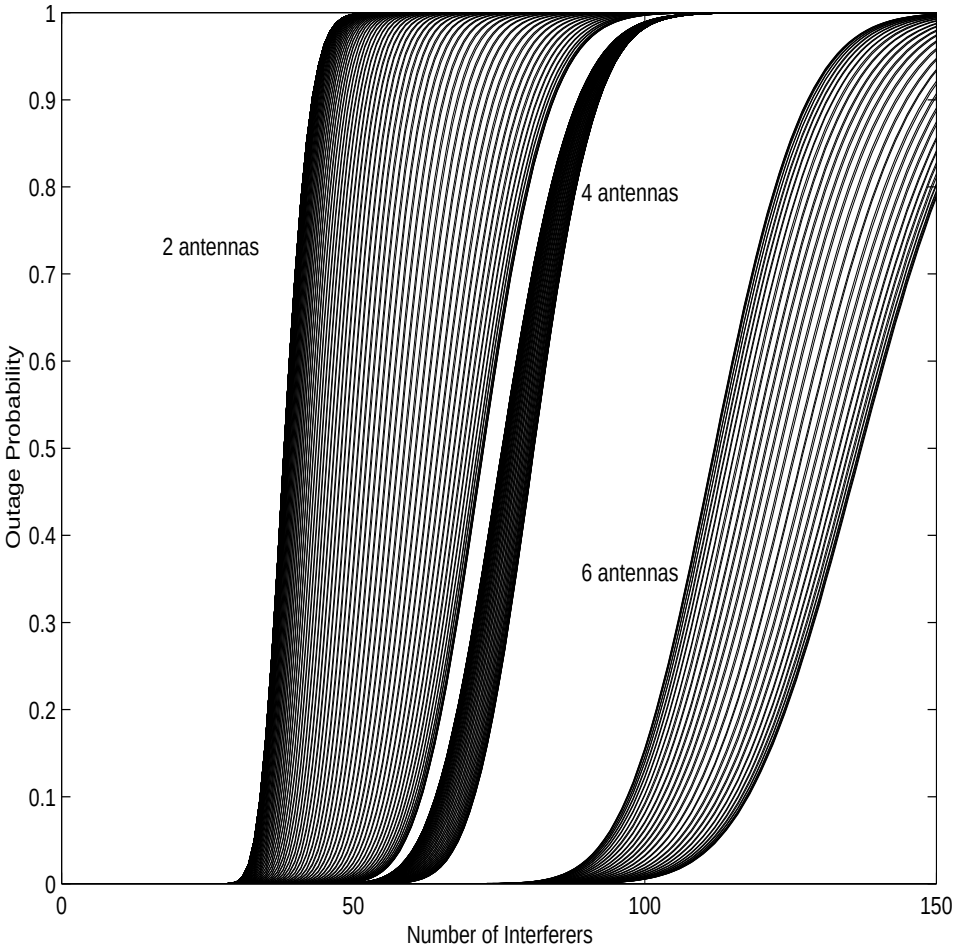

Figure 4.8: *Outage probabilities for increasing interferers and 2,4, and 6 antenna elements. Each curve represents a different DOA in increments of* 1^o.

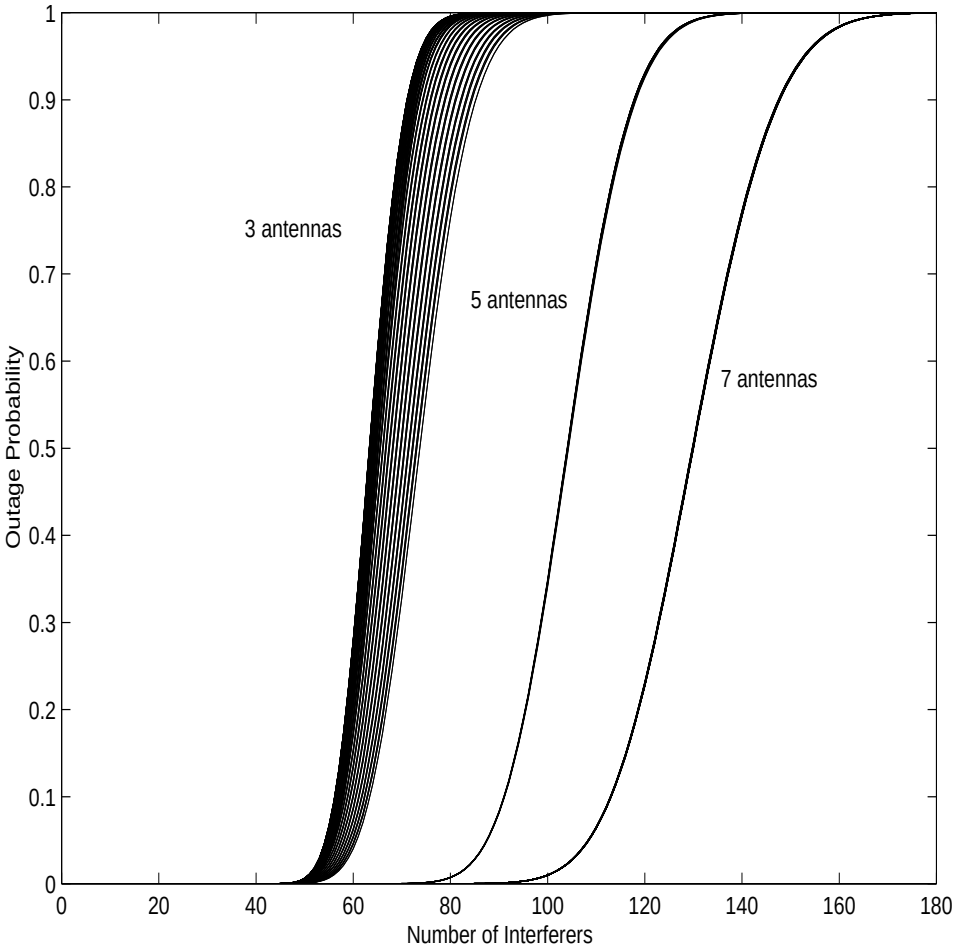

Figure 4.9: *Outage probabilities for increasing interferers and 3,5, and 7 antenna elements. Each curve represents a different DOA in increments of* 1^o.

Outage Probability	0.0001	0.001	0.01	0.05	0.1	0.25	0.5
1 Antenna	26	26	26	26	26	26	26
2 Antennas	30	31	33	35	36	37	40
3 Antennas	46	49	52	56	58	61	65
4 Antennas	49	52	57	63	66	71	77
5 Antennas	70	75	82	88	91	98	104
6 Antennas	74	80	87	94	99	105	113
7 Antennas	87	93	101	110	114	122	131

Table 4.11: Worst-case capacity over all DOA's as a function of the outage probability and the number of antenna elements. Computed from Figs. 4.8 and 4.9

By increasing the number of interferers in the system, and seeing the total percentage of the distribution that falls above a total interference of $25.5P_R$, the capacities corresponding to different outage probabilities can be determined.

Figures 4.8 and 4.9 show that antenna arrays with an odd number of elements are much less sensitive to DOA effects than the arrays with an even number of elements. In Figures 4.8 and 4.9, the outage probabilities for arrays with 2-7 antenna elements are plotted aginst the number of interference mobiles N_I, and each curve represents a different DOA in increments of 1^o.

Using the outage probabilities from Figures 4.8 and 4.9, a more complete estimate of system capacity can be made. Table 4.12 shows the worst-case capacity over all DOA's as a function of the outage probability. As can be seen from Table 4.12, data mobiles have a large effect on the overall system performance. For acceptable outage probabilities (0.001), the addition of a single data mobile reduces the overall capacity by 16 mobiles. This motivates the need for nulling of heavy interferers which is investigated in Chapter 5.

Outage Probability	0.0001	0.001	0.01	0.05	0.1	0.25	0.5
0 data	70	75	82	88	91	98	104
1 data	54	59	67	76	82	90	98
2 data	37	43	55	66	72	82	92
3 data	21	31	44	57	63	74	85
4 data	8	18	33	47	54	66	78

Table 4.12: Worst-case capacity over all DOA's as a function of the outage probability and the number of data mobiles; computed from Fig. 4.11, it represents the case of 5 antennas and 0-4 data mobiles

4.5 Multi-Service/Rate Systems

In calculating the power statistics for a multi-service or multi-rate system, many of the same techniques can be used as presented in the previous sections to give an initial indication of how data mobiles will co-exist within a voice mobile system. By assuming that the net effect of a data mobile is that of a number voice mobiles clustered together in a small area, it will act as a heavy interferer. By modifying the probability density function for the single voice mobile to produce a larger amount of transmitted power (for our calculations one data mobile produces 7 times the power of a voice mobile). This assumes a voice activity factor of unity, making our results pessimistic. The density of the interference power due to a single data mobile is then shown in Fig. 4.10. Again, as in the previous section, as the number of voice mobiles increases, more of the interference distribution will lie above the point where power control will start to break down. Fig. 4.11 shows the percentage of all cases of mobile placement for which power control will break down for 0-4 data mobiles in a 5 element array.

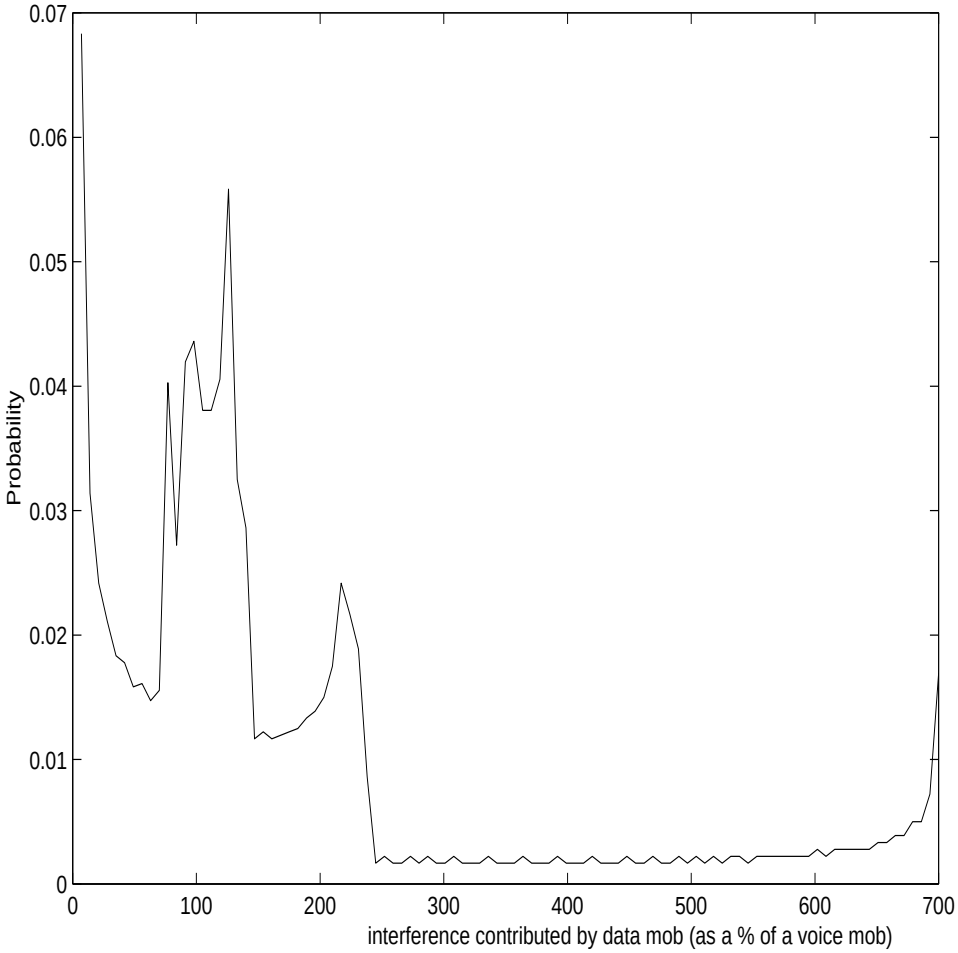

Figure 4.10: *Density function for the amount of interference relative to a voice mobile that a data mobile will contribute.*

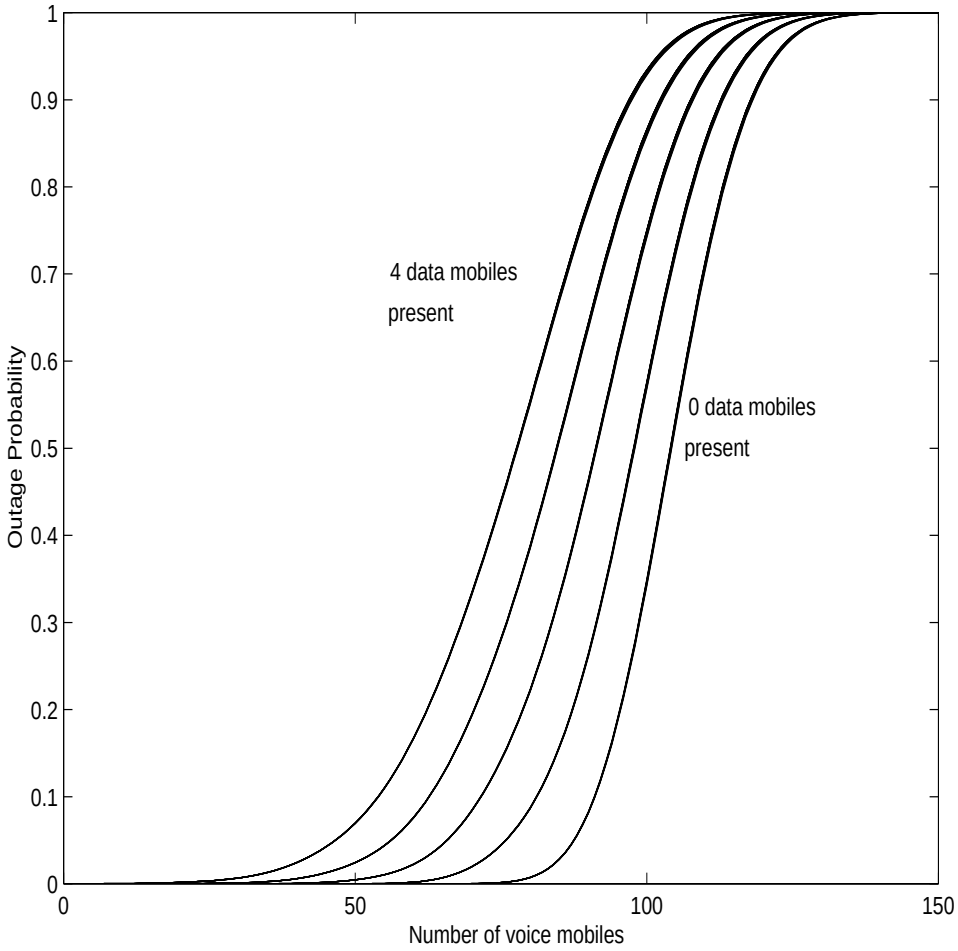

Figure 4.11: *Effect of number of data mobiles on system outage probability for the case of a 5 elements array.*

4.6 Summary

The effects of using beamforming in a cellular CDMA system were analysed in this chapter. Both the mean signal and interference power of a multi-user CDMA environment were predicted and compared to computer simulations. This was then applied to the problem of capacity estimation of the system. It was found that significant increases in capacity are achieved as the number of antennas in the base station are increased.

Then the analysis was extended to include a scattering environment. In section 4.4.1, we have shown that the effect of the spatial filtering of scattered energy is not sufficient to obtain an accurate picture of the system performance . As a result, we have examined the effect of the scattering on both the signal and interference through evaluating the cross-correlation statistics of the antenna array. In conclusion, the effects due to inter-element cross-correlation on system capacity were minimal for low scatter and only small ($\sim 10\%$) for high scatter environments.

Finally, a more in-depth look was taken into system capacity under non-uniform environments. It was shown that in maintaining an acceptable Quality-of-Service (outage probabiltity < 0.001) with non-uniform mobile placement, the system capacity is decreased by about 30%. This analysis also illustrated the effects on system capacity due to DOA effects. It was shown that antenna arrays with certain numbers of antenna elements are more susceptible to DOA effects. The addition of high rate data mobiles was shown to decrease system capacity by about 16 voice mobiles per data mobile in a 5 element array. This result motivates the implementation of more sophisticated beamforming algorithms to null heavy interferers.

Chapter 5

Application to Different Beamforming Scenarios

5.1 Introduction

The method shown in Chapter 4 for predicting mobile power and capacity in a CDMA environment using maximum SNR beamforming is not limited to this specific type of beamforming, and in fact can be used for other beamforming situations (both uplink and downlink). In order to illustrate this, in this chapter we show an initial study into two scenarios employing different methods of beamforming. The first is an extension to a multi-service environment utilising a direct matrix inversion algorithm [7] to reduce the effect of high interference data mobiles in a predominantly voice mobile environment. The second scenario is that of utilising beamforming in the downlink of a mobile environment.

These two examples are used to show the versatility of the methods developed in Chapter 4 to calculate system performance, and are by no means optimized in terms of the type of beamforming. In this chapter, we show that the proposed framework of capacity evaluation can be applied to different beamforming applications: the direct matrix inversion (DMI) algorithm in order to reduce the effect of heavy interferers is shown, as well as a type of transmission beamforming as required in the downlink.

5.2 Methods of Beamforming

In Chapter 4, beamforming was used in order to maximize the desired signal while minimizing a large number of interfering signals arriving from many directions in the uplink of a CDMA system. This was accomplished through individual-user maximum SNR beamforming. In this method of beamforming, the weights are chosen to maximize the desired signal, without taking into account any of the information from the interfering user (i.e. the weights are set equal to the complex conjugate of the array response vector of the desired mobile).

Other methods of beamforming exist which consider the effects of other mobiles in the system. These methods are used both for the uplink and downlink problems. Some examples of this type include maximum SINR beamforming [28], and other methods presented in the tutorial paper by Van Veen and Buckley in [49].

The process of beamforming in the downlink is a completely different and more difficult problem than that of the uplink [14]. In the uplink, the goal is to maximize the received signal power in the direction of arrival of the desired user while minimizing the received signal power from all other directions. In the downlink, however, a single set of beamforming weights is used to transmit the signals to all users simultaneously. Beamforming in the downlink has been studied more extensively in [14],[28] and [55].

5.2.1 Beamforming in a Multi-Service Environment Using the Direct Matrix Inversion Algorithm

The direct matrix inversion method for determining beamforming weights is presented by Compton in [7]. In this method, K samples of a known signal vector X are obtained, and an estimate of the covariance matrix $\hat{\Phi}$ is formed by

$$\hat{\Phi} = \frac{1}{K} \sum_{k=1}^{K} X^*(k) X^T(k) \tag{5.1}$$

where $X^*(k)$ denotes the conjugate of $X(k)$ and $X^T(k)$ denotes the transpose of $X(k)$. The weights W are then calculated through inversion of the covariace matrix.

Outage Probability	0.0001	0.01	0.05	0.1	0.25	0.5
3 data	48	56	60	62	66	71

Table 5.1: Capacity as a function of the outage probability with 5 antenna elements, the desired voice mobile DOA at 70^o and data mobiles at DOAs of 150^o,210^o, and 290^o using the DMI algorithm to determine beamforming weights.

$$W = \hat{\Phi}^{-1} U_d^* \tag{5.2}$$

where U_d^* represents the array response vector of the desired signal. For CDMA systems, the PN code structure may be employed to obtain $X(k)$ rather than using training sequences [35].

Using this algorithm, heavy interferers can be spatially filtered. As an example of this, a beampattern is shown for the desired voice user at 70^o with data mobiles at 150^o, 210^o, and 290^o in Figure 5.3.

Now, using the information contained within this beampattern, the same type of analysis can be performed in order to determine the capacity of the system. As discussed previously, capacity is defined here as the maximum number of mobile for which a solution to the power control equations can be found. Table 5.1 shows the system capacity as a function of outage probability and Figure 5.2 shows the outage probability curve for the desired voice mobile at 70^o. This compares favourably with the corresponding row of Table 4.12, where the capacity for an outage probability of 0.0001 is 21 voice mobiles.

This analysis has been performed on a single beampattern for which the DMI algorithm produces good results. The DMI algorithm starts to break down in cases where the the desired mobile is close to one of the heavy interferers, yielding a beampattern that will produce poor results. As an example of this, a beampattern is shown in Figure 5.3 for the case where the desired mobile is moved to within 10 degrees of

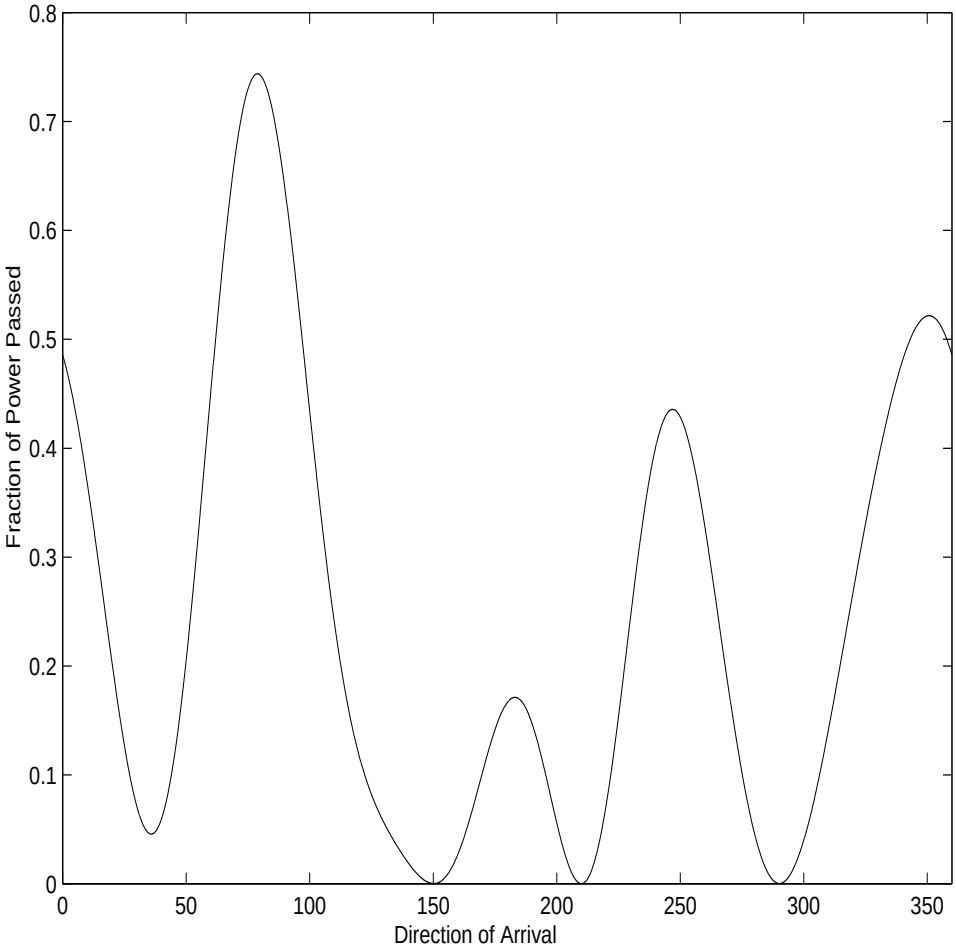

Figure 5.1: *Beampattern produced using the DMI algorithm to generate weights for a desired voice user at* 70° *with data mobiles at* 150°, 210°, *and* 290°.

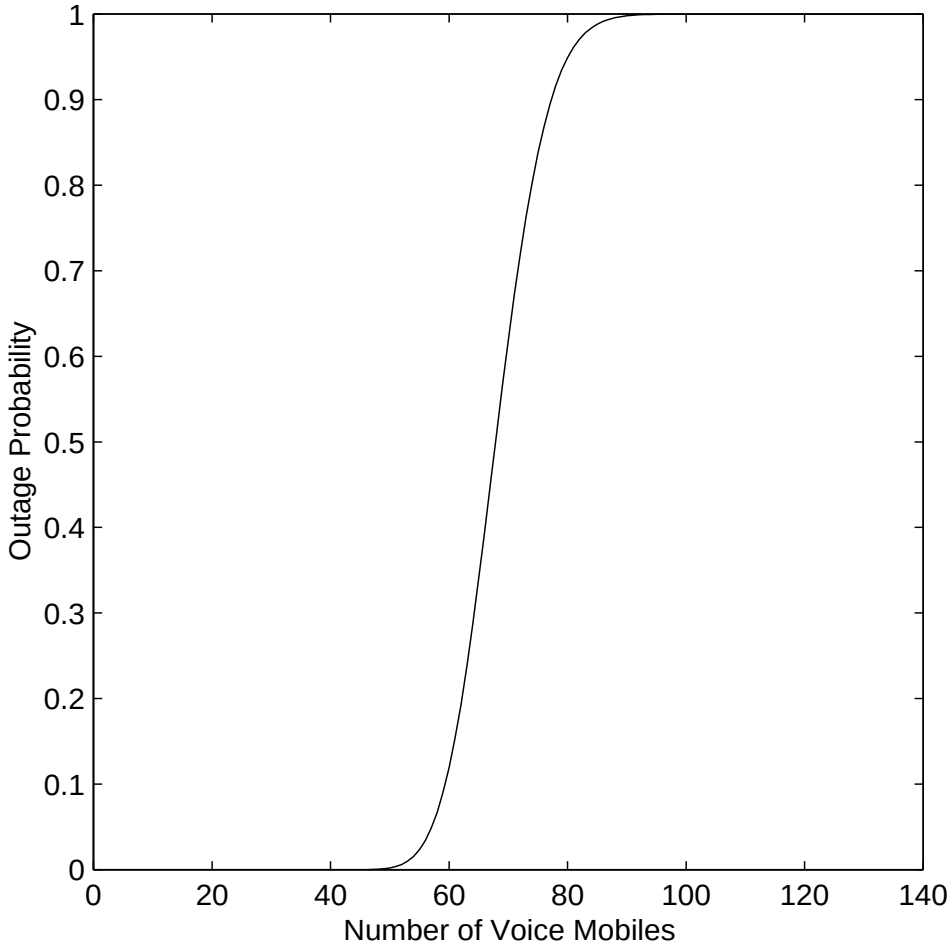

Figure 5.2: *Outage probability for increasing interferers and 5 antenna elements for the desired mobile at* 70^o *and 3 data mobiles at* 150^o,210^o, *and* 290^o *using the DMI algorithm to determine beamforming weights.*

a heavy interferer.

5.2.2 Maximum Sum of SNR Beamforming Algorithm

One method for determining the beamforming weights for transmission beamforming has been proposed by Luo in Chapter 5 of [28], and is summarized below.

The received signal at the kth mobile after despreading is given by:

$$r_k = \bar{w}^H \bar{a}_k b_k + n_k \tag{5.3}$$

where $\bar{w}$ represents the beamforming weights used at the base station, $\bar{a}_k$ represents the array response vector of the kth mobile, b_k represents the current BPSK bit, and n_k represents the white thermal noise with variance σ^2.

The received output of the decorrelator, y_k will then be

$$y_k = (\bar{w}^H \bar{a}_k b_k + n_k)(\bar{w}^H \bar{a}_k)^* \tag{5.4}$$

and the average SNR of the kth mobile is

$$SNR_k = \frac{E[\|\bar{w}^H \bar{a}_k\|^4]}{E[\|(\bar{w}^H \bar{a}_k)^* n_k\|^2]} \tag{5.5}$$

$$= \frac{E[\|\bar{w}^H \bar{a}_k\|^2]}{\sigma^2} \tag{5.6}$$

For the case of N users, we wish to maximize the SNR for several mobiles simultaneously. One way to do this is to maximize

$$\sum_{k=1}^{N_M} E[\|\bar{w}_k^H \bar{a}_k\|^2] \tag{5.7}$$

$$= \bar{w}_k^H E[\sum_{k=1}^{N_M} \bar{a}_k \bar{a}_k^H] \bar{w} \tag{5.8}$$

The solution of this is to choose $\bar{w}$ as the eigenvector corresponding to the largest eigenvalue of $E[\sum_{k=1}^{N_M} \bar{a}_k \bar{a}_k^H]$. This solution for the weights used in beamforming tends to raise the beampattern in the direction of mobile users and lower it in other directions.

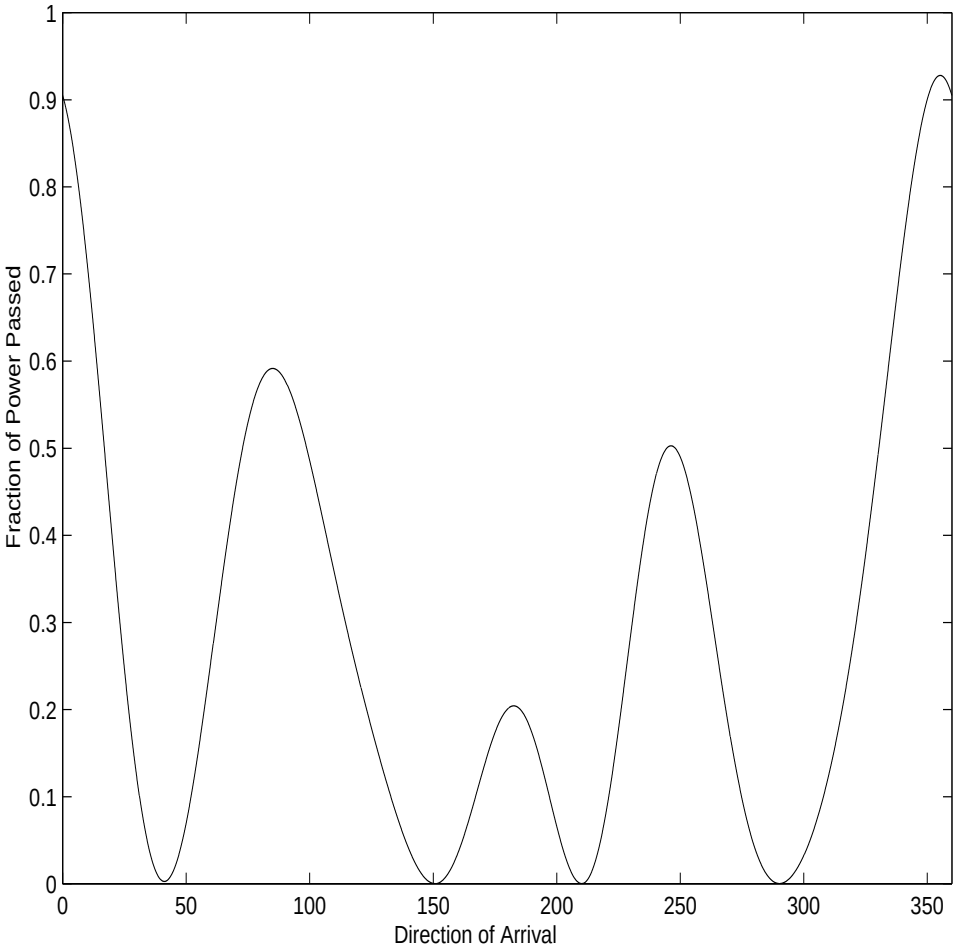

Figure 5.3: *Beampattern produced using the DMI algorithm to generate weights for a desired voice user at* 140^o *with data mobiles at* 150^o,210^o, *and* 290^o.

5.2.3 Beamforming in the Downlink

In their paper [17], Gilhousen et al. studied both the uplink and downlink CDMA system capacity. In this section, we examine the effect of beamforming on the capacity of the downlink. For the downlink, the expression for the signal to noise ratio at the ith mobile is given by

$$\left(\frac{E_b}{N_0}\right)_i \geq \frac{\kappa \vartheta_i S_{T_{1i}}/R_B}{\left[\left(\sum_{j=1}^{K} S_{T_{ji}}\right) + \sigma_n^2\right]/B} \tag{5.9}$$

where $S_{T_{ji}}$ is the power received by mobile i due to base station j, assuming a maximum of K cells from which interference power is received (for the purposes of this work, it is assumed that only cells within the second ring of cells contribute interference, and so $K = 19$), κ is the fraction of the total cell site power devoted to the mobiles (1-κ) is devoted to the pilot, and ϑ_i is the fraction of κ devoted to user i. From (5.9), the following is obtained

$$\vartheta_i \leq \frac{(E_b/N_0)}{\kappa B/R_B}\left[1 + \left(\frac{\sum_{j=2}^{K} S_{T_{ji}}}{S_{T_{1i}}}\right) + \frac{\sigma_n^2}{(S_{T_{1i}})}\right] \tag{5.10}$$

where the apportionment of the total power to individual users must sum to no more than one

$$\sum_{i=1}^{N_M} \vartheta_i \leq 1 \tag{5.11}$$

If the relative received cell-site power measurements are defined as

$$f_i \equiv \left(1 + \sum_{j=2}^{K} S_{T_{ji}}/S_{T_{1i}}\right), \quad i = 1, \ldots, N_M \tag{5.12}$$

then it follows from (5.10) and (5.11) that the sum over all mobiles of the given cell is bounded by

$$\sum_{i=1}^{N_M} f_i \leq \frac{\kappa B/R_B}{E_b/N_0} - \sum_{i=1}^{N_M} \frac{\sigma_n^2}{S_{T_{1i}}} \tag{5.13}$$

Gilhousen et al. [17] also state that the sum on the right-hand side of (5.13) is negligible, and for our Monte Carlo simulations, we assume $R_B = 9600Hz$, $B = 128 \times 9600Hz$, $\kappa = 0.8$ and $E_b/N_0 = 5$dB to ensure a BER of $\leq 10^{-3}$ justified by the coherent reception using the pilot as reference. Using this information, the capacity can be estimated through Monte Carlo simulation, adding users to all cells until an unacceptable percentage of the cases do not satisfy Eq.(5.13). In order to simulate the power that a mobile i can expect to receive from base station j, received power $S_{T_{ji}}$ is defined by the path loss and shadowing effects in [17] as

$$S_{T_{ji}} = 10^{\zeta/10} d_{ji}^{-4} \tag{5.14}$$

where d_{ji} is the distance between the mobile i and one of the 19 base stations j, and ζ is a Gaussian distributed random variable with variance = 8dB. We have performed Monte Carlo simulation using a voice activity factor of one with the method described above using a hexagonal cell structure with interference received from base stations in two rings around the centre base station. We have extended the above approach to the case of beamforming to examine its effect on the system. The outage probability curve as a function of the number of mobiles in each cell is given in Figure 5.6.

With the addition of transmission beamforming, we modify the power $S_{T_{ji}}$ that a mobile i can expect to receive from base station j to include path loss and shadowing as well as the transmitted beam power from the jth base station, $|\bar{w}_j^H \bar{a}_{ij}|^2$ where $\bar{w}_j$ represents the transmission beamforming weights at base station j and $\bar{a}_{ij}$ is the array response vector of mobile i with respect to base station j. For the case of transmission beamforming, $S_{T_{ji}}$ is given by:

$$S_{T_{ji}} = 10^{\zeta/10} d_j^{-4} |\bar{w}_j^H \bar{a}_{ij}|^2 \tag{5.15}$$

In the Monte Carlo simulations with beamforming, the locations of mobiles were chosen in all 19 cells, and beamforming weights $\bar{w}_j$ were determined using the transmission beamforming method developed in [28] and outlined in Section 5.2.2. This was done in order to determine the spatial suppression due to beamforming for each of the 19 cells in the direction of the desired mobile in the centre cell. Figure (5.4) depicts a beampattern where the algorithm works well. However, under other circumstances some mobiles may end up in a lower power part of the beampattern as illustrated by Figure (5.5), significantly decreasing the SNR for that mobile, and significantly increasing the contribution due to that mobile in Equation (5.13). It is this effect that may severely degrade the performace of the system with the type of beamforming outlined below. The overall performance of the system is shown in Figure (5.6) using the Monte Carlo approach; and as can be seen in this figure, the capacity of the system is actually higher without beamforming than it is with beamforming. This can be explained by the presence of the intra-cell interference, which was not taken into account in the determination of the beamforming weights.

The goal of this section was to illustrate a method that could be used to test a method of downlink beamforming. The type of beamforming tested in this section proved ineffective. Other methods of downlink beamforming, however, may prove to increase the capacity of the downlink. A method of allocating power to beamforming weights that maximizes the SNR of the mobile with the minimum SNR such as that presented in [55] may perform better than that of [28], since intra-cell interference is taken into account. However, its complexity is higher than that of [28]. The optimal choice of weights is still an open problem.

5.3 Summary

Initial studies were made into the multi-service/multi-rate environment. The use of the DMI algorithm for heavy interferer cancellation was shown to be an effective method to reduce interference contributed by data mobiles in a predominantly voice

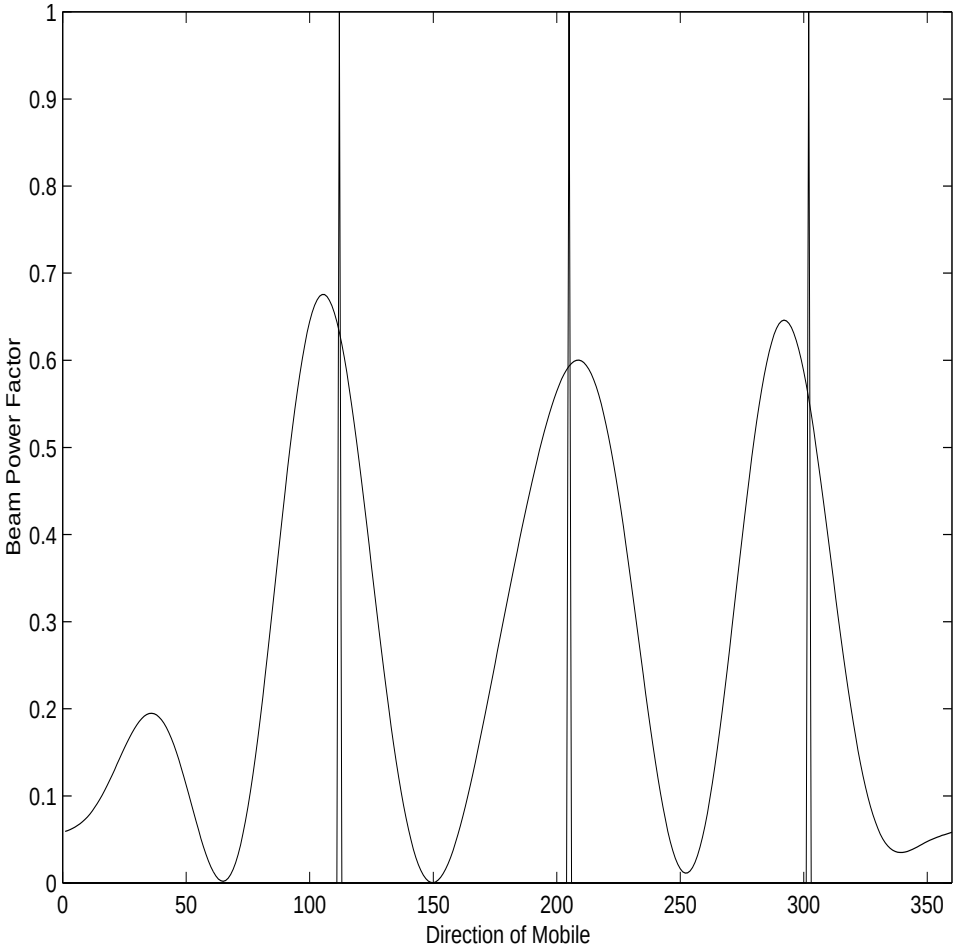

Figure 5.4: *One of the beampatterns produced using the algorithm for transmission beamforming from [28] for mobiles at* 112^o, 205^o, *and* 303^o. *Vertical spikes indicate desired directions for maximal transmission power.*

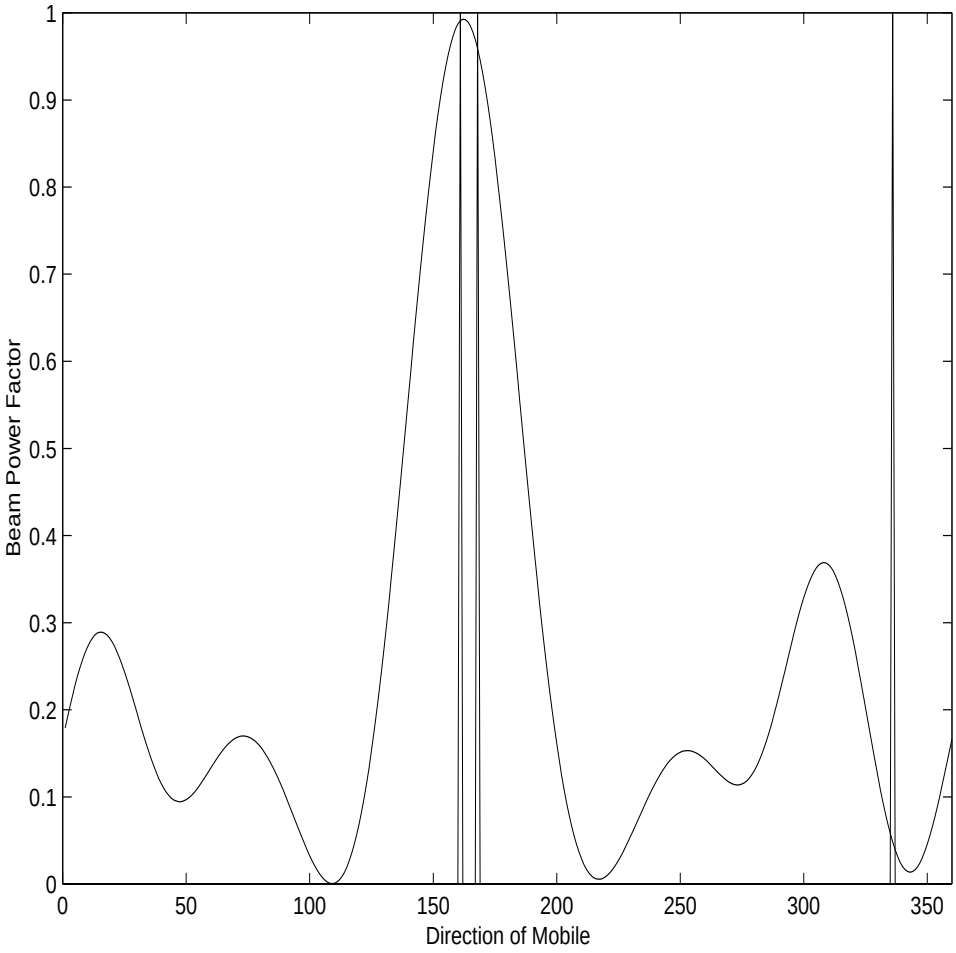

Figure 5.5: *Another beampattern produced using the algorithm for transmission beamforming from [28] for mobiles at* 161^o, 168^o, *and* 335^o. *Vertical spikes indicate desired directions for maximal transmission power.*

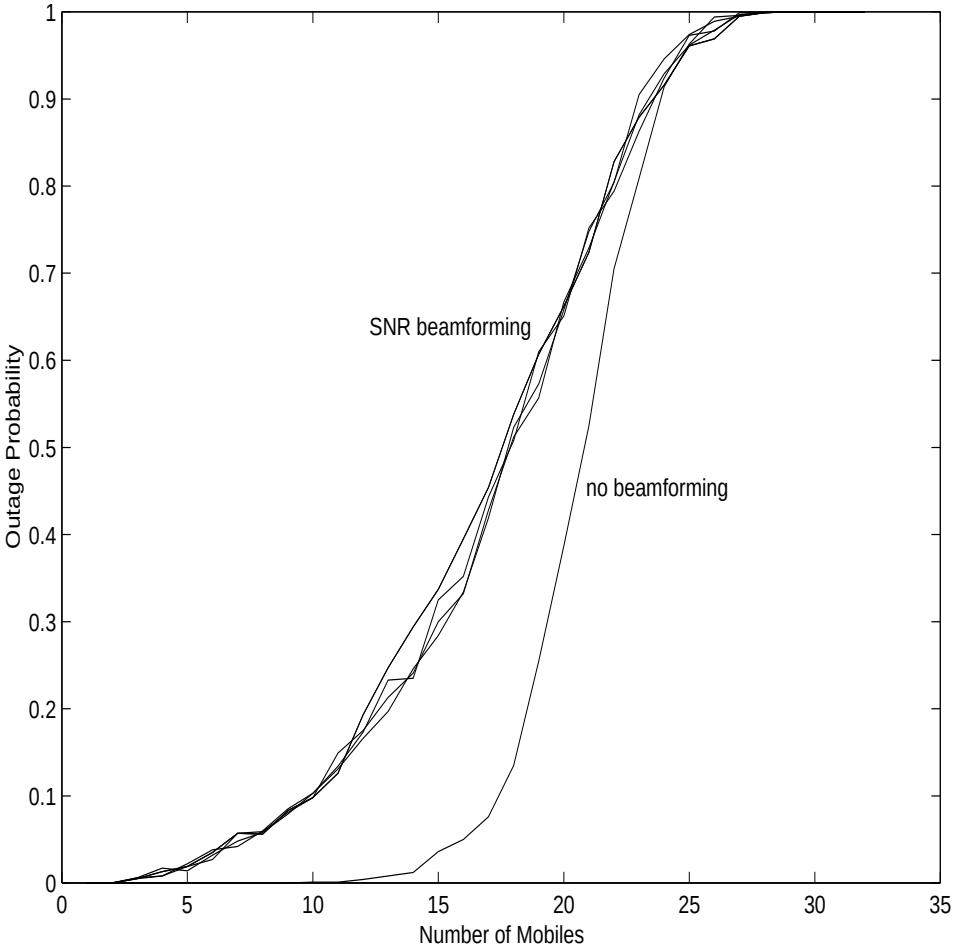

Figure 5.6: *Overall performance comparison of downlink performace with and without beamforming under a maximum sum of SNR criterion. Beamforming with 5,9,13,17 and 21 element circular arrays.*

mobile environment. It was also shown, however, that this method beaks down when a desired user comes close to a data mobile.

The application of transmission beamforming in the downlink of a CDMA system was also examined. A method developed by Gilhousen et al. [17] for calculating downlink capacity was extended to include beamforming. A method of maximum sum of SNR transmission beamforming developed in [28] was tested and shown to perform poorly. However, intra-cell interference was not taken into account in the development of the beamforming method in [28]. A method of transmission beamforming developed in [55] may give better performance than the method outline here.

Chapter 6

Conclusion

6.1 Introduction

This chapter reiterates some of the major contributions of this work, and outlines some possible extensions and improvements that could be made.

6.2 Summary of Contributions

This section presents a list of the major contributions of this thesis.

- A study was made into the effectiveness of the use of ARMA modelling to create a low-order filter to generate a sequence with the autocorrelation outlined by Jakes in [23]. It was found that traditional methods of ARMA modelling were ineffective for the Jakes autocorrelation function as the true order of the model is infinite. By using the AR(7) model as found above with a comb filter with a carefully selected null location in its PSD, it was found that the Bessel autocorrelation could be matched quite closely for the first 100 lags.

- A model given by Salz and Winters in [46] for cross-correlation statistics between two antenna elements assuming uniform angle-of-arrival statistics was generalized to the case of any angle-of-arrival probability distribution $P(\theta)$. A Gaussian angle-of-arrival distribution was chosen as an example for the purposes

of this thesis, and the the cross correlation statistics were used to generate signals that would have the Jakes' autocorrelation statistics and cross correlation statistics matching the GAA model.

- The most significant contribution of this thesis is the improvement of the power and capacity predictions of a CDMA system in the multiple antenna element beamforming case from [11], and the extension of this to include power and capacity prediction and simulation incorporating inter-element cross-correlation effects due to scatter. Beampatterns were used to determine the amount of interference that would be expected in a multiple user system, and the effect of the inter-element cross-correlation on the desired mobile power and interference power was helpful in determining the overall capacity of the system. Analysis was verified by simulations involving antennas with correlated signals as outlined above. We have shown that significant increases in capacity may be achieveable using beamforming, even in environments with moderate to high amounts of scatter. It was also shown that the directional nature of antenna arrays can lower the capacity of the system. However, circular antenna arrays with certain numbers of antenna elements (e.g. $N_A = 5$ and $N_A = 7$) are minimally affected by DOA.

- Other beamforming applications were then explored. It was shown how the direct matrix inversion (DMI) algorithm may be an effective means to eliminate the effects of heavy interferers in a multi-service system. However, it was also noted that the DMI algorithm tended to break down in cases where the desired user came within 10^o of a heavy interferer. A method for determining the capacity of the downlink developed in [17] was extended to include transmission beamforming. It was shown that the system capacity using the transmission beamforming method developed in [28] may be lower without beamforming. However, improved transmission beamforming methods may outperform the single element case.

6.3 Future Work

We will now suggest areas where further study could be made to complement this work

- In Chapter 2, an attempt was made to minimize the mean square error between the autocorrelation of the ARMA filter's output sequence and the desired Bessel ACF, while trying to minimize the order of the ARMA filter. An initial study was made into methods of optimum model order selection, but a more in-depth study to determine the order of the optimal filter is needed.

- In Chapter 4, power and capacity values were predicted for the uplink of a CDMA system. This study neglected effects due to the delay spread of the environment. A necessary extension of this work is the inclusion of the effects of delay spread on the system.

- In Chapter 5, the DMI algorithm was used to minimize the effects of heavy interferers in a predominantly voice mobile system. It was found that in cases where the desired mobile was at a direction of arrival within 10^o of a heavy interferer, the performance of the system is poor. A possible improvement of this algorithm would be to employ more sophisticated constraints to determine how to cope with heavy interferers close to the desired mobile.

- In Chapter 5, a method of transmission beamforming developed in [28] was shown to be outperformed by the same test performed without beamforming. It would be useful to investigate improved methods of transmission beamforming based on preliminary work in [55] to compare performance with that of [28].

6.4 Conclusions

In this thesis we applied a specific improvement to ARMA modelling of fading channels and a model based on the work of Salz and Winters in [46] in order to

simulate the auto- and cross-correlation statistics of the fading envelopes received by the elements of an antenna array. We then developed a method for determining the power levels and capacity of a CDMA system using beamforming with a multi-element antenna array. This analysis and simulation was extended to the case of the scattering environment where it was shown that large capacity gains may be obtainable using beamforming, even in high-scatter environments.

Appendix A

Application to Fading Channel Gain Tracking

To detect an information sequence transmitted coherently and reliably over a fading channel, it is necessary to estimate the channel phase and amplitude. This is motivated by the fact that coherent detection of signals over fading channels is superior to non-coherent detection if accurate channel state information is available [43]. Prediction of fading dynamics can be applied to channel estimation in systems employing coherent modulation.

Because of this, we present an algorithm given in [27] in order to illustrate an application of the channel simulator developed in Chapter 2. This will show that the accuracy of the chosen channel simulator can have a significant effect on the BER curves produced during simulation.

Let I_k denote a binary information sequence, and x_k the $q-$ary output of a low-pass equivalent discrete-time encoder/modulator. The complex signal x_k is transmitted over a frequency-nonselective Rayleigh or Rician fading channel. The received low-pass equivalent discrete-time signal is then [43]

$$y_k = x_k c_k + n_k \tag{A.1}$$

where c_k is channel gain, a complex Gaussian process with memory. The mean of c_k is $a = E\{c_k\}$. When $a = 0$, the fading channel is Rayleigh. Otherwise it is Rician. The covariance function of c_k is $r_{k,k-n} = r_n \stackrel{\triangle}{=} E\{(c_k - a)(c_{k-n} - a)^*\}$. A special

case of the above model is the Jakes-Reudink fading channel [23] with r_n given by $r_n = r_0 J_0(2\pi f_m nT) = r_0 \frac{1}{2\pi} \int_{-\pi}^{\pi} e^{j2\pi f_m nT \sin\theta} d\theta$, where $J_0()$ is the zeroth order Bessel function, T is the symbol period and f_m is the maximum Doppler frequency given by $f_m = \frac{v}{\lambda}$ with v and λ defined as mobile vehicle speed and transmission wavelength, respectively.

The channel gain c_k can be divided into two parts: the line-of-sight (LOS) part with average power a^2 and the random scattering part with average power r_0. The K factor is defined as the ratio [32] $K \triangleq \frac{a^2}{r_0}$. If r_0 is normalized to 1, then $K = a^2$. The K factor is equal to zero for Rayleigh fading channels and is greater than zero for Rician fading channels. The average signal-to-noise (SNR) ratio per symbol is then $\gamma_s = \frac{a^2+r_0}{\sigma_n^2}$, where σ_n^2 is the variance of the additive white Gaussian noise (AWGN) n_k. The average signal-to-noise (SNR) ratio per bit for q-ary constant-envelope modulation is $\gamma = \frac{a^2+r_0}{\sigma_n^2 \log_2 q}$.

If x_k is a known training symbol and if the signal-to-noise ratio (SNR) is high, a good estimate of c_k can be easily computed as

$$c_k \approx y_k / x_k \triangleq \tilde{c}_k \tag{A.2}$$

according to Eq.(A.1), where y_k is the received signal. However, most of the received symbols are not training symbols. In these cases the available information for estimating c_k can be based upon prediction from the past detected data-bearing symbols $\bar{x}_i$ $(i < k)$. Since a fading channel is usually correlated [23], it is possible to use an adaptive linear filter to estimate the current complex channel gain c_k using the past detected symbols $\bar{x}_i$ $(i < k)$ and the current observed signal y_k. The idea of decision-feedback has long been used in adaptive equalization of deterministic telephone channels [43]. The same idea was also used in [22]. However, [22] mainly used training-symbol information and did not consider the high correlation of both Rayleigh and Rician fading channels.

We now summarize the decision feedback and adaptive linear prediction (DFALP) algorithm: Let the past detected data symbols be $\bar{x}_{k-1}, \bar{x}_{k-2}, \ldots \bar{x}_{k-N}$. The past received signals are $y_{k-1}, y_{k-2}, \ldots y_{k-N}$. Notice that $\bar{x}_i$ and y_i are complex, and that

$\bar{x}_i$ takes on a finite number of values (e.g., four values for QPSK). Then the past decision feedback complex channel gains are

$$\frac{y_{k-i}}{\bar{x}_{k-i}} \quad i = 1, 2, ..., N. \tag{A.3}$$

If the fed back data symbol happens to be correct, that is, $\bar{x}_{k-i} = x_{k-i}$, the estimate $y_{k-i}/\bar{x}_{k-i}$ would be reliable. However, this may not be always true. Therefore the estimate $y_{k-i}/\bar{x}_{k-i}$ should be corrected in a manner to be described later in this section. Let $\tilde{c}_{k-i}$ denote the corrected fading channel estimate from $y_{k-i}/\bar{x}_{k-i}$, or the fading channel estimate if training symbols were available (Eq.(A.2)). Using a standard linear prediction approach [20], the predicted fading channel gain at time k is

$$\hat{c}_k = \sum_{i=1}^{N} b_i^* \tilde{c}_{k-i} = \vec{b}(k)\vec{\tilde{c}}(k) \tag{A.4}$$

where

$$\vec{\tilde{c}}(k) = (\tilde{c}_{k-1}, \tilde{c}_{k-2}, ..., \tilde{c}_{k-N})^T \tag{A.5}$$

is a vector of past corrected channel gain estimates and

$$\vec{b}(k) = (b_1, b_2, ..., b_N)^T \tag{A.6}$$

are the filter (linear predictor) coefficients at time k. The constant N is the order of the linear predictor. The objective is to minimize the estimation error adaptively, i.e.,

$$\min \eta_k = |c_k = \hat{c}_k|^2 \tag{A.7}$$

where c_k is the actual complex channel gain. Liu and Blostein suggest using the Widrow-Hoff's least-mean-square algorithm [53] in order to determine the filter coefficients of the next time step $\vec{b}(k+1)$. This is given by

$$\vec{b}(k+1) = \vec{b}(k) + \mu(c_k - \hat{c}_k)^* \vec{\tilde{c}}(k) \tag{A.8}$$

where μ is the adaptation parameter controlling the convergence-rate and the steady-state error of the algorithm. Since the actual channel gain c_k is not available, the current corrected channel gain estimate is substituted.

$$\vec{b}(k+1) = \vec{b}(k) + \mu(\tilde{c}_k - \hat{c}_k)^* \vec{\tilde{c}}(k) \tag{A.9}$$

Now the problem of using decision feedback and correction to obtain the corrected channel gain estimate $\tilde{c}_k$ from the predicted channel gain $\hat{c}_k$ is addressed. First, Liu and Blostein [27] estimate the data symbol using the predicted channel gain $\hat{c}_k$:

$$\hat{x}_k = \frac{y_k}{\hat{c}_k} \tag{A.10}$$

where y_k is the current received signal plus noise, and $\hat{c}_k$ is a channel estimate given by the linear predictor (A.4). Second, [27] use the minimum distance decision rule

$$\min_{x_k \in D} |\hat{x}_k - x_k| \tag{A.11}$$

where D is the signal constellation of the modulated complex low-pass equivalent signal x_k. For QPSK, $D = \{e^{jn\pi/4}, n = 1, 3, 5, 7\}$. Let $\bar{x}_k$ denote the detected data symbol, i.e.,

$$|\hat{x}_k - \bar{x}_k| = \min_{x_k \in D} |\hat{x}_k - x_k|. \tag{A.12}$$

Using the detected data symbol $\bar{x}_k$, a new estimate of the channel gain is formulated.

$$\frac{y_k}{\bar{x}_k}. \tag{A.13}$$

There exist two possibilities for the decision rule (A.12). One possibility is that the decision is correct, i.e., $\bar{x}_k = x_k$. Then the estimate $y_k/\bar{x}_k$ would be reliable. On the other hand, if the decision is wrong, i.e., $\bar{x}_k \neq x_k$, the estimate $y_k/\bar{x}_k$ will certainly be very poor. To solve this problem, a thresholding idea similar to that proposed in [22] is used. In most cases, if the decision is correct, the distance between the predicted channel gain $\hat{c}_k$ and the decision feedback estimate $y_k/\bar{x}_k$ would not be large, i.e., the probability that $|\hat{c}_k - y_k/\bar{x}_k| < \beta$ would be high, where β is a chosen threshold. On the other hand, if the decision is wrong, the distance between the predicted channel

gain $\hat{c}_k$ and the decision-feedback estimate $y_k/\bar{x}_k$ would be large, i.e., the probability that $|\hat{c}_k - y_k/\bar{x}_k| \geq \beta$ would be high. Therefore the corrected channel estimate may be expressed as

$$\check{c}_k = \begin{cases} y_k/\bar{x}_k & \text{if } |\hat{c}_k - y_k/\bar{x}_k| < \beta \\ \hat{c}_k & \text{if } |\hat{c}_k - y_k/\bar{x}_k| \geq \beta \end{cases} \tag{A.14}$$

The justification for thresholding appears in [22]. There exists no analytical approach to choosing the threshold β. In [22], it was proposed that for q-ary PSK β is chosen to be $e^{j\pi/(2q)}$.

The corrected channel estimate $\check{c}_k$ is then low-pass filtered using a linear phase low-pass filter (LPF) with $2D_f + 1$ taps to reduce the noise. That is, the final channel gain estimate is

$$\bar{c}_{k-D_f} = \sum_{i=0}^{2D_f} h_i \check{c}_{k-i} \tag{A.15}$$

where h_i is the impulse response of a LPF with $2D_f + 1$ taps. The choice of filter cutoff frequency is discussed in [27]. A linear phase FIR filter is used and a delay of D_f samples is incurred after the above final low-pass filtering. The algorithm steps are summarized below:

DFALP Fading Channel Tracker

Repeat Steps 1-3:

- Step 1: If a training symbol x_k is available, set $\check{c}_k = y_k/x_k$. Otherwise,

  1.1 Predict channel gain:$\hat{c}_k = \sum_{i=1}^{N} b_i^* \check{c}_{k-i} = \vec{b}(k)\vec{\check{c}}(k)$;

  1.2 Estimate data symbol: $\hat{x}_k = y_k/\hat{c}_k$;

  1.3 Tentative decision: find $\bar{x}_k$ such that $|\hat{x}_k - \bar{x}_k| = \min_{x_k \in D} |\hat{x}_k - x_k|$;

  1.4 Correction:

  If predicted gain agrees with decision feedback estimate, use the fed back estimate,

i.e., if $|\hat{c}_k - y_k/\bar{x}_k| < \beta$, then $\tilde{c}_k = y_k/\bar{x}_k$,

else use predicted gain only, i.e., if $|\hat{c}_k - y_k/\bar{x}_k| \geq \beta$ then $\tilde{c}_k = \hat{c}_k$;

- Step 2: Low pass filter $\tilde{c}_k$: $\bar{c}_{k-D_f} = \sum_{i=0}^{2D_f} h_i \tilde{c}_{k-i}$
- Step 3: Output $\bar{c}_{k-D_f}$, increment k and go to Step 1.

The notations are:

$\bar{c}_{k-D_f}$ = final (delayed) channel gain estimate;

a_k, b_k = ARMA filter coefficients;

$\vec{\tilde{c}}(k)$ = past corrected channel gain estimate;

y_k = received signal plus noise at time kT;

$\bar{x}_k$ = detected data symbol at time kT.

One training symbol is sent for transmitting every $K_t - 1$ data symbols. The initial conditions for the filter coefficients vb are chosen to be

$$\vec{b}(0) = (1, 0, ..., 0)^T \tag{A.16}$$

A block diagram of the DFALP algorithm is shown in Figure A.1. The received signal y_k is divided by a channel estimate $\hat{c}_k$ from the adaptive linear predictor. The estimated data symbol is detected using a minimum distance decision rule. Then the corrected channel estimate $\tilde{c}_k$ is obtained. The corrected channel estimate $\tilde{c}_k$ is then passed through a LPF with $2D_f + 1$ taps to reduce the noise, resulting in a decision delay D_f. The final smoothed channel estimate $\bar{c}_{k-D_f}$ is sent out for soft Viterbi decoding. Note that only $\tilde{c}_k$ can be fed back and the smoothed estimate $\bar{c}_{k-D_f}$ cannot be fed back since it is delayed by D_f.

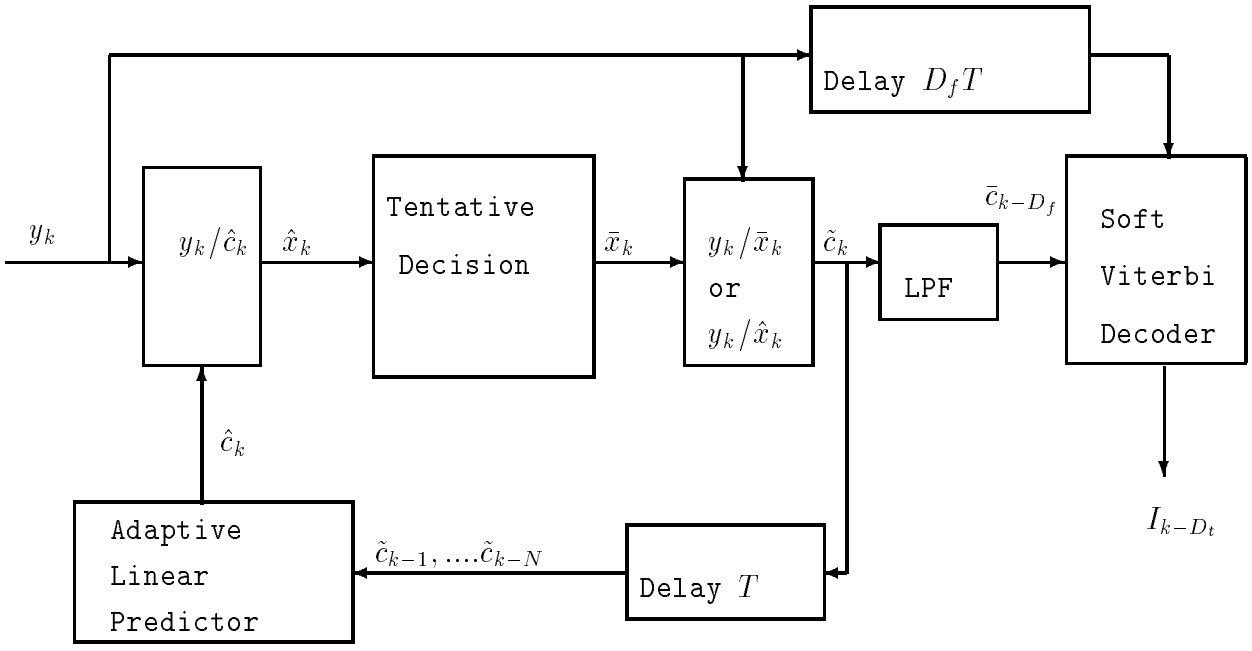

Figure A.1: *The DFALP algorithm for tracking phase and amplitude of frequency nonselective fading channels.*

Bibliography

[1] Sidney P. Applebaum. "Adaptive arrays". *IEEE Transactions on Antennas and Propagation*, 24(5):585–598, 1976.

[2] David Aszetly. *On Antenna Arrays in Mobile Communication Systems: Fast Fading and GSM Base Station Receiver Algorithms.* PhD thesis, Dept. of Signals, Sensors and Systems Signal Processing, Royal Institute of Technology, 1996.

[3] S. Barberis, L. Bonzano, E. Gaiani and M. Tosalli. "Capacity of a CDMA Wireless Communication System in Picocellular Environment". In *1996 International Conference on Communications*, volume 3, pages 1824–1828, 1996.

[4] E. N. Bramley "Diversity Effects in Spaced-Aerial Reception of Ionospheric Waves". *IEE Proceedings*, 98(3):19-25, Jan 1951.

[5] Rick Cameron and Brian Woerner. "Performance analysis of CDMA with imperfect power control". *IEEE Transactions on Communications*, 44(7):777–781, 1996.

[6] Geoffrey W.K. Colman, Steven D. Blostein, and Norman C. Beaulieu. "An ARMA multipath fading simulator". In *The 7th Annual Virginia Tech Symposium on Wireless Personal Communications*, 1997.

[7] R.T. Compton Jr. *Adaptive Arrays, Concepts and Performance.* Prentice Hall Inc., 1988.

[8] Giovanni Emanuele Corazza, Giovanni De Maio and Francesco Vatalaro. "CDMA Cellular Systems Performance with Fading, Shadowing, and Imperfect Power Control". *IEEE Transactions on Vehicular Technology*, 47(2):450–459, 1998.

[9] Wilbur B. Davenport and William L. Root *An Introduction to the Theory of Random Signals and Noise*. McGraw-Hill, 1958.

[10] Dariush Divsalar, Marvin K. Simon and Dan Raphaeli. "Improved Parallel Interference Cancellation for CDMA". *IEEE Transactions on Communications*, 46(2):258–268, 1998.

[11] A. Mark Earnshaw. *An Investigation into Improving Performance of Cellular CDMA Communication Systems with Digital Beamforming*. PhD thesis, Dept. of Electrical and Computer Engineering, Queen's University, 1997.

[12] A. Mark Earnshaw and Steven D. Blostein. "Investigating the effects of imperfect digital beamforming on cell capacity in a cellular CDMA communication system". In *1996 International Conference on Universal Personal Communications*, pages 458–462, 1996.

[13] Richard B. Ertel, Paolo Cardieri, Kevin W. Sowerby, Theodore S. Rappaport, Jeffrey H. Reed. "Overview of Spatial Channel Models for Antenna Array Communication Systems". *IEEE Personal Communications*, pages 10–22, February 1998.

[14] A. Gerlach. *Adaptive Transmitting Antenna Arrays at the Base Station in Mobile Radio Networks*. PhD thesis, Dept. of Electrical Engineering, Stanford University, 1995.

[15] Filippo Giannetti. "Capacity evaluation of a cellular CDMA system operating in the 63-64 GHz band". *IEEE Transactions on Vehicular Technology*, 46(1):55–64, 1997.

[16] Filippo Giannetti, Marco Luise and Ruggero Reggiannini. "The Capacity of Cellular CDMA in the 63-64 GHz Band". In *1997 International Conference on Communications*, pages 989–993, 1997.

[17] Klein S. Gilhousen, Irwin M. Jacobs, Roberto Padovani, Andrew J. Viterbi, Jr. Lindsay A. Weaver, and Charles E. Wheatley III. "On the capacity of a cellular CDMA system". *IEEE Transactions on Vehicular Technology*, 40(2):303–312, 1991.

[18] R. Haeb and H. Meyr. "A systematic approach to carrier recovery and detection of digitally phase modulated signals on fading channels". *IEEE Transactions on Communications*, 37(7):748–754, 1989.

[19] E. J. Hannan and J. Rissanen. "Recursive Estimation of Mixed Autoregressive-Moving Average Order". *Biometrika*, 69(1):81–94, 1982.

[20] S. S. Haykin. *Adaptive Filter Theory*. Englewood Cliffs: Prentice Hall, 1991.

[21] Steven J. Howard and Kaveh Pahlavan. "Autoregressive modelling of wide-band indoor radio propagation". *IEEE Transactions on Communications*, 40(9):1540–1552, 1992.

[22] G.T. Irvine and P.J. McLane. "Symbol-aided plus decision-directed reception for PSK/TCM modulation on shadowed mobile satellite fading channels". *IEEE Journal on Selected Areas in Communications*, 10(8):1289–1299, 1992.

[23] William C. Jakes. *Microwave Mobile Communications*. John Wiley & Sons, Inc., 1974.

[24] Akihiro Kajiwara. "Effects of Cell Size, Directional Antenna, Diversity, and Shadowing on Indoor Radio CDMA Capacity". *IEEE Transactions on Vehicular Technology*, 46(1):242–247, 1991.

[25] Steven M. Kay. *Modern Spectral Estimation*. Prentice Hall, Inc., 1988.

[26] Joseph C. Liberti, Jr. and Theodore S. Rappaport. "Analytical results for capacity improvements in CDMA". *IEEE Transactions on Vehicular Technology*, 43(3):680–690, 1994.

[27] Yong Liu and Steven D. Blostein. "Identification of frequency non-selective fading channels usinfg decision feedback and adaptive linear prediction". *IEEE Transactions on Communications*, 43(2/3/4):1484–1492, 1995.

[28] Tao Luo. *Beamforming in the Uplink and Downlink Channels of a Cellular CDMA Communication System.* MSc. thesis, Dept. of Electrical and Computer Engineering, Queen's University, 1998 .

[29] Salim Manji and Weihua Zhuang. "Capacity Analysis of an Integrated Voice/Data DS-CDMA Network". In *1997 International Conference on Communications*, volume 2, pages 979–983, 1997.

[30] Neri Merhav. "The Estimation of the Model Order in Exponential Families". *IEEE Transactions on Information Theory*, 35(5):1109–1114, Sept. 1989.

[31] Laurence B. Milstein, Theodore S. Rappaport, and Rashad Barghouti. "Performance evaluation for cellular CDMA". *IEEE Journal on Selected Areas in Communications*, 10(4):680–689, 1992.

[32] M.L. Moher and J.H. Lodge. "TCMP-A modulation and coding strategy for Rician fading channels". *IEEE Journal on Selected Areas in Communications*, 7(9):1347–1355, 1989.

[33] Robert A. Monzingo and Thomas W. Miller. *Introduction to Adaptive Arrays.* John Wiley & Sons, Inc., 1980.

[34] Jerome L. Myers and Arnold D. Well. *Research Design & Statistical Analysis.* Harper Collins Publishers Inc., 1991.

[35] Ayman F. Naguib. *Adaptive Antennas for CDMA Wireless Networks.* PhD thesis, Dept. of Electrical Engineering, Stanford University, 1995.

[36] Ayman F. Naguib and Arogyaswami Paulraj. "Performance of DS/CDMA with M-ary orthogonal modulation cell site antenna arrays". In *1995 International Conference on Communications*, pages 697–702, 1995.

[37] Ayman F. Naguib and Arogyaswami Paulraj. "Recursive adaptive beamforming for wireless CDMA". In *1995 International Conference on Communications*, pages 1515–1519, 1995.

[38] Ayman F. Naguib and Arogyaswami Paulraj. "Performance of wireless CDMA with M-ary orthogonal modulation and cell site antenna arrays". *IEEE Journal on Selected Areas in Communications*, 14(9):1770–1783, 1996.

[39] Ayman F. Naguib, Arogyaswami Paulraj, and Thomas Kailath. "Capacity improvement with base-station antenna arrays in cellular CDMA". *IEEE Transactions on Vehicular Technology*, 43(3):691–698, 1994.

[40] Athanasios Papoulis. *Probability, Random Variables, and Stochastic Processes.* McGraw-Hill, Inc., 1984.

[41] Vijayanand K. Paulrajan, James A. Roberts and D. L. Machamer. "Capacity of a CDMA Cellular System with Variable User Data Rates". In *1996 IEEE Global Telecommunications Conference*, volume 2, pages 1458–1462, 1996.

[42] Arogyaswami J. Paulraj, and Constantinos B. Papadias. "Space-Time Processing for Wireless Communication". *IEEE Signal Processing Magazine*, pages 49–83, Nov. 1997.

[43] John G. Proakis. *Digital Communications.* McGraw-Hill, Inc., 1989.

[44] John G. Proakis and Dimitris G. Manolakis. *Digital Signal Processing.* Macmillan Publishing Co., 1992.

[45] Jack Salz and Jack H. Winters. "Effect of fading correlation on adaptive arrays in digital wireless communications". In *1993 International Conference on Communications*, volume 3, pages 1768–1774, 1993.

[46] Jack Salz and Jack H. Winters. "Effect of fading correlation on adaptive arrays in digital mobile radio". *IEEE Transactions on Vehicular Technology*, 43(4):1049–1057, 1994.

[47] John I. Smith. "A computer generated multipath fading simulation for mobile radio". *IEEE Transactions on Vehicular Technology*, 24(3):39–40, 1975.

[48] Gordon L. Stüber and Chamroeun Kchao. "Analysis of a multiple-cell direct-sequence CDMA cellular mobile radio system". *IEEE Journal on Selected Areas in Communications*, 10(4):669–679, 1992.

[49] Barry D. Van Veen and Kevin M. Buckley. "Beamforming: A versatile approach to spatial filtering". *IEEE ASSP Magazine*, pages 4–24, April 1988.

[50] Audrey M. Viterbi and Andrew J. Viterbi. "Erlang Capacity of a Power Controlled CDMA System". *IEEE Journal on Selected Areas in Communications*, 11(6):892–899, 1993.

[51] Andrew J. Viterbi, Audrey M. Viterbi, Klein S. Gilhousen and Arogyaswami Ephraim Zehavi. "Soft Handoff Extends CDMA Cell Coverage and Increases Reverse Link Capacity". *IEEE Journal on Selected Areas in Communications*, 12(8):1281–1287, 1994.

[52] Yiping Wang and J.R. Cruz. "Performance Analysis of CDMA Cellular Systems with Adaptive Antenna Arrays over Multipath Channels". In *1996 International Conference on Communications*, pages 536–540, 1996.

[53] B. Widrow, J.M. McCool, and M. Ball. "The Complex LMS Algorithm". In *Proceeding of IEEE*, pages Vol 63, pages 96–104, 1975.

[54] Hsin-Yu Wu and Alexandra Duel-Hallen. "On the performance of coherent and noncoherent multiuser detectors for mobile radio CDMA channels". In *5th IEEE International Conference on Universal Personal Communications*, pages 76–80, 1996.

[55] Weidong Yang and Guanghan Xu. "Optimal Downlink Power Assignment for Smart Antenna System". In *International Conference on Acoustics, Speech, and Signal Processing* 1998.

[56] David J. Young and Norman C. Beaulieu. "On the generation of correlated Rayleigh random variates by inverse discrete time fourier transform". In *5th IEEE International Conference on Universal Personal Communications*, pages 231–235, 1996.

Vita

Geoffrey W. K. Colman

EDUCATION

Queen's University	M.Sc.(Eng.)	Electrical Engineering	1996–98
Queen's University	B.Sc.(Eng.)	Electrical Engineering	1991–96

EXPERIENCE

Defence Scientist (1998–),
Defence Research Establishment Ottawa, Ottawa, Ontario
Research Assistant (1996–1998),
Electrical and Computer Engineering, Queen's University
Teaching Assistant (1996–1996),
Electrical and Computer Engineering, Queen's University

PUBLICATIONS

Geoffrey W.K. Colman and Steven D. Blostein (1998), "Improved Power and Capacity Predictions of a CDMA System with Base-Station Antenna Arrays and Digital Beamforming", *19th Biennial Symposium on Communications, Queen's University, 1998.*

Geoffrey W.K. Colman, Steven D. Blostein and Norman C. Beaulieu (1997), "An ARMA Multipath Fading Simulator", *7th Virginia Tech/MPRG Symposium on Wireless Personal Communications.*